iScience

CellPress
OPEN ACCESS

Article

A proton-inhibited DEG/ENaC ion channel maintains neuronal ionstasis and promotes neuronal survival under stress

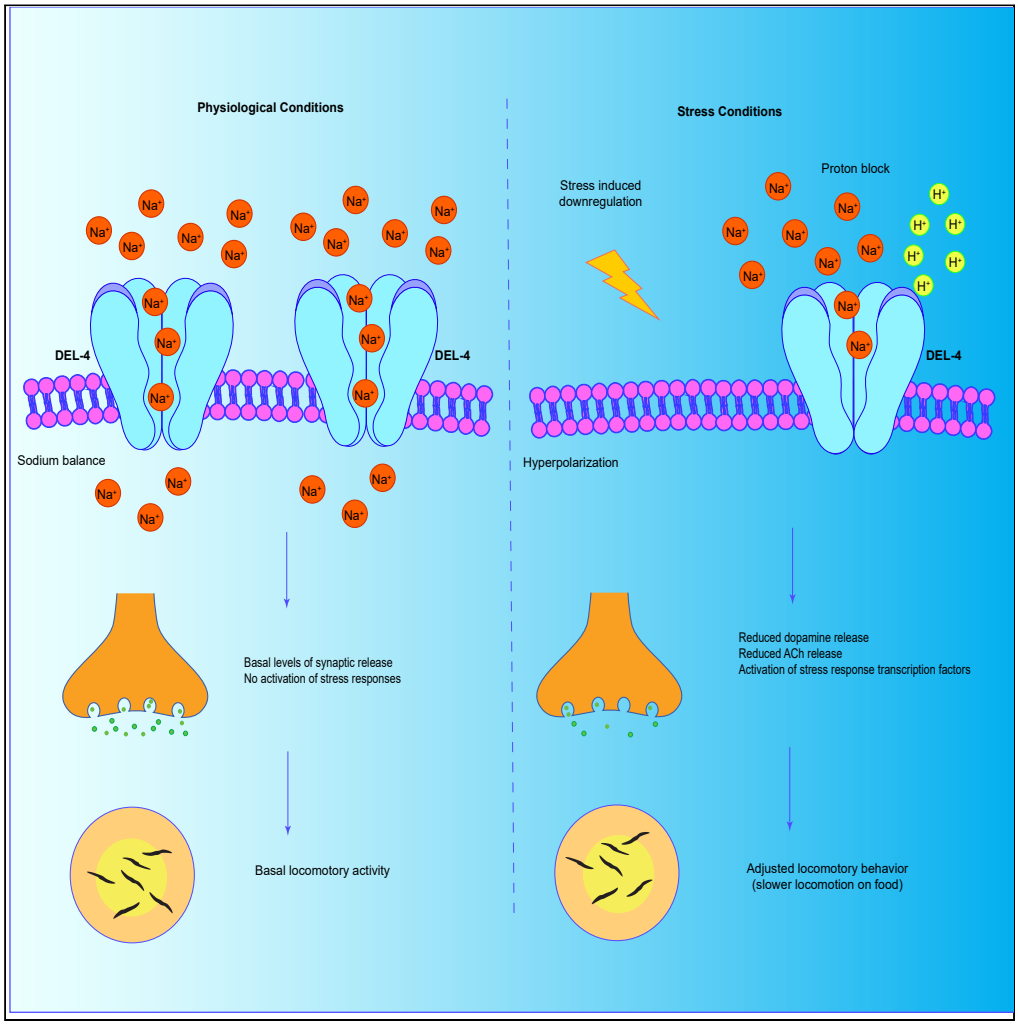

Dionysia Petratou, Martha Gjikolaj, Eva Kaulich, William Schafer, Nektarios Tavernarakis

tavernarakis@imbb.forth.gr

Highlights

The degenerin DEL-4 forms a sodium leak homomeric proton-inhibited channel

DEL-4 regulates neuronal membrane potential and neurotransmission

Heat stress and starvation reduce DEL-4 expression

DEL-4 depletion triggers systemic stress responses and neurodegeneration

Petratou et al., iScience 26, 107117
July 21, 2023
https://doi.org/10.1016/j.isci.2023.107117

iScience

CellPress
OPEN ACCESS

Article

A proton-inhibited DEG/ENaC ion channel maintains neuronal ionstasis and promotes neuronal survival under stress

Dionysia Petratou,[1,2] Martha Gjikolaj,[1,2] Eva Kaulich,[3] William Schafer,[3] and Nektarios Tavernarakis[1,2,4,*]

SUMMARY

The nervous system participates in the initiation and modulation of systemic stress. Ionstasis is of utmost importance for neuronal function. Imbalance in neuronal sodium homeostasis is associated with pathologies of the nervous system. However, the effects of stress on neuronal Na^+ homeostasis, excitability, and survival remain unclear. We report that the DEG/ENaC family member DEL-4 assembles into a proton-inactivated sodium channel. DEL-4 operates at the neuronal membrane and synapse to modulate *Caenorhabditis elegans* locomotion. Heat stress and starvation alter DEL-4 expression, which in turn alters the expression and activity of key stress-response transcription factors and triggers appropriate motor adaptations. Similar to heat stress and starvation, DEL-4 deficiency causes hyperpolarization of dopaminergic neurons and affects neurotransmission. Using humanized models of neurodegenerative diseases in *C. elegans*, we showed that DEL-4 promotes neuronal survival. Our findings provide insights into the molecular mechanisms by which sodium channels promote neuronal function and adaptation under stress.

INTRODUCTION

Physiological stress, perceived by the sensory system, induces cellular stress responses that trigger organismal adaptation. Organisms have adapted to overcome different types of stress that emerge throughout their lives. Organismal homeostasis, behavior, and survival are altered by environmental stresses, such as heat, starvation, hypoxia, and oxidative stress.[1–3] The nervous system is an essential sensor of environmental changes.[4] Stress perception and decision-making for specific behavioral responses occur through adjustments in neuronal activity, plasticity, or signal transduction.[3] Neurons modify their properties and excitation patterns via structural and functional plasticity to convey stressful messages. Functional neuronal plasticity in response to stress is contingent on the regulation of neurotransmitter receptors, transporters, and ion channels. Several studies in mammals have demonstrated the effects of diverse types of stress on neurotransmitter and receptor levels. Gamma-aminobutyric acid (GABA), glutamate, acetylcholine, corticoid, serotonin, and dopamine receptors compose indicative signaling initiators whose expression levels depend on distinct types of stress.[5–9]

Nevertheless, how stressful stimuli are perceived and what molecular modifications modulate excitation and intrinsic neuronal properties are not fully understood. Recent studies have revealed that stress modifies ion channel abundance or activation. In mammals, acute and chronic stress differentially coordinates the expression of voltage-gated potassium channels.[10,11] Activation of AMP-activated protein kinase (AMPK) potentially mediates the effects of acute stress on potassium-conducting channels.[11] In *Drosophila melanogaster*, starvation suppresses KCNQ potassium channel activity via sodium/solute cotransporter-like 5A11.[12] Oxidative stress modulates the expression of calcium-conducting channels.[13,14] Likewise, reactive oxygen species activate the TRP ankyrin1 channel, which acts as an oxidative and nitrative stress sensor.[15] However, the regulation of sodium channels in neuronal cells and their participation in signal transduction in response to stress remain unclear.[16]

Early studies have indicated that neural conduction in the nematode *Caenorhabditis elegans* differs from that in vertebrates.[17] Research on neuronal electrical properties has revealed that several *C. elegans* neurons only generate graded responses. This notion prevailed until the recent discovery that specific

[1]Institute of Molecular Biology and Biotechnology, Foundation for Research and Technology, Heraklion, 70013 Crete, Greece

[2]Department of Basic Sciences, Medical School, University of Crete, Heraklion, 71003 Crete, Greece

[3]Neurobiology Division, MRC Laboratory of Molecular Biology, Cambridge Biomedical Campus, CB2 0QH Cambridge, UK

[4]Lead contact

*Correspondence: tavernarakis@imbb.forth.gr

https://doi.org/10.1016/j.isci.2023.107117

C. elegans sensory neurons may fire action potentials.[18] Nevertheless, the potassium and calcium currents generate both graded and action potentials in *C. elegans*. Classical voltage-gated sodium channels and sodium-dependent potentials have not yet been identified.[19] Despite the lack of voltage-dependent sodium channels, several findings suggest that Na+ currents contribute to neuronal firing in *C. elegans*. Patch-clamp recordings revealed that the absence of extracellular Na+ abolishes action potentials.[20]

Degenerin/epithelial sodium channels (DEG/ENaCs) constitute a large family of voltage-insensitive sodium channels, expressed in the nervous system and epithelial tissues.[21] They have been implicated in several human pathologies, including respiratory syndromes, vascular, cardiac, and neurodegenerative diseases.[22] Few studies have pinpointed their implications in stress responses. In vertebrates, pharmacological inhibition of acid-sensing sodium ion channels (ASICs) (Table S1) reduces stress-associated reactions in behavioral models and exhibits antidepressant-like effects.[23,24] Oxidative stress inhibits the expression of α-ENaC[25,26] and regulates the activation of ASICs.[27,28] SGK1, a Ser-Thr kinase induced by the corticosteroid signaling pathway, modulates the abundance of ENaC and ASIC1 in the plasma membrane.[29–31] Elevation of corticosterone by acute stress causes a protein kinase C (PKC)-dependent increase of ASIC currents in cultured hippocampal neurons.[32,33]

In this study, we sought to delineate the participation of DEG/ENaC family members in stress perception and subsequent integration to modify behavioral responses in animals. We used *C. elegans* as a model organism for its extensively characterized nervous system, exceptional genetic tractability, and significant conservation with mammalian systems. We show that the degenerin-like (DEL) proteins DEL-2, DEL-3, and DEL-4, three members of the degenerin family, are expressed in chemosensory and dopaminergic neurons. DEL-3 and DEL-4 are additionally expressed in serotonergic, with DEL-4 also expressed in cholinergic motor neurons. The dopamine-mediated basal slowing response revealed that DEL-4 affects dopaminergic signaling. Interestingly, we found that DEL-4 forms a proton-blocked homomeric amiloride-sensitive sodium channel. Using reverse genetics, pharmacological analysis, and imaging techniques, we provide evidence that DEL-4 is regulated by specific types of stress and contributes to the adaptation of neuronal signaling to modify the locomotory rate of the animal. Analysis of neurodegenerative disease models revealed the neuroprotective properties of DEL-4. Discerning the neuronal mechanisms that drive the effects of stress on sensory integration and neuronal cohesion will provide valuable insights into how stress advances the progression of neurodegenerative diseases and may provide new pharmaceutical targets.

RESULTS

Localization pattern of degenerins DEL-2, DEL-3, and DEL-4

The degenerin DEG/ENaC subfamily of *C. elegans* comprises approximately 30 members. We focused on the three members, DEL-2, DEL-3, and DEL-4, previously identified in a serial analysis of gene expression to localize in ASE neurons, the primary set of gustatory neurons in *C. elegans*.[34]

To determine the expression patterns of these three degenerins, we generated transcriptional reporters (STAR Methods, Table 2). Epifluorescence imaging revealed that all three DELs were localized to the head, midbody, and tail neurons (Figures 1, S1A and S2). To identify neurons that express DEL-2, DEL-3, and DEL-4, we crossed their transcriptional reporters with several neuron-specific fluorescent markers, specifically for sensory, dopaminergic, serotonergic, and cholinergic motor neurons (Table 1, S2 and S3). We verified the expression of these three channels in ASE neurons, as previously described,[34] using a transcriptional reporter of FLP-8 (Figure 1). Further analysis revealed that DEL-2 localizes in the amphids ASH and ASI (apart from ASE), phasmids PHA and PHB, and dopaminergic neurons CEPDL/R (Figures 1A and S2A). DEL-3 is present in the chemosensory neurons ASE, PHA, PHB, and PHC, in most dopaminergic neurons (CEPDL/R, CEPVL, ADEL, and PDE), and in the serotonergic neurons NSML/R (Figures 1B and S2B). DEL-4 displayed broad expression. It localizes at the chemosensory neurons ASE, ASI, ASH, and PHA, in all dopaminergic neurons (CEPDL/R, CEPVL/R, ADEL/R, and PDE) and the serotonergic neuron NSMR (Figures 1C and S2C). Moreover, DEL-4 subsists in cholinergic motor neurons VA/B, DA/B, and mechanosensory PVM neurons (Figures 1C and S2C). Additionally, we looked at the CenGen data for neurons identified to express DEL-2, DEL-3, and DEL-4. Indeed, some of the neurons that we propose that express DELs coincide with those identified in the CenGen (Key Resources Table - KRT), specifically, the DEL-2 expression in the neurons ASH, ASE, ASI, PHB, and CEP and the DEL-3 expression in the neurons CEP, ADE,

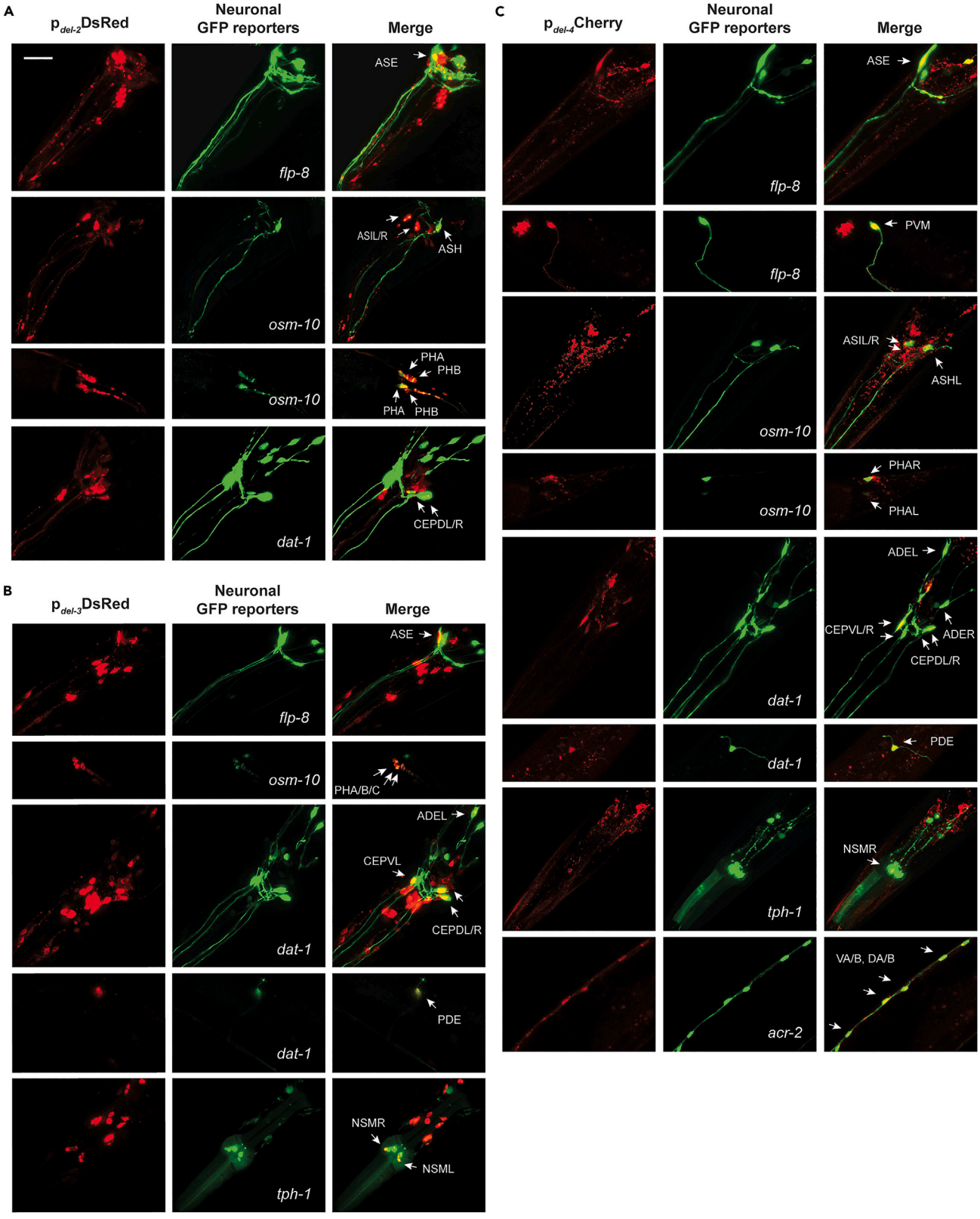
A
p del-2 DsRed
Neuronal GFP reporters
Merge
ASE
flp-8
ASIL/R
ASH
osm-10
PHA
PHB
PHA PHB
osm-10
dat-1
CEPDL/R
B
p del-3 DsRed
Neuronal GFP reporters
Merge
ASE
flp-8
osm-10
PHA/B/C
ADEL
CEPVL
CEPDL/R
dat-1
dat-1
PDE
tph-1
NSML
NSMR
C
p del-4 Cherry
Neuronal GFP reporters
Merge
ASE
flp-8
PVM
flp-8
ASIL/R
ASHL
osm-10
PHAR
PHAL
osm-10
ADEL
CEPVL/R
ADER
CEPDL/R
dat-1
dat-1
PDE
NSMR
tph-1
VA/B, DA/B
acr-2

Figure 1. Neuronal expression of DEL-2, DEL-3, and DEL-4

(A) Expression of DEL-2 in the chemosensory neurons ASE, ASH, ASI, PHA, and PHB and in the set of dopaminergic neurons CEPDL/R in the head (Tables S2 and S3).

(B) Expression of DEL-3 in the chemosensory neurons ASE, PHA, PHB, and PHC, in the dopaminergic neurons CEPDL/R, CEPVL, ADEL, and PDE in the head and midbody, and the serotonergic neurons NSMR/L (Tables S2 and S3).

(C) Identification of DEL-4 expression in the chemosensory neurons ASE, ASI, ASH, and PHA, in the mechanosensory neuron PVM, in all six dopaminergic neurons CEPDL/R, CEPVL/R, ADEL/R in the head, and PDE in the midbody, in the serotonergic neuron NSMR and cholinergic motor neurons VA/B and DA/B (Tables S2 and S3). (A–C) Confocal images at 40x lens (maximum intensity projections) of strains that were generated by crossing *del-2, del-3*, or *del-4* transcriptional reporters (red – left column) with the respective neuronal reporters (green – middle column). Left columns: *del-2*, *del-3*, and *del-4* promoters drive the expression of mCherry or dsRed in the nervous system. Middle columns: transcriptional GFP neuronal reporters are shown in green. Promoters of *flp-8* and *osm-10* drive expression in the sensory neurons ASE, URX, PVM, and ASH, ASI, PHA, and PHB, respectively. The promoter of *dat-1* drives expression of GFP in the dopaminergic neurons (CEPD, CEPV, ADE, and PDE), the *tph-1* promoter in the serotonergic neurons (NSM and ADF), and the *acr-2* promoter in the cholinergic motor neurons (VA/B and DA/B) (Tables S2 and S3). (right columns) The right column of each panel corresponds to merged images. We utilized the merged images of z-stacks to assess colocalization (see also Figure S2). One day adult animals. Arrows indicate neuronal cell somas where mCherry or dsRed is co-expressed with GFP (left is anterior). Scale bar 20 μM. See also Figure S2.

PDE, and NSM. Therefore, we conclude that DEL-2, DEL-3, and DEL-4 show a neuronal localization pattern, which in the case of DEL-4 expands from sensory to motor neurons.

DEL-4 exhibits high similarity to human ENaCs and ASICs (ENaC1b and ASIC1b), as identified by protein BLAST (see Methods section). *In silico* analysis using the tool Phobius of the Stockholm Bioinformatics Center (http://phobius.sbc.su.se/)[35] predicted that DEL-4 shares a topology analogous to that of the rest of the DEG/ENaC family members (Figure S1B, green, yellow, red, and orange boxes). It adopts a characteristic structural model consisting of two transmembrane domains, two small intracellular regions at the N- and C-terminus, and one large extracellular loop. The broader expression pattern of DEL-4 both in sensory and motor neurons together with its similarity to human ENaCs and ASICs led us to focus our study on DEL-4 as a putative regulator of neuronal ionstasis, and further examined its role in regulation of stress response.

DEL-4 downregulation simulates a stress-like state

To investigate the possible effects of stress on DEL-4 ion channel, we measured its expression under various types of stress (Figures 2 and S3). Heat stress and long-term starvation reduced DEL-4 levels (Figures 2A, 2E, S3F and S3G). In contrast, oxidative stress, ER, and acidic pH stress did not affect them (Figures 2B–2E). These finding suggest that heat stress (HS) and long-term starvation can modulate DEL-4-mediated signaling.

Heat shock transcription factor 1 (HSF-1) is the homolog of the mammalian HSF1 and master regulator of heat shock response.[36–38] Interestingly, heat stress in the absence of *hsf-1* further reduces *del-4* expression (Figures 2E–2G). This implies that *del-4* suppression upon HS is not HSF-1 dependent; however, the presence of HSF-1 ameliorates DEL-4 depletion upon HS. Consistently, *in silico* analysis revealed the presence of HSF-1 binding sites in *del-4* promoter region (Figures S1B and S1C). Since heat stress curtailed the abundance of DEL-4 in the neuronal cell membrane, we hypothesized that the null *del-4* mutant (Figure S1D) where DEL-4 is permanently absent would experience sustained stress. Indeed, alleviation of DEL-4 resulted in a statistically significant increase of HSF-1 protein levels throughout the whole-body (Figure 2G) and hypodermis nuclei (Figures 2H, S4A and S4I). HSP-16.2 expression levels, directly regulated by HSF-1, are also increased in *del-4* mutant background (Figures 2I, S4B and S4I). To further verify the activation of HSF-1 in the absence of *del-4*, we tested the thermotolerance of *del-4* mutants and overexpressing animals. As predicted, *del-4* mutants were HS resistant as they survived longer than wild type (wt) after HS, while DEL-4-overexpressing animals were sensitive to thermal stress (Figure 2J). These findings underline the role of DEL-4 in the regulation of heat shock response.

As mentioned previously, long-term starvation depletes DEL-4 protein levels (Figures 2A and 2E). DAF-16, the homolog of mammalian FOXO, is a key transcription factor activated in response to starvation. Upon starvation, DAF-16 translocates to the nucleus to promote metabolic adaptations necessary for resistance to stress.[39] Nonetheless, long-term starvation reduces DAF-16 expression and triggers its translocation back to the cytoplasm in an AGE-1/PI3K-dependent manner.[40] We found that downregulation of *del-4* reduced DAF-16 protein levels in the whole body (Figures 3A and 3K) and decreased the nucleus/cytoplasm ratio of DAF-16 (Figures 3B, 3K, S4C and S4I), mimicking the response to long-term starvation. We also observed a reduction in the expression of a well-established DAF-16-target gene, namely

Table 1. *C. elegans* strains and lines used in this study

REAGENT or RESOURCE	SOURCE	IDENTIFIER
Experimental model: *C. elegans* Strains		
Wild type: Bristol (N2) isolate	*Caenorhabditis* Genetics Center	RRID: WB-STRAIN: WBStrain00000001; WormBase ID: WBStrain00000001
$p_{del\text{-}2}$DsRed: *unc-119(ed3)*;Ex[$p_{del\text{-}2}$DEL-$2_{1\text{-}27}$::DsRed; *unc-119*(+)]	This paper	N/A
$p_{del\text{-}3}$DsRed: *unc-119(ed3)*;Ex[$p_{del\text{-}3}$DEL-$3_{1\text{-}45}$::DsRed; *unc-119*(+)]	This paper	N/A
$p_{del\text{-}4}$Cherry: *unc-119(ed3)*;Ex[$p_{del\text{-}4}$DEL-$4_{1\text{-}36}$::mCherry; *unc-119*(+)]	This paper	N/A
$p_{osm\text{-}10}$GFP: HA3 nuls11[osm-10::GFP + *lin-15*(+)]	*Caenorhabditis* Genetics Center	RRID: WB-STRAIN: WBStrain00008277; WormBase ID: WBStrain00008277
$p_{flp\text{-}8}$GFP: NY2078 ynls78[flp-8p::GFP]	*Caenorhabditis* Genetics Center	RRID: WB-STRAIN:WBStrain00029169; WormBase ID: WBStrain00029169
$p_{dat\text{-}1}$GFP: BZ555 egls1[$p_{dat\text{-}1}$GFP]	*Caenorhabditis* Genetics Center	RRID: WB-STRAIN:WBStrain00004039; WormBase ID: WBStrain00004039
$p_{tph\text{-}1}$GFP: GR1366 mgls42 [tph-1::GFP + *rol-6(su1006)*]	*Caenorhabditis* Genetics Center	RRID: WB-STRAIN:WBStrain00007909; WormBase ID: WBStrain00007909
$p_{acr\text{-}2}$GFP: CZ631 juls14[acr-2p::GFP + lin-15(+)]	*Caenorhabditis* Genetics Center	RRID:WB-STRAIN:WBStrain00005354; WormBase ID: WBStrain00005354
$p_{del\text{-}2}$DsRed; $p_{flp\text{-}8}$GFP: *unc-119(ed3)*;Ex[$p_{del\text{-}2}$ DEL-$2_{1\text{-}27}$::DsRed; $p_{flp\text{-}8}$GFP;*unc-119*(+)]	This paper	N/A
$p_{del\text{-}2}$DsRed; $p_{osm\text{-}10}$GFP: *unc-119(ed3)*;Ex[$p_{del\text{-}2}$ DEL-$2_{1\text{-}27}$::DsRed; OSM-10:: GFP;*unc-119*(+)]	This paper	N/A
$p_{del\text{-}2}$DsRed; $p_{dat\text{-}1}$GFP: *unc-119(ed3)*;Ex[$p_{del\text{-}2}$ DEL-$2_{1\text{-}27}$::DsRed; $p_{dat\text{-}1}$GFP;*unc-119*(+)]	This paper	N/A
$p_{del\text{-}3}$DsRed; $p_{flp\text{-}8}$GFP: *unc-119(ed3)*;Ex[$p_{del\text{-}3}$ DEL-$3_{1\text{-}45}$::DsRed; $p_{flp\text{-}8}$GFP;*unc-119*(+)]	This paper	N/A
$p_{del\text{-}3}$DsRed; $p_{osm\text{-}10}$GFP: *unc-119(ed3)*;Ex[$p_{del\text{-}3}$ DEL-$3_{1\text{-}45}$::DsRed; OSM-10:: GFP;*unc-119*(+)]	This paper	N/A
$p_{del\text{-}3}$DsRed; $p_{dat\text{-}1}$GFP: *unc-119(ed3)*;Ex[$p_{del\text{-}3}$ DEL-$3_{1\text{-}45}$::DsRed; $p_{dat\text{-}1}$GFP;*unc-119*(+)]	This paper	N/A
$p_{del\text{-}3}$DsRed; $p_{tph\text{-}1}$GFP: *unc-119(ed3)*;Ex[$p_{del\text{-}3}$ DEL-$3_{1\text{-}45}$::DsRed;TPH-1::GFP;*unc-119*(+); *rol-6(su1006)*]	This paper	N/A
$p_{del\text{-}4}$Cherry; $p_{flp\text{-}8}$GFP: *unc-119(ed3)*;Ex[$p_{del\text{-}4}$ DEL-$4_{1\text{-}36}$::mCherry; $p_{flp\text{-}8}$GFP;*unc-119*(+)]	This paper	N/A
$p_{del\text{-}4}$Cherry; $p_{osm\text{-}10}$GFP: *unc-119(ed3)*;Ex[$p_{del\text{-}4}$ DEL-$4_{1\text{-}36}$::mCherry; OSM-10::GFP;*unc-119*(+)]	This paper	N/A
$p_{del\text{-}4}$Cherry; $p_{dat\text{-}1}$GFP: *unc119(ed3)*; Ex[p_{del4} $DEL4_{1\text{-}36}$::mCherry; p_{dat1}GFP;*unc-119*(+)]	This paper	N/A
$p_{del\text{-}4}$Cherry; $p_{tph\text{-}1}$GFP: *unc119(ed3)*; Ex[p_{del4} $DEL4_{1\text{-}36}$::mCherry; TPH1::GFP;*unc-119*(+); *rol-6(su1006)*]	This paper	N/A
$p_{del\text{-}4}$Cherry; $p_{acr\text{-}2}$GFP: *unc-119(ed3)*;Ex[$p_{del\text{-}4}$ DEL-$4_{1\text{-}36}$::mCherry; $p_{acr\text{-}2}$GFP; *unc-119*(+)]	This paper	N/A

(*Continued on next page*)

Table 1. *Continued*

REAGENT or RESOURCE	SOURCE	IDENTIFIER
del-4 mutant: T28B8.5 *del-4(tm717)*	National Bioresource Project, Japan	WormBase ID: WBVar00250586
DEL-2::mCherry: *unc-119(ed3)*;Ex[p_{del-2} DEL-2::mCherry; *unc-119*(+)]	This paper	N/A
DEL-3::DsRed: *unc-119(ed3)*;Ex[p_{del-3} DEL-3::DsRed; *unc-119*(+)]	This paper	N/A
DEL-4::DsRed: *unc-119(ed3)*;Ex[p_{del-4} DEL-4::DsRed; *unc-119*(+)]	This paper	N/A
DEL-4::GFP: *unc-119(ed3)*;Ex[p_{del-4} DEL-4::GFP;*unc-119*(+)]	This paper	N/A
DEL-4::DsRed: N2; Ex [p_{del-4} DEL-4::DsRed; *rol-6(su1006)*]	This paper	N/A
dop-1(vs100): LX645 *dop-1(vs100)*	*Caenorhabditis* Genetics Center	RRID:WB-STRAIN:WBStrain00026369; WormBase ID: WBStrain00026369
dop-2(vs105): LX702 *dop-2(vs105)*	*Caenorhabditis* Genetics Center	WB-STRAIN:WBStrain00026373; WormBase ID: WBStrain00026373
dop-3(vs106): LX703 *dop-3(vs106)*	*Caenorhabditis* Genetics Center	RRID:WB-STRAIN:WBStrain00026374; WormBase ID: WBStrain00026374
pkc-1(ok563): RB781 *pkc-1(ok563)*	*Caenorhabditis* Genetics Center	RRID:WB-STRAIN:WBStrain00031494; WormBase ID: WBStrain00031494
pkc-2 (ok328): VC127 *pkc-2 (ok328)*	*Caenorhabditis* Genetics Center	RRID:WB-STRAIN:WBStrain00035524; WormBase ID: WBStrain00035524
tpa-1 (k501): MJ500 *tpa-1 (k501)*	*Caenorhabditis* Genetics Center	RRID:WB-STRAIN:WBStrain00026559; WormBase ID: WBStrain00026559
kin-2(ce179): KG532 *kin-2(ce179)*	*Caenorhabditis* Genetics Center	RRID:WB-STRAIN:WBStrain00023482; WormBase ID: WBStrain00023482
unc-43(tm1605): K11E8.1 *unc-43(tm1605)*	National Bioresource Project, Japan	WormBase ID: WBVar00250586
del-4(tm717);dop-1(vs100)	This paper	N/A
del-4(tm717);dop-2(vs105)	This paper	N/A
del-4(tm717);dop-3(vs106)	This paper	N/A
del-4(tm717);pkc-1(ok563)	This paper	N/A
del-4(tm717);pkc-2 (ok328)	This paper	N/A
del-4(tm717);tpa-1 (k501)	This paper	N/A
del-4(tm717);kin-2(ce179)	This paper	N/A
del-4(tm717);unc-43(tm1605)	This paper	N/A
$p_{hsp-16.2}$GFP: TJ375 gpIs1 [*hsp-16.2*p::GFP]	*Caenorhabditis* Genetics Center	RRID:WB-STRAIN:WBStrain00034895; WormBase ID: WBStrain00034895
p_{sod-3}GFP: CF1553 muIs84 [(pAD76) sod-3p::GFP) + *rol-6(su1006)*]	*Caenorhabditis* Genetics Center	RRID:WB-STRAIN:WBStrain0000486; WormBase ID: WBStrain00004861
p_{gst-4}GFP: CL2166 dvIs19 [(pAF15) gst-4p::GFP::NLS)]	*Caenorhabditis* Genetics Center	RRID:WB-STRAIN:WBStrain00005102; WormBase ID: WBStrain00005102
p_{hsp-4}GFP: SJ4005 zcls4 [*hsp-4*::GFP]	*Caenorhabditis* Genetics Center	RRID:WB-STRAIN:WBStrain00007694; WormBase ID:WBStrain00007694
hsf-1(sy441): PS3551 *hsf-1(sy441)*	*Caenorhabditis* Genetics Center	RRID:WB-STRAIN:WBStrain00007673; WormBase ID:WBStrain00007673
daf-16(mu86): CF1038 *daf-16(mu86)*	*Caenorhabditis* Genetics Center	RRID:WB-STRAIN:WBStrain00007210; WormBase ID: WBStrain00007210

(*Continued on next page*)

Table 1. *Continued*

REAGENT or RESOURCE	SOURCE	IDENTIFIER
p_{hsf-1}HSF-1::GFP: *EQ87* iqIs28 *[pAH71 P*hsf-1::hsf-1::gfp*; pRF4* rol-6 (su1006)*]*	Ao-Lin Hsu (University of Michigan, USA)	N/A
p_{daf-16}DAF-16::GFP: p_{daf-16}DAF-16(d/f/h)::GFP	Tibor Vellai (Eötvös Loránd University, Budapest)	N/A
p_{skn-1}SKN-1::GFP: LD1008 ldEx9 [skn-1(operon)::GFP + rol-6(su1006)	*Caenorhabditis* Genetics Center	RRID:WB-STRAIN:WBStrain00024127; WormBase ID: WBStrain00024127
p_{skn-1}SKN-$1^{B/C}$::GFP: LD1 ldIs7 [skn-1b/c::GFP + rol-6(su1006)]	*Caenorhabditis* Genetics Center	RRID:WB-STRAIN:WBStrain00024125; WormBase ID: WBStrain00024125
$p_{let-858}$GCaMP2.0: IR1155 N2; Ex[$P_{let-858}$GCaMP2.0; *rol-6(su1006)*]	This paper	Palikaras et al., 2015
p_{aak-2}AAK-2::Tomato: AGD383 uthls202 [aak-2(intron1)::aak-2(aa1-aa321)::Tomato:: unc-54 3'UTR + *rol-6(su1006)*]	*Caenorhabditis* Genetics Center	RRID:WB-STRAIN:WBStrain0000009; WormBase ID: WBStrain00000095
del-4(tm717); p_{hsp-4}GFP: *del-4(tm717)*; zcls4[p_{hsp-4}GFP]	This paper	N/A
del-4(tm717); p_{aak-2}AAK-2::Tomato: *del-4(tm717)*; uthls202[aak-2(intron1):: aak-2(aa1-aa321)::Tomato::unc-54 3'UTR ; *rol-6(su1006)]*	This paper	N/A
del-4(tm717);p_{skn-1}SKN-$1^{B/C}$::GFP: *del-4(tm717)*; ldIs7 [skn-1b/c::GFP + rol-6(su1006)]	This paper	N/A
p_{asic-1}SNB-1::SEpHluorin: IR723 N2; Ex [p_{asic-1} SNB-1::SEpHluorin; *rol-6(su1006)*]	Voglis et al.[77]	N/A
del-4(tm717); p_{asic-1}SNB-1::SEpHluorin: *del-4 (tm717)*; N2; Ex [p_{asic-1}SNB-1::SEpHluorin; *rol-6(su1006)*]	This paper	N/A
p_{acr-2}SNB-1::SEpHluorin: KP3085 nuls122 [p_{acr-2}::pHluorin:: SNB-1; p_{myo-2}DsRed]	*Caenorhabditis* Genetics Center	WormBase ID: WBStrain00047338
goa-1(sa734): DG1856 *goa-1(sa734)*	*Caenorhabditis* Genetics Center	RRID: WB-STRAIN:WBStrain00022814
unc-49(e407): CB407 *unc-49(e407)*	*Caenorhabditis* Genetics Center	WormBase ID: WBStrain00004164
DEL-4::GFP;p_{del-4}SNB-1::DsRed: *unc-119(ed3)*;Ex[p_{del-4} DEL-4::GFP;p_{del-4}SNB-1::DsRed ;*unc-119*(+)]	This paper	N/A
GFP::SNB-1: EG8244 [*unc-119(ed3)*; oxSi834 [P_{unc-47} GFP::SNB-1::*unc-54* UTR; *unc-119*(+)]	E. Jorgensen (University of UTAH, Salt Lake City); Nonet et al.[95]	N/A
NLP-21::YFP: KP3947 nuls183 [p_{unc129}NLP-21:: Venus + p_{myo-2}NLS::GFP]	*Caenorhabditis* Genetics Center	RRID:WB-STRAIN:WBStrain00023636; WormBase ID: WBStrain00023636
del-4(tm717); GFP::SNB-1: *del-4(tm717)*; [*unc-119(ed3)*; oxSi834[P_{unc-47}GFP::SNB-::unc-54 UTR; *unc-119*(+)]	This paper	N/A
del-4(tm717); NLP-21::YFP: nuls183 [p_{unc129}NLP-21:: Venus; p_{myo-2}NLS::GFP]	This paper	N/A
p_{dat-1}ASAP-1:N2; Ex [p_{dat-1}ASAP-1; *rol-6(su1006)*]	This paper	N/A
del-4(tm717); p_{dat-1}ASAP-1: *del-4(tm717)*; p_{dat-1} ASAP-1; *rol-6(su1006)*]	This paper	N/A
del-4(tm717); p_{dat-1}GFP: *del-4(tm717)*; egls1[p_{dat-1}GFP]	This paper	N/A
DEL-4::DsRed; p_{dat-1}GFP: p_{del-4} DEL-4:: DsRed; egls1 [p_{dat-1}GFP]; *rol-6(su1006)*	This paper	N/A

(*Continued on next page*)

Table 1. *Continued*

REAGENT or RESOURCE	SOURCE	IDENTIFIER
BR5270: BR5270 byIs161 [p_{rab-3}F3(delta) K280 + p_{myo-2}mCherry]	*Caenorhabditis* Genetics Center	RRID:WB-STRAIN:WBStrain00003901; WormBase ID: WBStrain00003901
BR5270; p_{dat-1}GFP: byIs161 [p_{rab-3}F3(delta) K280 + p_{myo-2}mCherry]; egIs1 [p_{dat-1}GFP]	This paper	N/A
del-4(tm717);BR5270; p_{dat-1}GFP: *del-4(tm717)*; byIs161 [p_{rab-3}F3(delta)K280 + p_{myo-2}mCherry]; egIs1 [p_{dat-1}GFP]	This paper	N/A
DEL-4::DsRed; BR5270; p_{dat-1}GFP: p_{del-4} DEL-4::DsRed; *rol-6(su1006)*; byIs161 [p_{rab-3}F3(delta)K280 + p_{myo-2}mCherry]; egIs1 [p_{dat-1}GFP]	This paper	N/A
UA44: UA44 baIn11[p_{dat-1}a-Synuclein; p_{dat-1}GFP]	Guy Caldwell (University of Alabama, AL, USA); Sanjib Guha et al.[96]	RRID:WB-STRAIN:WBStrain00035179; WormBase ID: WBStrain00035179
del-4(tm717); UA44: *del-4(tm717)*; baIn11 [p_{dat-1}::a-Synuclein; p_{dat-1}GFP]	This paper	N/A
DEL-4:: DsRed; UA44: p_{del-4}DEL-4:: DsRed; *rol-6(su1006)*; baIn11[p_{dat-1}a-Synuclein; p_{dat-1}GFP]	This paper	N/A
che-2 (e1033): CB1033 *che-2 (e1033)*	*Caenorhabditis* Genetics Center	RRID:WB-STRAIN:WBStrain00004231; WormBase ID: WB-STRAIN:WBStrain00004231
dat-1(tm903)	National Bioresource Project, Japan	WormBase ID: WBVar00249925
del-4(tm717) rescue: *del-4(tm717)*; Ex [p_{del-4}DEL-4,p_{myo-2}] (rescue)	This paper	N/A
cat-2(e1112): *CB1112 cat-2(e1112)*	*Caenorhabditis* Genetics Center	RRID:WB-STRAIN:WBStrain00004246; WormBase ID: WBStrain00004246
del-4(tm717); $p_{hsp-16.2}$GFP: *del-4(tm717)*; TJ375 gpIs1 [*hsp-16.2*p::GFP]	This paper	N/A
del-4(tm717); p_{gst-4}GFP: *del-4(tm717)*; dvIs19 [(pAF15) gst-4p::GFP::NLS)]	This paper	N/A
del-4(tm717); p_{sod-3}GFP: *del-4(tm717)*; muIs84 [(pAD76) sod-3p::GFP) + *rol-6(su1006)*]	This paper	N/A
del-4(tm717); $P_{let-858}$GCaMP2.0: *del-4(tm717)*; $P_{let-858}$GCaMP2.0; *rol-6(su1006)*	This paper	N/A

sod-3, upon *del-4* suppression (Figures 3C, 3K, S4D and S4I). L1 larvae required DAF-16 activation and nuclear translocation to enter into starvation-induced diapause and endure starvation.[40,41] Since *del-4* downregulation reduced DAF-16 levels and activity, we hypothesized that arrested L1 survival would be reduced in a *del-4* mutant background. In accordance with our hypothesis, we discovered that *del-4* mutants were more sensitive to long-term starvation compared to wt (Figure 3D), while DEL-4-overexpressing animals were more resistant corroborating the notion that DEL-4 is required for an intact response to prolonged starvation.

To determine whether DEL-4 deficiency triggers other types of metabolic stress responses, we assessed the activation of the ER unfolded protein response (ER^{UPR}) and oxidative stress response in the *del-4* mutant background. We observed that depletion of DEL-4 upregulated *hsp-4*, a well-established target of ER^{UPR} and a homolog of the mammalian BiP (Figures 3E, 3K, S4E and S4I). ER stress triggers cytosolic Ca^{2+} release from the sarco-endoplasmic reticulum which in turn induces Ca^{2+}-calmodulin protein kinase β-dependent AMPK activation (Arias-Del-Val et al., 2019).[42] To determine whether DEL-4 is a mediator of this pathway, we suppressed *del-4* in animals carrying the genetically encoded calcium indicator GCaMP2.0 expressed throughout the body ($p_{let-858}$GCaMP2.0) or an AMPK translational reporter (p_{aak-2}AAK-2::Tomato). In both cases, the reduction or absence of DEL-4 induced a systemic increase in the cytoplasmic calcium and AMPK levels (Figures 3F, 3G, 3K, S4F, S4G and S4I).

Table 2. Oligonucleotides used in this study

REAGENT or RESOURCE	SOURCE	IDENTIFIER
Oligonucleotides		
Primer for the *del-4(tm717)* variation (Forward): 5′-AAAAGTGTGGACCCGGATAT-3′	This paper	N/A
Primer for the *del-4(tm717)* variation (Reverse): 5′-AAAAGTGTGGACCCGGATAT-3′	This paper	N/A
Primer for the *del-3(tm5642)* variation (Forward): 5′-ATGTGGCTCCGAGGACTTTTC-3′	This paper	N/A
Primer for the *del-3(tm5642)* variation (Reverse): 5′- GCAATCAGACACCACACCCAGTA-3′	This paper	N/A
Primer for the *dop-1(vs100)* variation (Forward): TGTGCTGAAATGAACGAATGAGAC	This paper	N/A
Primer for the *dop-1(vs100)* variation (Reverse): TCGGATCATTCAAGTCCCGTC	This paper	N/A
Primer for the *dop-2(vs105)* variation (Forward): AACGATTCCTTGCGATTCTGG	This paper	N/A
Primer for the *dop-2(vs105)* variation (Reverse): AACCATAAATCTGTGTGAGCAAAGC	This paper	N/A
Primer for the *dop-3(vs106)* variation (Forward): TGTGGGCACCTCATTCACTGG	This paper	N/A
Primer for the *dop-3(vs106)* variation (Reverse): ACCGCGCTGAACCAAAGTATG	This paper	N/A
Primer for the *pkc-1(ok563)* variation (Forward): TTGAGCGTGCTCGGGTCC	This paper	N/A
Primer for the *pkc-1(ok563)* variation (Reverse): ACCTTCCACGTTTGTTCCGTG	This paper	N/A
Primer for the *pkc-2(ok328)* variation (Forward): ACTTGCGACGTCGAATTTGTAGG	This paper	N/A
Primer for the *pkc-2(ok328)* variation (Reverse): CCATAAGCCCACCAATCCACAG	This paper	N/A
Primer for the *tpa-1(k501)* variation (Forward): CGCCATTGGTGCTAACATGAC	This paper	N/A
Primer for the *tpa-1(k501)* variation (Reverse): CCGACGAGCATTTCATACATCAA	This paper	N/A
Primer for the *kin-2(ce 179)* variation (Forward): AATAGCAGAGGGTCAGTAATTGACTG	This paper	N/A
Primer for the *kin-2(ce179)* variation (Reverse): AGTACGGATAAGCTCTTAGAGAGAAGC	This paper	N/A
Primer for the *unc-43(tm1605)* variation (Forward): TAAACTACTGCCATCAGCGTGG	This paper	N/A
Primer for the *unc-43(tm1605)* variation (Reverse): CCAAATTTTCTCATTCGCGC	This paper	N/A
Primer for *del-4* (exons 1-10) (Forward): 5′-GATGGGTGTATTTTGGACCG-3′	This paper	N/A
Primer for *del-4* (exons 1-10) (Reverse): 5′-TCAAGACACGATTCTCCTGA-3′	This paper	N/A
Primer for *del-2* transcriptional reporter (Forward): 5′-TCTTATGATGCACGGCG-3′	This paper	N/A
Primer for *del-2* transcriptional reporter (Reverse): 5′-GGTACCCGTCCACTATTAGTAAT-3′	This paper	N/A

(*Continued on next page*)

Table 2. *Continued*

REAGENT or RESOURCE	SOURCE	IDENTIFIER
Primer for *del-3* transcriptional reporter (Forward): 5′-5′-GCATGCTTACATTTGAGGGTTTAG-3′	This paper	N/A
Primer for *del-3* transcriptional reporter (Reverse): 5′-ACCGGTGTTTTCGATTCAGTTTT-3′	This paper	N/A
Primer for *del-4* transcriptional reporter (Forward): 5′-CTGCAGGTCGACACATCATAAATC-3′	This paper	N/A
Primer for *del-4* transcriptional reporter (Reverse): 5′-ACCGGTCCTCAACCATCGAGCATTT-3′	This paper	N/A
Primer for *del-2* translational reporter with mCherry (exons 5-11) (Forward): 5′-CTGCAGGATTTCTCTGTCAAGTGG-3′	This paper	N/A
Primer for *del-2* translational reporter with mCherry (exons 5-11) (Reverse): 5′-ACCGGTCATATTGTCAGGCAAGTT-3′	This paper	N/A
Primer for *del-2* translational reporter with mCherry (exons 2-4) (Forward): 5′-CTGCAGAGTTGATGATGATTAAAGAA-3′	This paper	N/A
Primer for *del-2* translational reporter with mCherry (exons 2-4) (Reverse): 5′-CTGCAGTGAAAATGCTCAAACAAA-3′	This paper	N/A
Primer for del-3 translational reporter (exons 2-7) (Forward): 5′-ACCGGTTGTTCACGATGATCAACTATT-3′	This paper	N/A
Primer for del-3 translational reporter (exons 2-7) (Reverse): 5′- ACCGGTGGTGTGTCTCCTGAAGCTA-3′	This paper	N/A
Primer for del-4 translational reporter with GFP (promoter and CDS) (Forward): 5′-ACGCGTCGACACATCATAAATCTCCACCCAC-3′	This paper	N/A
Primer for del-4 translational reporter with GFP (promoter and CDS) (Reverse): 5′-CGGGGTACCCCATCATTAGAATGAGGCTTTGG-3′	This paper	N/A
Primer for SNB-1 coding gene (Forward): 5′-CGG GGTACCGAA TTCGGACGCTCAAGGAGATGCCGGC-3′	This paper	N/A
Primer for SNB-1 coding gene (Reverse): 5′-CGGGGTACCGAA TTCTTTTCCTCCAGCCCATAAAACG-3′	This paper	N/A
Primer for *del-4* promoter (Forward): 5′-CTGCAGGTCGA CACATCATAAATC-3′	This paper	N/A
Primer for *del-4* promoter (Reverse): 5′-GGATCCCATCTG CAATTTTATTTT-3′	This paper	N/A
Primer for ASAP1 voltage indicator (Forward): 5′-TAGCCG CCACCATGGAGAC-3′	This paper	N/A
Primer for ASAP1 voltage indicator (Reverse): 5′- AGATCTT TCATTAGGTTACCACTTCAAG -3′	This paper	N/A
Primer for *dat-1* promoter (Forward): 5′-CTGCAGATCCAT GAAATGGAACTTGA-3′	This paper	N/A
Primer for *dat-1* promoter (Reverse): 5′-GGATCCGGCTAAAAATTGTTGAG-3′	This paper	N/A
Primer for *del-4* cDNA for RTPCR (Forward): 5′-ATGACATGGTTGTTAGTTGCACG-3′	This paper	N/A
Primer for *del-4* cDNA for RTPCR (Reverse): GTGCAAAGTAACCGAATACATCAG	This paper	N/A
Primer for pmp-3 cDNA for RTPCR (Forward): 5′- ATGATAAATCAGCGTCCCGAC-3′	This paper	N/A
Primer for pmp-3 cDNA for RTPCR (Reverse): 5′- TTGCAACGAGAGCAACTGAAC -3′	This paper	N/A
Primer for KSM vector (Forward): 5′-AGATCTGGTTACCACTAAACCAGCC-3′	This paper	N/A
Primer for KSM vector (Reverse): 5′-TGCAGGAATTCGATATCAAGCTTATCGATACC-3′	This paper	N/A
Primer for *del-4* cDNA for expression on *Xenopus* oocytes (Forward): 5′-CTTGATATCGAATTCCTGCAATGGGTGTATTTTGGACCGGC-3′	This paper	N/A
Primer for *del-4* cDNA for expression on *Xenopus* oocytes (Reverse): 5′-GTTTAGTGGTAACCAGATCTTCAATCATTAGAATGAGGCTTTGGTGGAAC-3′	This paper	N/A

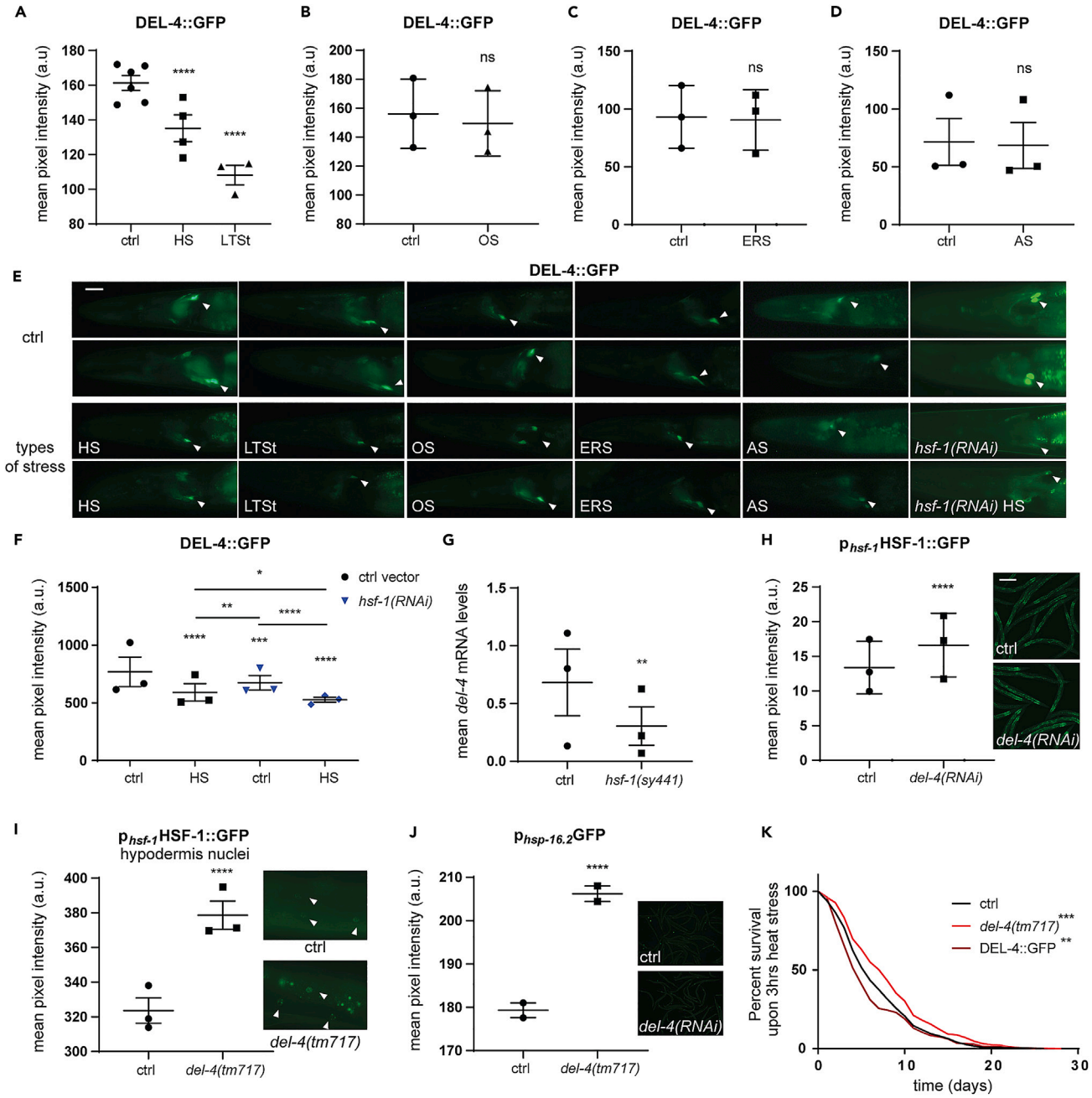

Figure 2. Regulation of DEL-4 expression by specific stress stimuli

(A) Expression levels of DEL-4 diminish upon heat stress and starvation. Imaging of 2-day adult animals, control or treated for 3 h at 37°C and left O/N for recovery or starved for 24 h (STAR Methods).

(B and C) Oxidative stress and ER stress do not alter the expression levels of DEL-4. For oxidative stress induction, we placed animals expressing the DEL-4 translational reporter on OP50 seeded NGM treated with paraquat to a final concentration of 8 mM (STAR Methods). We induced ER stress with tunicamycin, plated on OP50 seeded NGM at a final concentration of 2.5 μg/mL. Animals were placed on NGM with paraquat or tunicamycin at the L4 stage. Imaging was performed on day one of adulthood.

(D) Acidic stress does not affect DEL-4 levels. One-day adult animals were treated for 1 h in a 15 μL drop with M13 brought to pH3.5 with CH3COOHNa.

(E) Representative epifluorescent images of the head region of DEL-4::GFP-expressing animals under control conditions or upon heat stress, long-term starvation, oxidative stress, ER stress, and acidic stress (STAR Methods). We measured the intensity only in the neuronal cell body, which exhibited the highest expression level (arrowhead). Left is anterior. Lens 40x. Scale bar 20 μm.

(F and G) HSF-1 regulates the expression levels of DEL-4. (F) Downregulation of *hsf-1* with RNAi reduces the expression levels of DEL-4::GFP, upon control conditions and HS Imaging of 2-day adult animals, control or treated for 3 h at 37°C and left O/N for recovery (STAR Methods). (G) Reduced *del-4* mRNA

Figure 2. *Continued*

levels in the *hsf-1(sy441)* mutant. We measured with RT-PCR the mean *del-4* mRNA levels, using as template cDNA of 3-day adult wt and *hsf-1* mutant animals. We isolated total mRNA from wt and *hsf-1* mutants, reversely transcribed it into cDNA and used as template for RT-PCR. Dot plot, dots represent the mean *del-4* mRNA levels from independent biological replicates. We performed 3 independent biological replicates and for each biological we performed three technical replicates.

(H–K) *del-4* depletion activates HSF-1. (H) Increased HSF-1expression levels upon *del-4*(RNAi). The levels of HSF-1 were measured from the whole body at day 4 of adulthood. 5x lens, scale bar 20 μm. (I) The *del-4* mutant *(tm717)* displays increased nucleus to cytoplasm ratio of HSF-1 expression levels. HSF-1 levels in hypodermis nuclei are increased in the *del-4* mutant. We overlooked the nuclei located above the gut to avoid intestinal autofluorescence. 40x lens, scale bar 200 μm. (J) Absence of DEL-4 increases the expression levels of the HSF-1 target *hsp-16.2*. Measurements from the whole body of one-day adults. 5x lens, scale bar 20 μm. (K) Survival of wt, *del-4(tm717)* mutants and DEL-4 overexpressing animals after 2.5 h of heat stress applied on day 1 of adulthood. Death events were measured every second day. Mutants of *del-4* display enhanced resistance, while DEL-4-overexpressing animals exhibit reduced resistance to heat stress. For statistical significance, survival curve analysis was performed. (A–D, F–H, I, J) Dot plots, dots represent the number of independent biological replicates, error bars represent SEM Non-significant (ns) p = 0.1234, *p = 0.0332, **p = 0.0021, ***p = 0.0002, ****p < 0.0001. two-way ANOVA analysis. (A–D, F) n represents number of neuronal cell somas. (A) Control: n = 289; HS: n = 205; LTSt: n = 177. All HS and LTSt experiments were performed separately, except for one of the three repeats, but were plotted together for illustration purposes. (B) ctrl: n = 169, OS: n = 161. (C) ctrl: n = 97, ERS: n = 105. OS and ERS experiments were performed separately but plotted together for illustration purposes. (D) ctrl n = 105 and LpH n = 102. (F) ctrl: n = 243, HS: n = 233, hsf-1(RNAi): n = 213, HS and *hsf-1(RNAi)*: n = 286. (A–F) Control (ctrl), heat stress (HS), long-term starvation (LTSt), acidic (AS), oxidative stress (OS), and ER stress (ERS) (Table S1). (H) ctrl n = 219, *del-4(RNAi)* n = 237, n represents the number of individual animals measured (I) ctrl n = 279, HS n = 325, n represents the number of nucleuses (J) ctrl: n = 161, *del-4(tm717)*: n = 96, n represents number of animals. (K) 4 biological replicates, ctrl n = 356, *del-4(tm717)* n = 396, DEL-4::GFP n = 273, n represents number of animals participated in the lifespan assay. See also Figure S3.

SKN-1, the *C. elegans* homolog of mammalian Nrf2, is known for its role in Phase II detoxification genes transcription, thereby contributing to survival and resistance to oxidative stress.[43] We observed that systemic *del-4* knockdown enhanced the expression levels of *skn-1* and its target gene *gst-4* (Figures 3H, 3I, 3K, S4E and S4I). Specifically, SKN-1 increased both systemically and particularly in the ASI nuclei (Figures 3J and 3K). Collectively, these data indicate that DEL-4, acting in neurons, modulates the activation of several metabolic stress responses throughout the body. The question that rises is how this signal is transmitted from neurons to distal tissues and whether it is translated to behavioral adaptation to environmental stress.

DEL-4 modulates dopaminergic signaling

As previously described, DEL-4 is expressed in all dopaminergic neurons. Dopamine signaling is involved in several forms of behavioral plasticity, reward, stress processing, and control of motor output. Therefore, we reasoned that DEL-4 could integrate stress stimuli through dopaminergic signaling. In *C. elegans*, the functionality of the dopamine pathway can be readily assessed by monitoring a specific locomotory response to food availability cues, which is termed basal slowing response (BSR) (Table S1), and consists of a decrease in the animal's locomotory rate upon encountering food.[44] To assess whether DEL-4 modulates dopaminergic signalling, we tested the ability of animals to elicit a BSR in the presence or absence of DEL-4. Interestingly, *del-4* mutant animals exhibit a stronger BSR compared to wt (Figure 4A). In addition, transgenic animals overexpressing DEL-4 display a higher locomotory rate on food, and thus reduced BSR compared to wt (Figure 4A). These results suggest the involvement of DEL-4 in the regulation of dopaminergic signaling.

To examine the possible epistatic interaction of DEL-4 with the intracellular dopaminergic signaling pathway, we performed a BSR assay for the double mutants of *del-4* and each of the dopamine receptor genes (*dop-1*, *dop-2*, or *dop-3*) (Figures 4B and 4E; Tables 1 and S4) or their downstream kinase genes (*pkc-1*, *pkc-2*, *tpa-1*, *unc-43*, or *kin-2*) (Figures 4C–4E; Tables 1 and S4). In most instances, we observed that the BSR of the double mutants was equivalent to that of dopamine receptor or kinase single mutants. The only exceptions were the *del-4(tm717); pkc-2(ok328)* double mutants, which share the same phenotype as the single *del-4(tm717)* mutant. This observation suggests that PKC-2 either lies upstream of DEL-4 or that it functions independently (Figure 4C). These findings indicate that DEL-4 acts upstream of the dopaminergic signaling pathway.

To corroborate the effects of DEL-4 on dopaminergic signaling, we sought to estimate dopamine levels in the synapse of dopaminergic neurons, in the presence or absence of DEL-4. To this end, we used a pH-sensitive version of EGFP, the super ecliptic phluorin (Tables 1 and S1), fused to synaptobrevin, expressed specifically in dopaminergic neurons. We observed reduced basal levels of synaptic release in the absence of DEL-4 (Figure 5A). Moreover, *del-4(tm717)* mutants were resistant to paralysis in a dopamine resistance assay, further suggesting that the amount of dopamine in the synaptic cleft is reduced in the absence of DEL-4 (Figures 5B and S5).

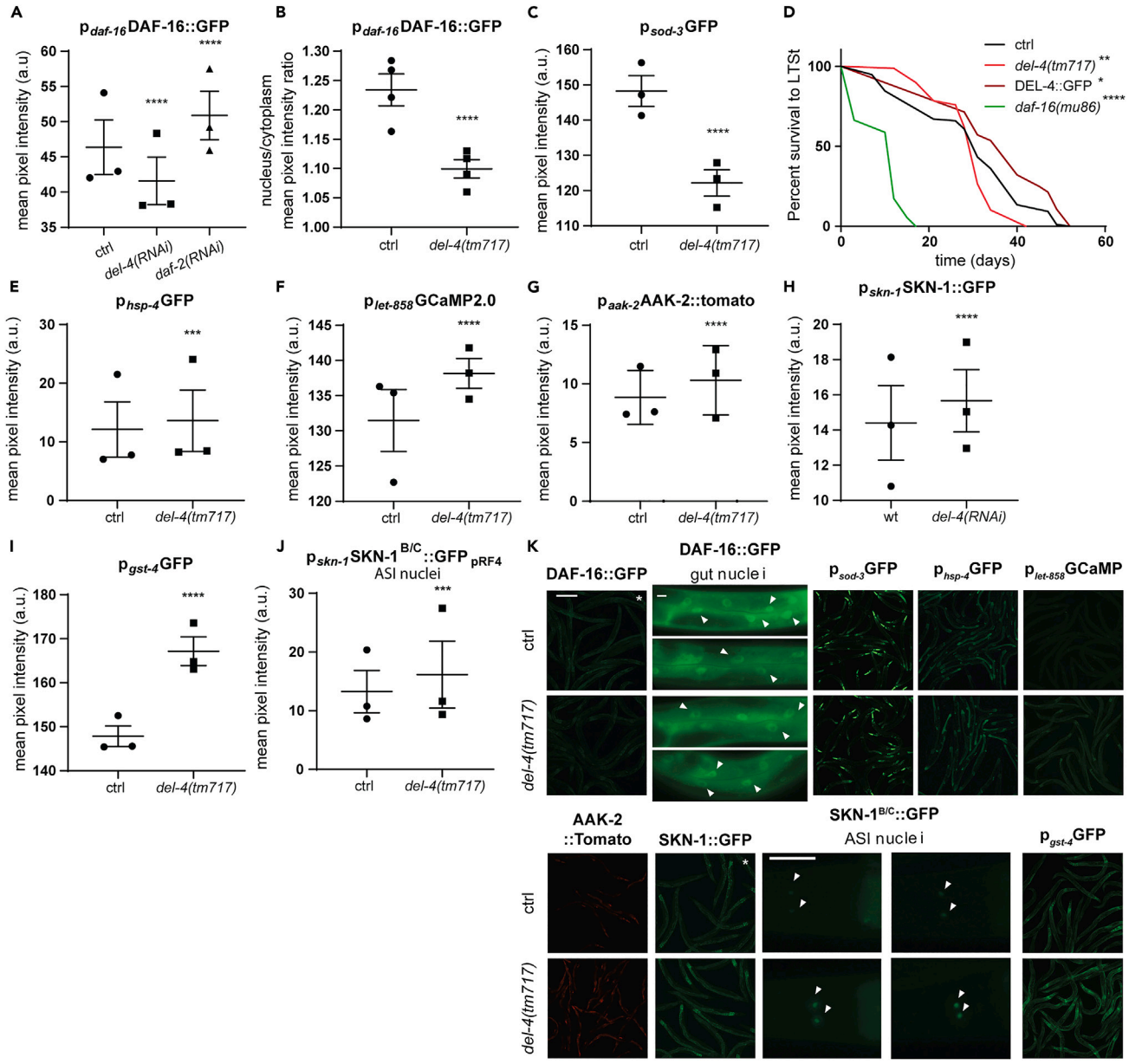

Figure 3. DEL-4 differentially regulates systemic stress responses

(A) Downregulation of *del-4* by RNAi decreases DAF-16 expression levels, measured in the whole body. *daf-2* RNAi was used as a positive control. Four-day adult animals.

(B) The DAF-16 ratio of nucleus to cytoplasm is decreased in the *del-4(tm717)* mutant. We measured the intensity levels of DAF-16 in the nuclei and adjacent cytoplasm of the gut and calculated the ratio. One-day adult animals.

(C) *del-4* elimination lowers the DAF-16 target SOD-3 expression levels. We measured the expression levels of *sod-3* from the whole body of animals expressing the transcriptional reporter p_{sod-3}GFP, under control conditions and in the *del-4(tm717)* mutant.

(D) *del-4(tm717)* mutant animals were sensitive to food deprivation compared to wt while animals overexpressing DEL-4 where more resistant. We measured the survival of wt, *del-4(tm717)* mutants, DEL-4::GFP-overexpressing animals, and *daf-16(mu86)* mutants during starvation. The *daf-16(mu86)* mutant was used as the positive control. Animals were bleached and placed as eggs in 1.5 mL M9. Every second day, 20 μL were retrieved from each genotype, put on OP50 seeded NGM as L1 larvae and allowed for three days to grow. We counted the animals that reached the L4 stage or adulthood (STAR Methods). Survival curve analyses were used for evaluation of statistical significance.

(E) The transcriptional reporter of HSP-4, an ER stress marker, displays elevated fluorescence intensity levels in the *del-4* mutant background compared to control. One-day adult animals.

(F) Cytoplasmic Ca^{2+} levels rise upon *del-4* depletion. Measurement of intracellular Ca^{2+} levels using the genetically encoded calcium indicator GCaMP2.0 driven by the *let-858* promoter for systemic expression.

Figure 3. *Continued*

(G) Increased AAK-2 levels in *del-4(tm717)* mutant animals. We measured the expression levels of AAK-2 from the whole body of animals expressing the translational reporter p_{aak-2}AAK-2::Tomato.

(H and I) DEL-4 downregulation increases systemic expression levels of SKN-1 (four-day adult animals) and its target GST-4 (one-day adult animals).

(J) SKN-1 expression levels of isoforms B and C are elevated in ASI nuclei in the *del-4* mutant background. One-day adults.

(K) Representative images of the designated reporters. Asterisks indicate *del-4(RNAi)* instead of the *del-4* mutant. Images illustrating whole animals were retrieved with a 5x lens and the scale bar corresponds to 20 μm. Images of p_{daf-16}DAF-16::GFP (gut nuclei) and were captured with a 20x lens and those of p_{skn-1}SKN-$1^{B/C}$::GFP in ASI nuclei with a 40x lens. In this case, the scale bar corresponds to 200 μm (left is anterior). (A–C, E–J) Dot plots, dots indicate mean levels of independent biological replicates. two-way ANOVA. Error bars represent SEM Non-significant (ns) p = 0.1234, *p = 0.0332, **p = 0.0021, ***p = 0.0002, ****p < 0.0001. One-way ANOVA. (A)ctrl n = 134, *del-4(RNAi)* n = 149, *daf-2(RNAi)* n = 152, n represents the number of animals. (B) ctrl n = 442, *del-4(tm717)* n = 375, n represents the number of nucleuses. (C) ctrl n = 178, *del-4(tm717)* n = 132, n represents number of animals. (D) ctrl n = 97, *del-4(tm717)* n = 79, DEL-4::GFP n = 28, *daf-16(mu86)* n = 92, n represents number of animals. (E) ctrl n = 120, *del-4(tm717)* n = 112, n represents number of animals. (F) ctrl n = 155, *del-4(tm717)* n = 161, n represents number of animals. (G) ctrl n = 128, *del-4(tm717)* n = 92, n represents number of animals. (H) ctrl n = 301, *del-4(RNAi)* n = 300, n represents number of animals. (I) ctrl n = 165, *del-4(tm717)* n = 162, n represents number of animals. (J) ctrl n = 143, *del-4(tm717)* n = 113, n represents number of ASI nuclei. See also Figure S4.

DEL-4 was present in the VA, VB, DA, and DB cholinergic motor neurons of the ventral nerve cord (Figure 1C). Muscle cells are innervated by cholinergic and GABAergic neurons. Firing through cholinergic neurons promotes muscle contraction, whereas the activation of GABAergic neurons evokes muscle relaxation. Both types of motor neurons express dopamine receptors, which act antagonistically to control *C. elegans* locomotion. The D1-like dopamine receptor, DOP-1, is confined to cholinergic motor neurons, where it stimulates acetylcholine (ACh) release (Table S1). The D2-like dopamine receptor, DOP-3, localizes primarily in GABAergic neurons and, to a much lesser extent, in cholinergic motor neurons. DOP-3 functions by inhibiting ACh release.[45] According to the BSR data (Figure 4B), all three dopamine receptors lie downstream of the effects of DEL-4 on BSR. To study the effect of DEL-4 downregulation on motor output, we estimated the degree of synaptic release initially at the cholinergic and subsequently at GABAergic neuromuscular junctions (NMJ). Interestingly, we saw that DEL-4 depletion results in reduced basal levels of synaptic release at the cholinergic NMJ, compared to wt (Figure 5C). To verify that the decreased cholinergic neurotransmission at the NMJ is due to presynaptic defect, we used a combination of aldicarb and levamisole resistance assays.[46] *del-4* mutants were resistant to the paralytic effects of aldicarb while animals overexpressing DEL-4 were sensitive, compared to wt (Figure 5D). However, DEL-4 depletion or overexpression did not alter the resistance of animals to levamisole (Figure 5E). These results indicate a presynaptic defect at the NMJ upon DEL-4 downregulation, causing a reduction in ACh synaptic release.

Subsequently, we sought to investigate the effects of DEL-4 depletion in GABAergic neurotransmission. DEL-4 is not expressed in GABAergic motor neurons. Therefore, we anticipated that alterations in GABAergic neurotransmission would rely solely on dopaminergic signaling. Notably, *del-4* mutants exhibit increased synaptic vesicle (SV) density in GABAergic motor neurons compared to control (Figures 5F, 5G, and 5J). This result indicates a dopamine-dependent increase in GABAergic motor neuron signaling upon DEL-4 downregulation. The activation of inhibitory motor neurons combined with the reduced cholinergic motor signaling explains the moderate locomotor activity of the *del-4* strain in the BSR.

Apart from neurotransmitters, neurons release neuropeptides that are packaged into dense core vesicles (DCVs) throughout the neuronal cell soma, axons, and dendrites. We determined the number of DCVs in the dorsal neural cord cholinergic motor neurons and did not observe any difference between *del-4* and control animals (Figures 5H, 5I, and 5K). These results suggest that DEL-4 specifically affects signaling through SVs but not through DCVs.

Collectively, the aforementioned findings support the notion that DEL-4 depletion decreases dopaminergic signaling, with an ultimate impact on downstream motor neuron neurotransmission and locomotory behavior. To shed light on the mechanism through which DEL-4 modulates neuronal function, we will investigate the physiological characteristics of a putative DEL-4 channel.

DEL-4 is a proton-gated sodium channel on neuronal cell membrane

To assess whether the subcellular localization of DEL-4 fits the known pattern of transmembrane channels, we labeled animals expressing the DEL-4::GFP with the lipophilic dye DiI. DiI stains the membranes of amphids, phasmids, and chemosensory neurons with nerve endings exposed to the environment (Table S2). Confocal imaging at high magnification revealed the colocalization of DEL-4 with DiI and its membranous localization (Figures 6A and S6A). To further examine DEL-4 site of action on neuronal membrane, we

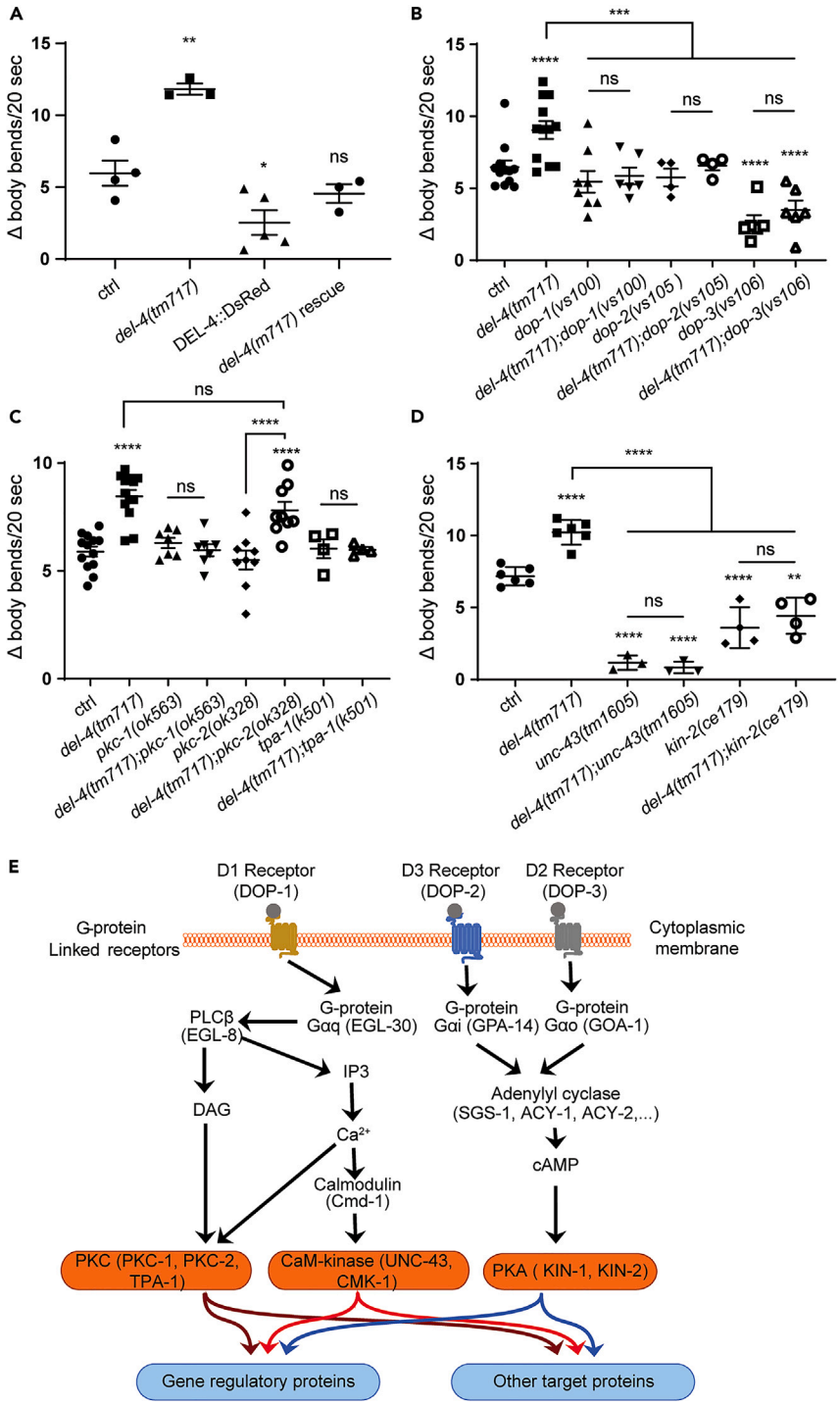

Figure 4. DEL-4 acts upstream in the dopaminergic signaling pathway to modulate *C. elegans* locomotory rate

(A) Basal slowing response (BSR) (STAR Methods and Table S1) of wt, *del-4(tm717)* mutants, DEL-4 overexpressing animals and *del-4(tm717)* rescue animals. *del-4* mutant animals display reduced number of body bends per 20 s on a plate with food compared to wild type and therefore show a strengthened BSR, while the BSR response of DEL-4 overexpressing animals which move faster on a plate with food is reduced. Mutant animals for *del-4* transformed with the endogenous DNA sequence of the *del-4* promoter and CDS (*del-4(tm717)* rescue animals) display the same BSR as the wt (ctrl).

Figure 4. *Continued*

(B) Dopamine receptors lie downstream of DEL-4. BSR of wt, *del-4(tm717)*, *dop-1*(vs*100*), *dop-2*(vs*105*), *dop-3*(vs*106*), *del-4(tm717);dop-1*(vs*100*), *del-4(tm717);dop-2*(vs*105*) and *del-4(tm717);dop-3*(vs*106*) animals (Tables 1 and S4). The phenotype of the double mutants for *del-4* and *dop-1*, *dop-2* or *dop-3* is the same as that of the single mutants of dopamine receptors.

(C) PKC-1 and TPA-1 are downstream of DEL-4, whereas PKC-2 may not contribute to the DEL-4 phenotype. BSR for homologs of mammalian PKC isoforms. BSR of wt, *del-4(tm717)*, *pkc-1(ok563)*, *del-4(tm717);pkc-1(ok563)*, *pkc-2(ok328)*, *del-4(tm717);pkc-2(ok328)*, *tpa-1(k501) and del-4(tm717);tpa-1(k501)* (Tables 1 and S4). Double-deficient mutants of *del-4(tm717);pkc-1(ok563)* and *del-4(tm717);tpa-1(k501)* exhibit the same phenotype as the *pkc-1(ok563)* or *tpa-1(k501)* single mutants, respectively. The BSR of *del-4(tm717);pkc-2(ok328)* double mutants is the same as in the *del-4(tm717)* single mutant.

(D) UNC-43 and KIN-2 lie downstream of DEL-4 in the dopaminergic signaling pathway. BSR of wt, *del-4(tm717)*, *unc-43(tm1605)*, *del-4(tm717);unc-43(tm1605)*, *kin-2(ce179)* and *del-4(tm717);kin-2(ce179)* animals. Double mutants *del-4(tm717);unc-43(tm1605) and del-4(tm717);kin-2(ce179)* present the same phenotype as *unc-43(tm1605)* and *kin-2(ce179)* single mutants, respectively (Tables 1 and S4). UNC-43 is an ortholog of the human calcium/calmodulin-dependent protein kinase II. KIN-2 is a regulator of KIN-1, which is an ortholog of the human cAMP-dependent protein kinase. The *kin-2(ce179)* mutant carries a gain of function mutation.

(E) Schematic representation of the dopamine signaling pathway. Dopamine receptors form G-protein coupled receptors, which upon binding of dopamine activated downstream G-proteins. D1 Receptors activate the IP3/DAG calcium pathway, and D3 and D2 receptors activate the adenylyl cyclase/cAMP signaling pathway. Inside parenthesis: *C. elegans* homologs. (A–D) Dot plots, dots represent the ratio Δ body bends/20s of independent biological replicates. The ratio Δ body bends/20s corresponds to body bends/20s on an empty plate minus body bends/20s on a plate with food. We tested 8–15 animals in every replicate of each BSR experiment. In all experiments, we used one-day-old adult animals. Error bars represent SEM Non-significant (ns) p = 0.1234, *p = 0.0332, **p = 0.0021, ***p = 0.0002, ****p < 0.0001. two-way ANOVA. (A) ctrl n = 36, *del-4(tm717)* n = 34, DEL-4::dsRed n = 42, *del-4(tm717)* rescue n = 45 (B) ctrl n = 116, *del-4(tm717)* n = 112, *dop-1*(vs*100*) n = 74, *del-4(tm717);dop-1*(vs*100*) n = 103, *dop-2*(vs*105*) n = 37, *del-4(tm717);dop-2*(vs*105*) n = 36, *dop-3*(vs*106*) n = 59, *del-4(tm717);dop-3*(vs*106*) n = 58, (C) ctrl n = 117, *del-4(tm717)* n = 117, *pkc-1(ok563)* n = 69, *del-4(tm717);pkc-1(ok563)* n = 66, *pkc-2(ok328)* n = 88, *del-4(tm717);pkc-2(ok328)* n = 84, *tpa-1(k501)* n = 41, *del-4(tm717);tpa-1(k501)* n = 51. (D) ctrl 6 n = 60, *del-4(tm717)* n = 60, *unc-43(tm1605)* n = 30, *del-4(tm717);unc-43(tm1605)* n = 30, *kin-2(ce179)* n = 40, *del-4(tm717);kin-2(ce179)* n = 40. In all cases, n represents the number of animals.

co-expressed DEL-4::GFP with SNB-1::dsRed, a synaptic vesicle marker, under the control of the *del-4* promoter. Despite their partial colocalization, the two reporters showed distinct expression patterns (Figure 6B). DEL-4 has a broader expression pattern, expands throughout cell somas and neuronal processes, and does not exhibit a punctate distribution, similar to SNB-1. Therefore, we conclude that DEL-4 is not exclusively located in synaptic regions.

Channels of the diverse DEG/ENaC family consist of three subunits. In mammals, ENaCs form heterotrimeric channels, whereas ASICs are both heterotrimeric and homotrimeric.[21,47] The subunit composition modifies the biophysical properties of the channel.[48] ENaCs are highly selective for Na^+ and Li^+ ions.[49] ASICs exhibit a weak preference for Na^+ and Li^+, but are also permeable for K^+ and in some cases Ca^{2+} ions.[50] We have previously shown that DEL-4 is a constitutively open channel mediating inward Na^+ current at neutral pH.[51] To further characterize DEL-4 channels' physiological properties, we implemented a two-electrode voltage clamp in *Xenopus laevis* oocytes, ectopically expressing either the wt protein DEL-4 or the protein product of the *del-4* mutant and nuclease-free water-injected oocytes as negative control (Figures 6C, 6D, 6F and S6B). The truncated protein from the *del-4* mutant was translated in frame from the N′ terminus up to a small part of the extracellular loop, comprising the first cytoplasmic domain at the N′ terminus, the first transmembrane domain, and the whole post-M1 domain (Figure S1B). We perfused oocytes with a sodium-rich solution (1XNDN96, see STAR Methods) and recorded the currents produced by stepping the membrane voltage from −150 to +75 mV, from a holding potential of −60 mV (Figure 6C). Amiloride, a common blocker of DEG/ENaC channels, abolished these currents in a dose-dependent manner, with an IC_{50} of 179 μM (Figures 6E, 6G and S6C). The truncated DEL-4 product did not elicit currents similar to the nuclease-free water-injected control (Figures 6D and 6F). The latter suggests that the missing parts of the protein are either responsible for the Na^+ currents or for the trafficking of the protein to the plasma membrane. Next, we investigated ion selectivity by carrying out ion substitution experiments. DEL-4 homomeric channel is permeable to monovalent cations, preferentially to Na^+ (selectivity sequence: $Na^+ = Li^+ > K^+ > Ca^{2+}$) but appears to be Ca^{2+} impermeable, at least in the *Xenopus* oocytes expression system (Figures 6H, 6I and S6D). These results revealed that DEL-4 subunits can form a homomeric channel in *Xenopus* oocytes. This channel localizes to the plasma membrane of neuronal cells, is blocked by amiloride in a dose-dependent manner, and is highly permeable to Na^+ and Li^+.

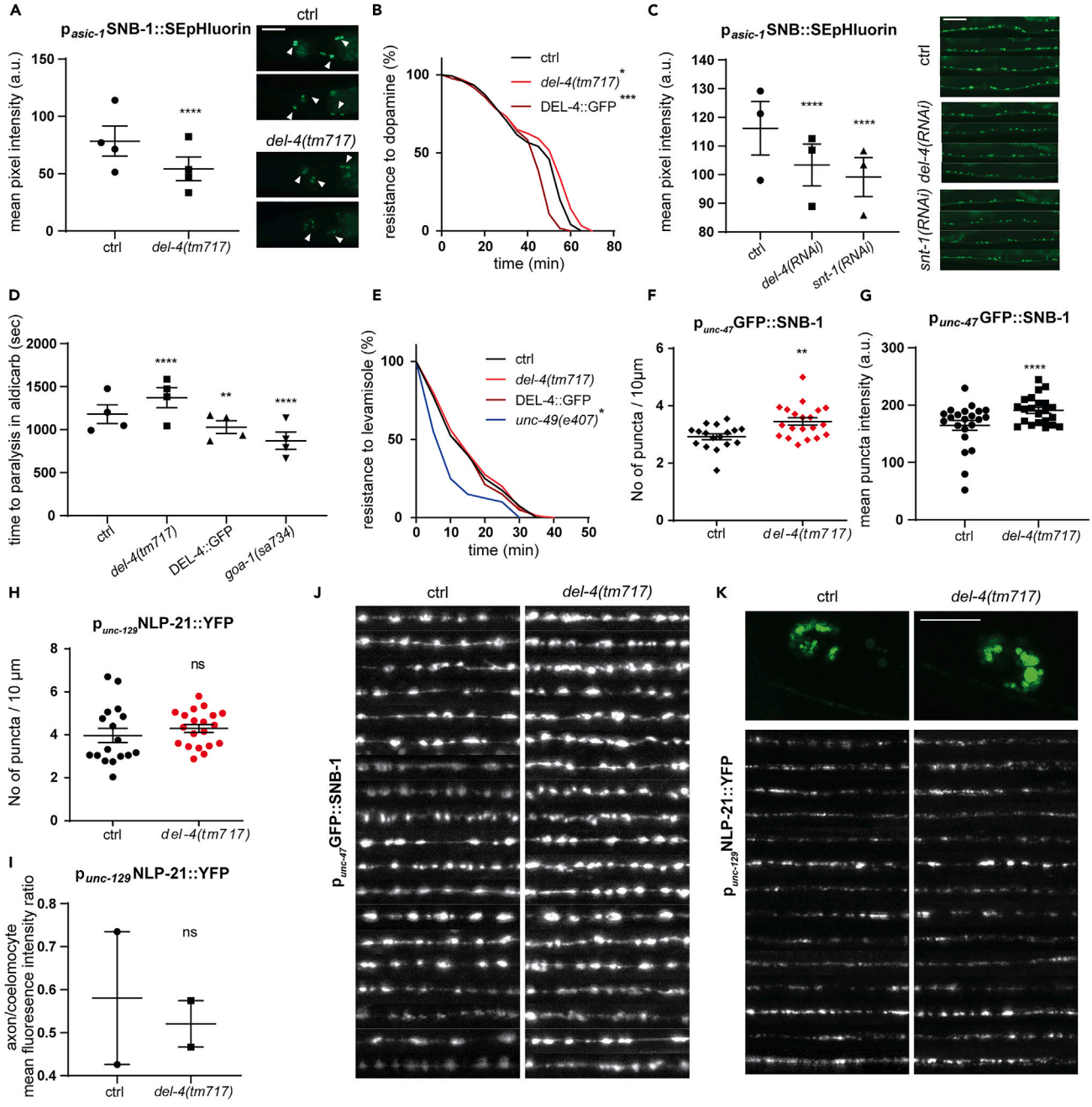

Figure 5. Synaptic vesicle exocytosis of dopaminergic and motor neurons is altered in response to DEL-4 abundance

(A) Basal levels of synaptic release from dopaminergic neurons are reduced in the *del-4(tm717)* mutant background. Left, measurements of Super Ecliptic pHluorin (STAR Methods) expressed in synaptic vesicles of dopamine-releasing neurons in controls and *del-4(tm717)* mutants. (Right) Representative images of p_{asic-1}SNB-1::SEpHluorin from control (top) and *del-4(tm717)* mutants (bottom). Some of the illustrated images came up by merging serial stacks using Adobe Photoshop CS5 (KRT) for illustration purposes only, so that all dopaminergic neurons may be visible in one image. We counted the mean pixel intensity in one-day adults from all cell bodies in the head (indicated with arrowheads). Left is anterior. Lens 40x. Scale bar 20 µM.

(B) Increased resistance of *del-4(tm717)* mutant animals to dopamine. Time course to paralysis of *del-4* mutant and overexpressing animals. We performed the time course assay with one-day adult animals in a 15 µL drop of 40 mM dopamine diluted with M9. Thirty animals per genotype were used in each experiment. Survival curve analysis was performed to estimate the statistical significance. Biological independent replicates were performed by two experimenters (MG and DP) and by one of them blindly. See also Figure S5.

(C) (Left) Reduced synaptic release from cholinergic motor neurons following *del-4* knockdown. We employed the Super Ecliptic pHluorin tagged with SNB-1 driven by the *acr-2* promoter to measure the basal levels of synaptic release in cholinergic motor neurons. The mean pixel intensity of neuronal somas was

Figure 5. *Continued*

calculated. We used *snt-1(RNAi)* as a positive control. (Right) Representative images of cholinergic motor neurons from animals expressing p_{acr-2}SEpHl::SNB-1, upon control (ctrl) (top), *del-4* (middle), or *snt-1* RNAi conditions. Scale bar 20 μm. Lens 20x. One-day adults.

(D) *del-4(tm717)* downregulation increases the resistance to aldicarb-mediated paralysis. We measured the time to paralysis of indicated genotypes at day one of adulthood in 15 μL of 10 mM aldicarb (STAR Methods). Positive control *goa-1(sa734)* (Tables 1 and S4) is an aldicarb hypersensitive strain. Survival curve analysis was performed to estimate statistical significance. Biological independent replicates were performed by two experimenters (MG and DP) and by one of them blindly.

(E) Absence or overexpression of DEL-4 causes the same phenotype as wt in the levamisole resistance assay. Time course to paralysis of the indicated genotypes at day one of adulthood in a 15 μL drop of 400 μM levamisole diluted with M9 (STAR Methods). We used the *unc-49(e407)* mutant strain (Tables 1 and S4) that exhibited sensitivity to levamisole as a positive control. For statistical analysis, survival curve analysis was performed.

(F, G, J) Synaptobrevin 1 positive puncta accumulate at the presynaptic terminals of dorsal cord GABAergic motor neurons in the *del-4(tm717)* mutant. Measurements were performed at day-one adult animals (STAR Methods). (F) Increased number of puncta/10 μm in the *del-4* mutant background. Scatterplot graph of control and *del-4(tm717)* animals showing the number of SNB-1 puncta per 10 μm. We measured the number of puncta per ten μm of GABAergic motor neurons from animals expressing the p_{unc-47}GFP::SNB-1 synaptic vesicle genetic reporter.

(G) Increased intensity of SNB-1 positive puncta in the *del-4(tm717)* mutant. We measured the mean puncta intensity along GABAergic motor neurons of control and *del-4(tm717)* mutants. (H, I, K) DEL-4 absence does not alter the release of dense core vesicles from the dorsal chord cholinergic motor neurons. Measurements were performed at day-one adult animals.

(H) Scatterplot demonstrating the number of NLP-21::YFP puncta per 10 μm of the dorsal neural chord. Cholinergic expression was achieved with the *unc-129* promoter (STAR Methods). Fluorescence of coelomocytes is a result of NLP-21::YFP endocytosis upon release. Control and *del-4(tm717)* mutant animals display the same phenotype.

(I) Quantification of neuropeptide release from cholinergic motor neurons, expressed as the mean pixel intensity ratio of axons to coelomocytes for control and *del-4* mutants. We measured the mean fluorescence intensity from axons of cholinergic motor neurons from animals expressing the neuropeptide NLP-21. We did not observe a statistically significant difference between control and *del-4* mutants.

(J) A panel of 19 images of dorsal neural cords expressing SNB-1::GFP in GABAergic motor neurons driven by the *unc-47* promoter. Left, control. Right, *del-4(tm717)*. Axons were straightened using the straightened function of ImageJ[94] (see KRT). The scale bar is the same as that in (K).

(K) Top, shown in green, representative images of the NLP-21::YFP strain indicating cholinergic motor neurons alongside coelomocytes in control (left) and *del-4(tm717)* (right) animals. Bottom, shown in black and white, panel of fragments of 14 straightened dorsal cord cholinergic motor neurons.

(K and L) Scale bar, 10 μm. Confocal images. Lens 63x. Day one of adulthood. (A, C, D, F–I) Dot plots, dots represent the mean values of biologically independent experiments. Error bars represent SEM ns $p = 0.1234$, *$p = 0.0332$, **$p = 0.0021$, ***$p = 0.0002$, ****$p < 0.0001$. two-way ANOVA analysis. (A) ctrl n = 301, *del-4(tm717)* n = 405, n = number of cell bodies, (B) ctrl n = 120, *del-4(tm717)* n = 120, DEL-4::GFP n = 120, n = number of animals (C) ctrl n = 494, *del-4(RNAi)* n = 618, *snt-1(RNAi)* n = 594, n = number of neuronal cell somas, (D) ctrl n = 21, *del-4(tm717)* n = 26, DEL-4::GFP n = 22, *goa-1(e407)* n = 21, n represents number of animals. (E) ctrl n = 80, *del-4(tm717)* n = 80, DEL-4::GFP n = 80, *unc-49(3407)* n = 20, n = number of animals. (F) ctrl n = 30, *del-4(tm717)* n = 34, n = number of animals (G) ctrl n = 272, *del-4(tm717)* n = 322, n = number of GFP::SNB-1 positive puncta counted from 30 ctrl and 34 *del-4(tm717)* animals, (H) ctrl n = 482, *del-4(tm717)* n = 646, n = number of NLP-21::YFP positive puncta counted from 25 ctrl and 31 *del-4(tm717)* animals, (I) ctrl n = 20, *del-4(tm717)* n = 35.

DEG/ENaC family members create sodium channels that are either constantly activated or gated by mechanical stimuli, peptides, or protons.[52] DEL-4 was previously shown to be a constitutively open channel at neutral pH and significantly inhibited by extracellular acidity[51] (Figure S6B). To further determine the DEL-4 homomeric channel's properties, we perfused DEL-4 expressing *Xenopus* oocytes with solutions of gradually reduced pH, starting from a baseline of pH 7.4. DEL-4-expressing oocytes showed a maximal current at around pH 5 and were inhibited by both high and lower pH, with pH_{50S} of 5.78 and 4.25 (Figures 7A–7C and S6E). Both the truncated control and the water-injected control oocytes did not show this inhibition with decreased pH (Figures S6B, S6F, and S6H). DEL-4 was not permeable to protons, as the ΔE_{rev} did not show statistically significant shift when extracellular proton concentration was increased from neutral pH to pH 4 (Figure S6G). It is likely that the pH_{50S} reflects the physiological range similar to what has been described for all the DEG/ENaC members such as the nematode ACD-5 or the human ENaCs. Their pH responses presumably reflect the environmental contexts, i.e. on the intestinal luminal membrane or epithelia, respectively, where they are expressed.[51,53] Therefore, inhibition of the DEL-4 homomeric channel by protons emerges in the limited range of pH 4.5–5.5, and this function is lost in the *del-4* mutant, which is incompetent to conduct current, in *Xenopus oocytes*.

Blocking a sodium channel in neurons may disrupt ion balance along the plasma membrane, since Na^+ stops entering the cytoplasm. Thus, the cytoplasmic membrane becomes more negatively charged, reducing the likelihood of an action potential. To verify this hypothesis, we used the genetically encoded voltage indicator, ASAP1 (Table S1), expressed in dopaminergic neurons. Changes in the membrane potential cause conformational changes in ASAP1 which lead to an increase in fluorescence upon hyperpolarization and a decrease in depolarization events.[54] As shown previously, DEL-4 is inhibited by extracellular low pH (Figures 7A–7C and S6E). Interestingly, treatment of ASAP1 reporter animals with low pH buffer leads to neuronal hyperpolarization in the presence of DEL-4 (Figures 7D and 7E). Similarly, *del-4* mutant animals displayed elevated levels of ASAP1 fluorescence compared to control animals under neutral pH

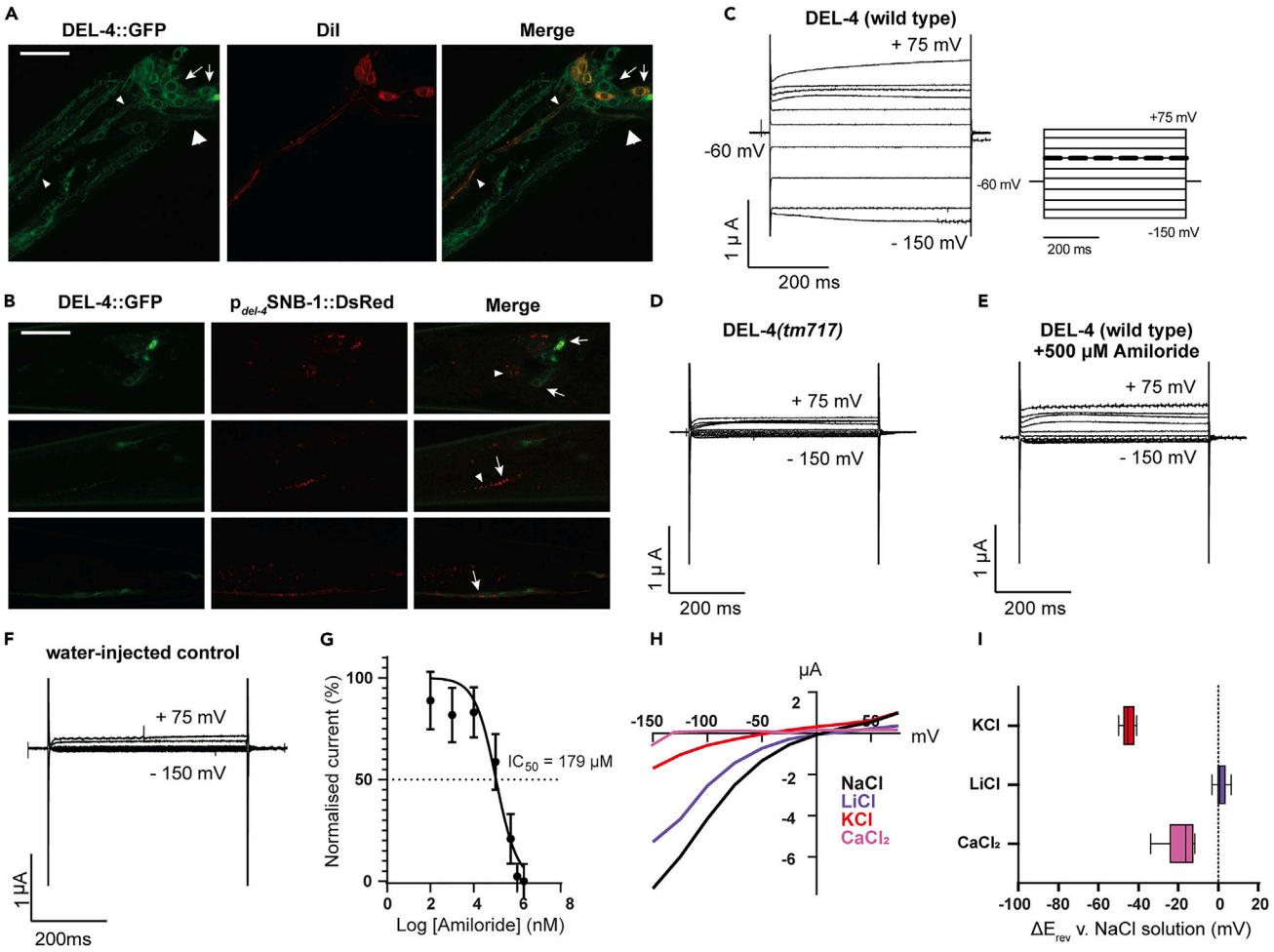

Figure 6. Subcellular localization, ion selectivity, and amiloride sensitivity of the homomeric DEL-4 channel

(A) DEL-4 localizes to the cytoplasmic membrane of neuronal cells. The DEL-4 translational reporter colocalized with DiI staining (KRT) on the surface of neuronal cell bodies and processes. Left: the *del-4* promoter drives the expression of DEL-4 tagged with GFP. Middle: DiI staining in seen in red. Right: merged images. We utilized the merged images of z-stacks to assess colocalization (see Figure S6A). Neuronal cell bodies (arrows), dendrites (small arrowheads) and axons (large arrowhead) are indicated. One-day adult animals. Left is anterior. Scale bar 20 µM. Confocal images (maximum intensity projections) with a 63x lens.

(B) Co-expression of DEL-4::GFP and SNB-1::dsRed driven by the same promoter (*del-4* promoter) revealed only random cases of colocalization. Left, expression of DEL-4 tagged with GFP in neurons driven by the *del-4* promoter (p_{del-4}DEL-4::GFP). Middle, *del-4* promoter drives the expression of *snb-1* (seen in red) in neurons (p_{del-4}SNB-1::dsRed. Right, merged images. Confocal images (Z-stacks). Lens 63x. Arrows indicate random cases of colocalization. Arrowheads indicate sites where DEL-4 and SNB-1 do not colocalize. We utilized merged z stack images to assess colocalization. Left is anterior. Scale bar 20 µm.

(C) DEL-4 subunits assemble into a constitutively open homomeric channel at neutral pH 7.4.

(D and F) Mutant *del-4(tm717)* or water-injected oocytes do not exhibit transient currents at neutral pH.

(E) DEL-4 currents at neutral pH can be blocked with 500 µM amiloride (STAR Methods).

(C–F) Representative transient currents in a *Xenopus* oocyte injected with *del-4* cRNA or *del-4(tm717)* cRNA or nuclease-free water and perfused with a physiological NaCl solution (ND96) at pH 7.4, in the absence (B) or presence (C) of 500 µM amiloride. The voltage steps applied were from −150 to +75 mV from a holding potential of −60 mV.

(G) Blocking of the DEL-4 homomeric channel by amiloride is dose-dependent. The normalized (I/Imax) current of the amiloride dose-response curves for the DEL-4 homomer revealed a half-maximal inhibitory concentration (IC_{50}) of 179 µM (LogIC50 = 4.61) (n = 5), as denoted by the dashed line. Currents were recorded at a holding potential of −60mV, normalized to maximal currents, and best fitted with Hill's equation (nonlinear fit log (inhibitor) vs. normalized response – variable slope) in GraphPad Prism.

(H and I) Representative normalized current-voltage (IV) relationships for *Xenopus* oocytes expressing DEL-4. The raw current for each oocyte and the leak current were subtracted at pH 7.4. We calculated the average ΔE_{rev} of 9 oocytes for each construct of when shifting from a NaCl solution to a KCl, LiCl or $CaCl_2$ solution. The interpolated curves displayed a shift in the reversal potential ΔE_{rev}. Replacement of NaCl with equimolar LiCl did not shift the reversal

Figure 6. *Continued*

potential ($E_{rev(Na/Li)}$ = −1.18 ± 0.93 mV) but replacement with equimolar KCl resulted in a reversal potential shift ($E_{rev(Na/K)}$ = 43.45 ± 1.86 mV) $E_{rev(Na/Ca)}$ 31.24 ± 7.77 mV (N = 10). A negative shift in E_{rev} indicates a preference for Na^+ over the respective ion, and a positive shift indicates a preference for the respective ion over Na^+. Data are presented as median and interquartile range (IQD), calculated using the Tukey method. See also Figure S6.

condition, while acidification did not affect membrane potential of *del-4* mutants (Figures 7D and 7E). Therefore, both extracellular acidification and DEL-4 channel deficiency hyperpolarizes the dopaminergic neurons *in vivo*, in accordance with our *in vitro* data.

DEL-4 participates in low pH sensory detection modulating behavioral responses to stress

Given DEL-4's ability to block Na^+ currents upon extracellular acidification, we wanted to test the behavioral response of control and *del-4* mutant animals upon encountering low pH environment. To this end, we performed a drop test assay, where the backward movement of animals upon contact with a drop of acidic buffer is monitored and quantified. This behavioral response is considered as avoidance to low pH stimulus. We challenged the animals with solutions of pH 2.2, 4.5, or 6.6. We observed that animals lacking DEL-4 were insensitive to pH 4.5, but not 2.2 or 6.6, while wt animals and animals that overexpress DEL-4 responded to all different buffers (Figure 8A). This finding indicates that closure of DEL-4 mediates the behavioral response to low pH stimuli.

Having established that DEL-4's ability to conduct current is affected by pH (Figures 7A–7C, S6B, S6E–S6H), and that blocking of Na^+ influx through DEL-4 leads to neuronal hyperpolarization Figures 7D and 7E), we sought to identify whether heat shock and long-term starvation could affect neuronal membrane potential in the presence or absence of DEL-4. To this end, we utilized again the reporter animals expressing ASAP1 in dopaminergic neurons and subjected them to prolonged starvation, thermal stress, or acidic stress (Figures 8B–8D). We found that all tested types of stress lead to hyperpolarization of dopaminergic neurons when DEL-4 is present. Interestingly, in the absence of DEL-4, neuronal membrane potential is not altered any further, than the state of the unstressed mutant, an effect that is also obvious upon DEL-4 depletion alone (Figures 8B–8D). Since starvation and heat stress limit the expression of DEL-4 (Figures 5A and 5D), while acidic stress blocks the channel's pore (Figures 7A–7C), we propose that different types of stress may hyperpolarize dopaminergic neurons by either reducing DEL-4 levels or by inhibiting conductance of current through DEL-4 channel. These findings put DEL-4 at the epicentre of stress stimuli sensation and integration.

DEL-4 displays neuroprotective effects on neurodegenerative human disease models in *C. elegans*

Several studies have shown that dysregulated dopaminergic signaling has a causative effect on the initiation and progression of neurodegenerative diseases, including Parkinson disease (PD) and Alzheimer disease (AD).[55,56] Both pathologies are complex disorders that depend on environmental and genetic factors. Data from gene expression profiling revealed the deregulation of neurotransmitters and ion channel receptors expression in PD.[57] Low levels of ACh and dopamine in the brain characterize AD and PD, respectively.[58] Moreover, chronic stress exacerbates AD and PD pathology.[59,60] In line with the effects of DEL-4 on neurotransmission and locomotion and the regulation of DEL-4 by stress, we hypothesized that downregulation of DEL-4 would aggravate the phenotype of these two neurodegenerative diseases. We utilized two *C. elegans* disease models, the UA44 as a Parkinson's model and the BR5270 as an Alzheimer disease models. These models express human α-synuclein in dopaminergic neurons, or the pro-aggregation F3ΔK280 tau fragment pan-neuronally.[61,62] In accordance to our hypothesis, we discovered that in both disease models overexpression of DEL-4 curtailed degeneration, whereas DEL-4 downregulation exacerbated this phenotype (Figure 9). In addition, depletion of DEL-4 induced dopaminergic neurodegeneration on day 5 and 7 of adulthood, even in the absence of aggregation prone proteins (Figure 9). Consequently, we propose that disruption of neuronal sodium homeostasis exacerbates neurodegeneration in control and in disease genetic background.

DISCUSSION

In this study, we characterized the contribution of a proton-inhibited DEG/ENaC channel to the perception and sensorimotor integration of specific types of stress. We observed that heat stress and starvation reduced the expression levels of DEL-4, which localizes to the plasma membrane of sensory, dopaminergic, serotonergic, and motor neurons while, vice versa, DEL-4 affects the activation of cellular stress responses throughout the body. Mechanistically, DEL-4 modifies the neuronal excitability pattern and alters synaptic

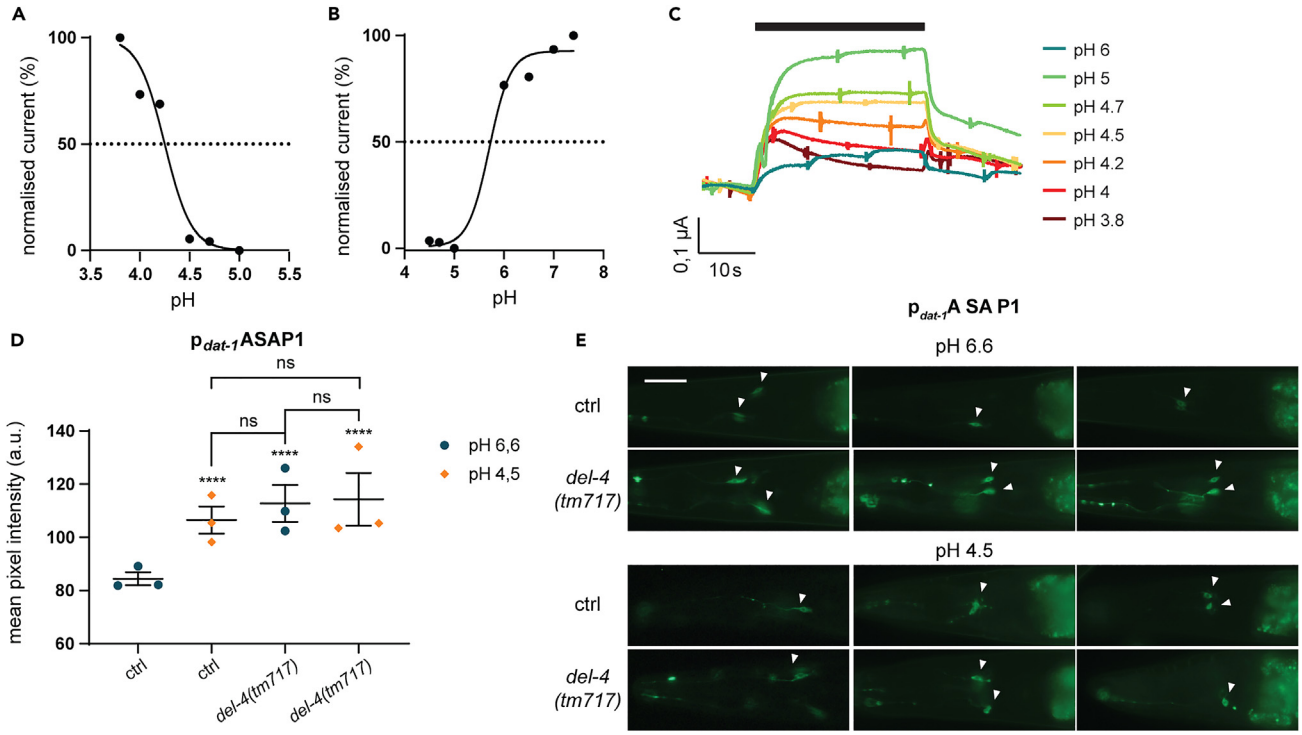

Figure 7. Acidic pH blocks the homomeric DEL-4 channel and hyperpolarizes dopaminergic neurons similar to DEL-4 depletion

(A and B) Extracellular protons inhibit the DEL-4 homomeric channel. Current to pH relationships of heterologously expressed DEL-4 homomeric channel, when perfused with solutions of increasing pH starting from 3.8 until 7.5 (n = 5). The channel is fully open at 100% current and closed at 0% current. Amount of total DEL-4 cRNA (500 ng/µL) injected. Only the mean values are presented. The voltage steps were from −150 to +75 mV from a holding potential of −60 mV. Currents were recorded at a holding potential of −60mV, normalized to maximal currents, and best fitted with Hill's equation in GraphPad Prism.

(C) Representative traces of DEL-4 expressing *Xenopus* oocytes when perfused with ND96 solution at various proton concentrations from a neutral baseline (pH 7.4). Currents were recorded at a holding potential of −60mV, and traces were baseline-subtracted and drift-corrected using Roboocyte2+ (Multichannels) software.

(D) Low pH enhances the intensity of ASAP1 in dopamine-releasing neurons. Quantification of resting membrane potential using a line expressing the genetic voltage indicator ASAP1 in dopaminergic neurons using the dat-1promoter. Control and *del-4(tm717)* mutant animals were imaged on day 2 of adulthood under control conditions and after acidic stress. Absence of DEL-4 and acidification increase ASAP1 fluorescence intensity, thus hyperpolarizing dopaminergic neurons. Mean pixel intensity was measured from cell bodies of dopaminergic neurons. Fluorescence intensity measurements of ASAP1 after 15 min incubation in M13 solution of pH 6.6 (ctrl) or pH 4.5, generated with $CH_3COOHNa$ (pH) (STAR Methods). The incubation time was followed by a recovery time of 10 min in M13 pH 6.6, to recover GFP fluorescence that quenched due to the pH sensitivity of GFP. Error bars represent the SEM ns p = 0.1234, *p = 0.0332, **p = 0.0021, ***p = 0.0002, ****p < 0.0001. two-way ANOVA analysis. Dot plot, dots represent the mean fluorescence of biological replicates. ctrl pH 6.6 n = 263, ctrl pH 4.5 n = 216, *del-4(tm717)* pH 6.6 n = 307, *del-4(tm717)* pH 4.5n = 317. n = number of dopaminergic neuron cell somas.

(E) Representative images of dopaminergic neurons expressing ASAP1 (p_{dat-1}ASAP1) in control and *del-4(tm717)* mutant animals under control or acidic stress conditions. Top, pH 6.6, bottom, pH 4.5. Scale bar 20 µm. Lens 20x. Left is anterior. See also Figure S6.

vesicle release from dopaminergic and motor neurons to adjust the locomotory rate of the animal. Finally, we demonstrated that DEL-4 modulation affects the integrity and viability of dopaminergic neurons. Our data highlight the significance of a DEG/ENaC member in neuronal sodium homeostasis and stabilization of resting membrane potential and provide valuable insight into DEG/ENaC sodium channel regulation upon stress. Our findings are consistent with those of previous studies, indicating that stress regulates mammalian ENaCs and ASICs.[25–29,31] However, our experiments represent the first *in vivo* study to illustrate that specific types of stress affect the abundance of a DEG/ENaC channel on the cytoplasmic membrane of neuronal cells.

Our electrophysiology and imaging results showed that low pH blocks the DEL-4 homomeric channel and hyperpolarizes the dopaminergic neurons. Acidification develops under physiological and pathological conditions, such as exercise,[63] ischemic stroke,[64] cardiac ischemia,[65] tumors,[66] and inflammation.[67] Similarly, in *C. elegans*, oxidative stress and mitochondrial fragmentation leads to cellular acidosis triggered by ROS production.[68,69] Pathogen infection and exercise also induce acidification.[69,70]

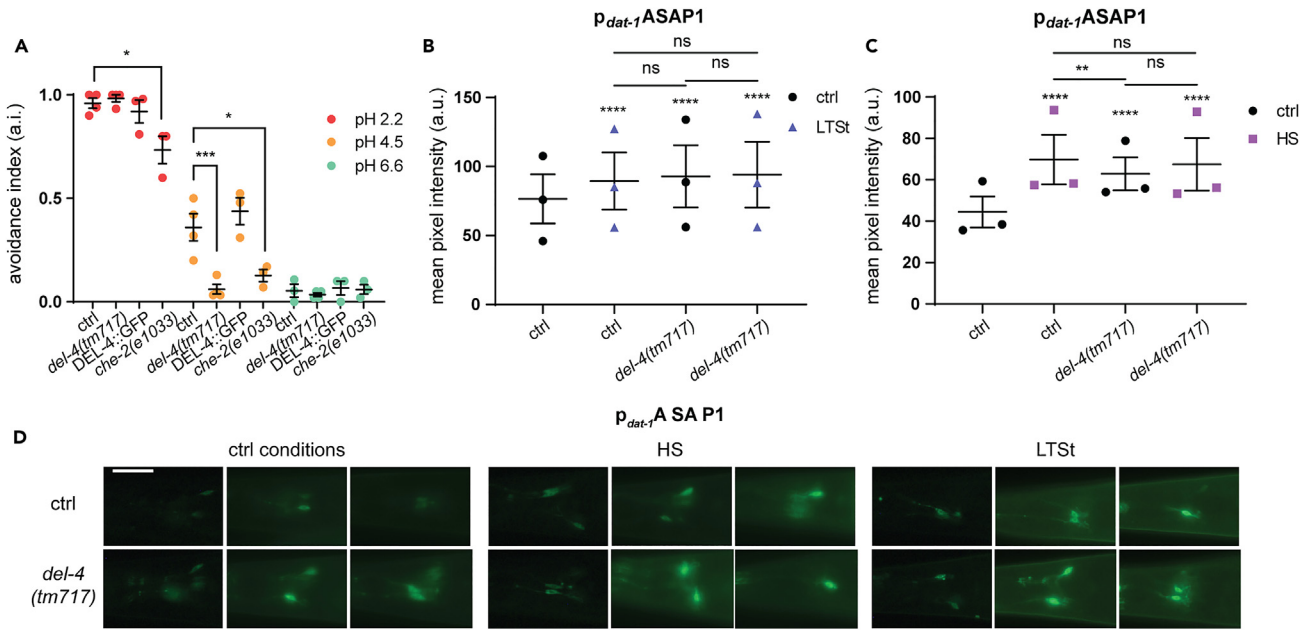

Figure 8. Dopaminergic neurons hyperpolarize upon heat stress and starvation

(A) Graph of avoidance index to M13 solutions of diverse pH values. We measured the responses of wt, *del-4(tm717)*, DEL-4::GFP, and *che-2(e1033)* (Tables 1 and S4) animals in the drop test assay. A drop of M13 buffer was applied with a syringe at the tail of each animal and a backward movement was accounted as avoidance. An avoidance index of 1 represents complete avoidance to the M13 solution, and 0 represents a total lack of avoidance response. The *che-2(e1033)* strain was used as a positive control. Animals were tested on day one of adulthood.

(B and C) Quantification of resting membrane potential using the line expressing ASAP1 in dopaminergic neurons. The voltage indicator ASAP1 was expressed under the *dat-1* promoter. Control and *del-4(tm717)* mutant animals were imaged on day 2 of adulthood under control conditions or after stress (STAR Methods). The absence of DEL-4, LTSt, and HS increases ASAP1 levels, thus hyperpolarizing dopaminergic neurons. The mean pixel intensity was measured from the neuronal cell bodies. (B) Long-term starvation (LTSt) hyperpolarizes dopaminergic neurons, similar to the *del-4(tm717)* mutant. We estimated the intensity levels of ASAP1 in control and *del-4(tm717)* animals after long-term starvation for 24 h on unseeded NGM. (C) The fluorescence of ASAP1 in dopaminergic neurons increases in the *del-4(tm717)* mutant and upon heat stress (HS). We calculated the intensity levels of ASAP1 in dopaminergic neuronal somas from control and *del-4(tm717)* animals after thermal stress for 1 h at 37°C.

(D) Representative images of dopaminergic neurons expressing ASAP1 in control and *del-4(tm717)* mutant animals under control or stress conditions. Scale bar 20 μm. Lens 20x. Left is anterior.Error bars represent SEM ns $p = 0.1234$, *$p = 0.0332$, **$p = 0.0021$, ***$p = 0.0002$, ****$p < 0.0001$. two-way ANOVA analysis. Dot plots, dots represent the mean of independent biological experiments (A) ctrl pH 2.2 n = 79, ctrl pH 4.2 n = 118, ctrl pH 6.6 n = 104, *del-4(tm717)* pH 2.2 n = 107, *del-4(tm717)* pH 4.5 n = 125, *del-4(tm717)* pH 6.6 n = 113, DEL-4::GFP pH 2.2 n = 106, DEL-4::GFP pH 4.5 n = 80, DEL-4::GFP pH 6.6 n = 123, *che-2(e1033)* pH 2.2 n = 108, *che-2(e1033)* pH 4.5 n = 93, *che-2(e1033)* pH 6.6 n = 104. n represents the total number of responses (positive and negative) counted in all experimental repeats. (B) ctrl ctrl n = 197, ctrl LTSt n = 212, del-4(tm717) ctrl n = 189, and del-4(tm717) LTSt n = 260. (C) Three trials, ctrl ctrl n = 177, ctrl HS n = 180, *del-4(tm717)* ctrl n = 213, and *del-4(tm717)* HS n = 186. (B, C) n represents number of dopaminergic neuron cell somas.

The site(s) of proton binding for channel opening in the mammalian ASICs are still relatively poorly understood with several candidate binding sites in the pore-forming and extracellular domains.[71] Among the *C. elegans* DEG/ENaCs, there are two groups of acid-sensitive DEG/ENaCs characterized by being either inhibited or activated by increasing proton concentrations. Three of these acid-sensitive DEG/ENaCs are activated by acidic pH, making them functionally similar to most of the vertebrate ASICs51. By contrast, DEL-4 is part of four acid-inhibited members which also include the degenerin ACD-1, a proton-inhibited glial sodium channel that participates in sensory perception and affects neuronal function.[72] Among mammalian members, low extracellular pH blocks the heteromeric αβ ENaC epithelial channel.[73] Although ENaCs are mainly localized in epithelial tissues, alpha and beta ENaC subunits are abundantly co-expressed in many brain regions.[74] Regarding its *in vivo* function, our results have shown that del-4 mutants are insensitive to solution at pH 4.5 indicating that DEL-4 could be directly involved in acid sensation. Additionally, we have also shown that DEL-4 may play a more modulatory role during neurotransmission. Consequently, DEL-4 could have dual roles depending on where it is expressed. This is similar to what has been suggested for another *C. elegans* DEG/ENaC, DEG-1, which in chemosensory neurons functions in responses to both attractive and repellent cues[72] but in nose nociceptor neurons is required for mechanoreceptor currents.[75] Overall, this work highlights the importance of proton homeostasis in the regulation of sodium channel gating and stress perception.

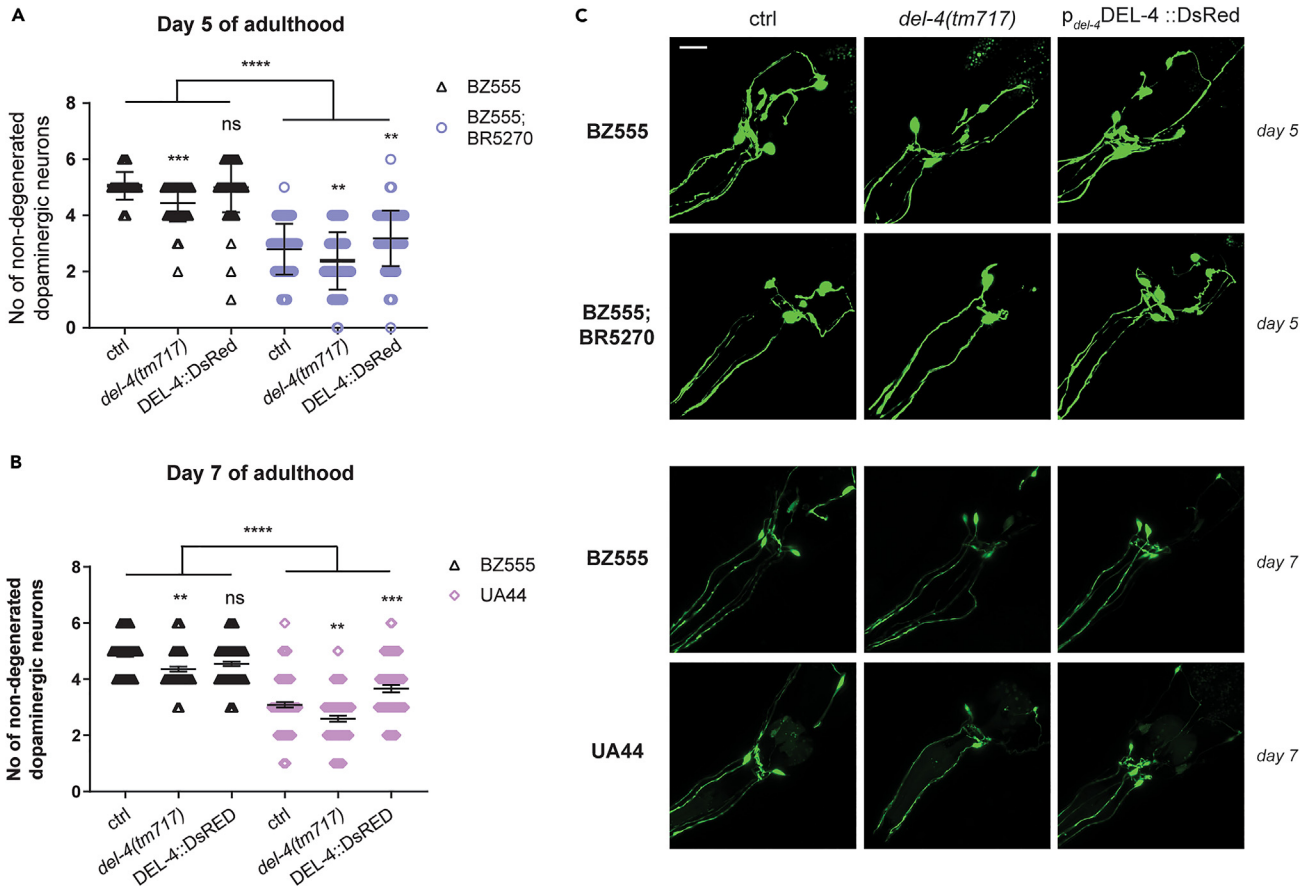

Figure 9. DEL-4 protects against neurodegeneration

(A) Overexpression of DEL-4 promotes survival of dopamine-releasing neurons in the head of *C. elegans* in an Alzheimer disease model. The graph indicates the number of surviving dopaminergic neurons in the head of control and *del-4(tm717)* mutant animals in control (BZ555) and disease conditions (BR5270) (Tables 1 and S4). DEL-4 elimination results in an increased number of degenerated neurons under control conditions and in the tauopathy model. The strain BR5270, which overexpresses the F3 pro-aggregation fragment of the human Tau protein with deleted K280, pan-neuronally, under the rab-3 promoter (p_{rab-3}F3(delta)K280), was used. Measurements were performed on 5-day adult animals.

(B) The *del-4(tm717)* mutant displays increased neurodegeneration under control conditions and in a model of Parkinson disease at day seven of adulthood. Comparison of surviving neurons of control and *del-4(tm717)* mutants under control conditions (BZ555) and in the UA44 model of Parkinson disease. DEL-4-overexpressing animals exhibit reduced degeneration compared to control. The UA44 strain (p_{dat-1}GFP; p_{dat-1}a-syn) expresses human α-synuclein and GFP in dopaminergic neurons. We used UA44 as the synucleinopathy model.(A, B) Error bars represent the SEM ns p = 0.1234, *p = 0.0332, **p = 0.0021, ***p = 0.0002, ****p < 0.0001. One-way ANOVA analysis.

(A–C) Dot plots, dots represent the number of non-degenerated neurons counted per animal.(C) Representative images from the head of control animals (left), *del-4(tm717)* mutants (middle), and DEL-4-overexpressing animals (DEL-4::dsRed) (right). Top, images from the BR5270 strain and the BZ555 control on day five of adulthood. Bottom, images from the UA44 strain and the BZ555 control on day seven of adulthood. Confocal images (maximum intensity projections). Lens 40x. Scale bar 20 μm. Left is anterior. (A–C) Strain BZ555 expresses GFP in dopaminergic neurons (p_{dat-1}GFP). We utilized BZ555 as a control for disease models. (A) BZ555 n = 73, *del-4(tm717)* n = 68, DEL-4::dsRed n = 88, BR5270 n = 158, BR5270;*del-4(tm717)* n = 134, BR5270; DEL-4::dsRed n = 151. (B) BZ555 n = 143, *del-4(tm717)* n = 67, DEL-4::dsRed n = 92, UA44 n = 117, UA44;*del-4(tm717)* n = 83, UA44; DEL-4::dsRed n = 63.

DEL-4 at steady-state conditions behaves as a permanently open channel. Thus, it may participate in neuronal resting membrane potential generation as a Na^+ leak channel. The subcellular localization pattern of DEL-4 supports this notion. DEL-4, unlike other ASICs,[76,77] is distributed throughout the plasma membrane and not specifically at the synapse. In addition, synaptic ASICs are mainly open in response to low pH, whereas DEL-4 would be closed under these conditions. The regulation of the DEL-4 channel by specific types of stress represents a mechanism that controls and alters neuronal excitability in response to environmental stress. DEL-4 modulates transcription factors that affect synaptic activity, neuronal structural maintenance, and survival.[78–82] Vice versa, HSF-1 participates in the regulation of DEL-4, thereby mediating stress signal transmission.

We observe altered neuronal signaling of motor neurons in the absence of DEL-4. We propose that in the case of *del-4* mutant there are two levels of regulation of ACh release from cholinergic motor neurons. First, DEL-4 is expressed in cholinergic motor neurons, therefore its absence could alter (similar to its effect on dopaminergic neurons) the resting membrane potential of cholinergic neurons due to defective ion homeostasis. The second level of regulation of cholinergic motor neurons arises from altered dopaminergic signaling in the *del-4* mutant. In *C. elegans*, the D1-like dopamine receptor, DOP-1, localizes on the cytosolic membrane of cholinergic motor neurons, where it stimulates ACh release. In addition, a deregulation of synaptic homeostasis has been observed in neurological diseases.[83] In *C. elegans*, released dopamine reaches dopamine receptors found on motor neurons through diffusion. We hypothesize that DOP-3 receptor expressed on GABAergic motor neurons is less activated in the *del-4* mutant, therefore increasing GABAergic signaling and further reducing ACh release. Overall, we believe that in the del-4 mutant there is a defected neuronal ionstasis and homeostasis that settle a new equilibrium concerning neuronal activation and synaptic release.

DEL-4 is essential for neural cell homeostasis and survival. The *del-4* mutant showed increased neuronal loss with age compared with the control. In contrast, heightened DEL-4 levels act in a neuroprotective manner in Parkinson and Alzheimer disease models. Conversely, blocking ASIC current attenuates α-synuclein accumulation and protects neurons from degeneration.[84] Mammalian ASICs have also been involved in brain ischemia. Inhibition of ASIC1a attenuates intracellular Ca^{2+} elevation due to cerebral ischemia.[85] Interestingly, acidity has been implicated in the onset and the progression of several features of amyotrophic lateral sclerosis.[86,87] ASIC2 and ASIC3 are upregulated in motor neurons of patients with amyotrophic lateral sclerosis.[88] Our results, concerning the proton-inhibition and the attenuated locomotory rate observed upon DEL-4 downregulation, corroborate the findings that ASICs are implicated in a variety of neurodegenerative diseases, in which acidification is observed.

The difference of DEL-4 to other ASICs is that it constitutes a sodium leak channel at physiological conditions, contrary to most of the mammalian ASICs that open upon acidification. The sodium background channel NALCN, a voltage-independent cation channel, regulates neuronal membrane conductance and coordinates its excitability.[89] Disruption of NALCN results in neuronal hyperpolarization and has been linked with neurodegenerative diseases, such as Alzheimer disease.[90] In view of these findings, the effects of DEL-4 on membrane potential and neurodegeneration are not contrary to a large body of evidence supporting that hyperpolarization is normally protective. In most of these cases, reduced depolarization is mediated by potassium or voltage-gated sodium channels.[91,92]

Several studies have linked chronic stress with the progression of AD and PD. In mammalian AD models, long-term adverse stress worsens cognitive functions and accelerates Aβ deposition.[60] Chronic stress in rodents reduces dopaminergic signaling in distinct brain regions and confines locomotory activity.[93] Research in animal models and humans with PD has revealed that stress worsens mental health and causes locomotion defects.[59] Our findings provide new insights into the molecular mechanisms underlying chronic stress that affects the onset and accelerates the progression of neurodegenerative diseases.

Our electrophysiological analysis indicates that DEL-4 forms a proton-gated homomeric channel. We note that DEL-4 shows extensive sequence similarity with human ENaC1b and ASIC1b. Therefore, it could potentially form either homomeric or heteromeric channels, *in vivo*. Whether the heteromeric channels will share the same electrophysiological properties as the DEL-4 homomeric channel remains to be elucidated. Nevertheless, depletion of DEL-4 is expected to affect all the types of DEL-4 containing channels *in vivo*.

We propose a model in which specific types of stress or acidity reduce or inhibit the DEL-4 channel, inducing hyperpolarization of dopamine neurons and the subsequent perturbation of synaptic release. Concomitantly, cell-non-autonomous modulation of several stress responses affects the excitation patterns of cholinergic and GABAergic motor neurons. This regulation adjusts the motor output of animals to elicit proper behavior in response to stress. Thus, neuronal ionstasis fine-tunes stress response mechanisms and neuroendocrine signaling to control physiological processes, such as locomotion (Figure 10).

Limitations of the study

We have not explored possible interactions of DEL-4 with other degenerin ion channels that could result in the formation of heteromeric sodium channels with distinct electrophysiological properties.

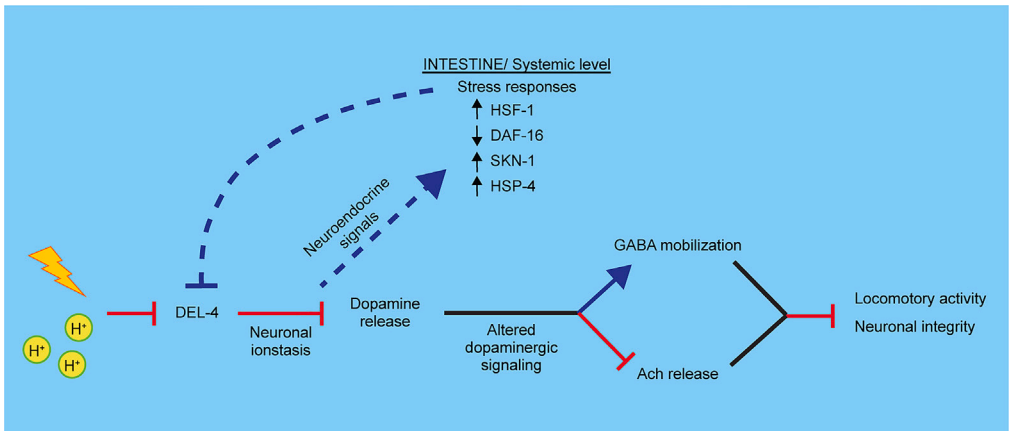

Figure 10. Proposed model

According to our results, we propose that several types of stress regulate the expression or the gating of the DEL-4 channel that acts in mediating stress perception. Consequently, modulation of DEL-4 by stress alters the downstream neuronal signaling through dopaminergic and motor neurons for the animal to adapt its behavioral response. Additionally, the altered neuronal signaling triggers the activation of stress response transcription factors that act through a feedback loop on the DEL-4 channel, to further modulate the stress response.

STAR★METHODS

Detailed methods are provided in the online version of this paper and include the following:

- KEY RESOURCES TABLE
- RESOURCE AVAILABILITY
  - Lead contact
  - Materials availability
  - Data and code availability
- EXPERIMENTAL MODEL AND STUDY PARTICIPANT DETAILS
  - Caenorhabditis elegans
  - Xenopus oocytes
- METHOD DETAILS
  - Generation of *C. elegans* transgenic lines
  - Genetic crosses
  - Molecular cloning
  - Total RNA isolation and qRT-analysis
  - Protein blast
  - RNAi treatment
  - Microscopy
  - Behavioural assays
  - DEL-4 expression and TEVC on Xenopus oocytes
  - Dil staining
  - Stress assays
  - Survival assays
  - Pharmacological assays
- QUANTIFICATION AND STATISTICAL ANALYSIS

SUPPLEMENTAL INFORMATION

Supplemental information can be found online at https://doi.org/10.1016/j.isci.2023.107117.

ACKNOWLEDGMENTS

We especially thank Eirini Lionaki for guidance with experiments and manuscript editing. We thank Angela Pasparaki for technical assistance and all members of our laboratory for useful discussions. Some nematode strains used in this work were provided by the *Caenorhabditis* Genetics Center, which is funded by

the National Center for Research Resources (NCRR) of the National Institutes of Health (NIH, USA), and S. Mitani (National Bioresource Project) in Japan. We thank A. Fire for plasmid vectors. We thank Nikos Kourtis for the construction of *del-4(tm717)* rescue strain. *C. elegans* strains *del-4(tm717)* and *unc-43(tm1605)* were generated by the International *C. elegans* gene knockout consortium. This project was supported by "Flagship Initiative for Neurodegenerative Diseases Research on the Basis of Precision Medicine, in the framework of Hellenic Precision Medicine Research Network for Neurodegenerative Diseases, of the project "Infrastructures for National Research Networks for Precision Medicine and Climate Change" no. 2018ΣΕ01300001 of the GSRT National Public Investments Programme. This project was supported by H2020 FETOPEN project "Dynamic" (EC-GA863203) to N.T. This project was also partially supported by the European Research Council under the grant agreement "ERC-GA695190-MANNA" to N.T. This research was also co-financed by the European Union (European Social Fund - ESF) and Greek national funds through the Operational Program "Education and Lifelong Learning" of the National Strategic Reference Framework (NSRF) 2007-2013 to N.T. Research Funding Program: THALES - Investing in Knowledge Society through the European Social Fund. Project "THALES - BSRC Alexander Fleming" - Development and employment of Minos-based genetic and functional genomic technologies in model organisms (MINOS) - MIS: 376898" to N.T. Additionally, through the Operational Program "Competitiveness, Entrepreneurship, Innovation" of the National Strategic Reference Framework (NSRF) 2014-2020, under the call RESEARCH – CREATE – INNOVATE (project code: T1EDK-01504, "EPHESIAN") to N.T.

AUTHOR CONTRIBUTIONS

Conceptualization, D.P. and N.T.; Methodology, D.P., M.G., E.K., and N.T.; Validation, D.P., M.G., and E.K.; Formal analysis, D.P., M.G., and E.K.; Investigation, D.P., M.G., and E.K.; Resources, W.S. and N.T.; Data curation, D.P., M.G., and E.K.; Writing - original draft, D.P., M.G., and E.K.; Writing - review and editing, D.P., M.G., E.K., W.S., and N.T.; Visualization, D.P., M.G., and E.K.; Supervision, W.S. and N.T.; Project administration, D.P. and N.T.; Funding acquisition, W.S. and N.T.

DECLARATION OF INTERESTS

The authors declare no competing interests.

INCLUSION AND DIVERSITY

We support inclusive, diverse, and equitable conduct of research.

Received: October 25, 2022
Revised: March 28, 2023
Accepted: June 9, 2023
Published: June 14, 2023

REFERENCES

1. Jang, M.S., Toyoshima, Y., Tomioka, M., Kunitomo, H., and Iino, Y. (2019). Multiple sensory neurons mediate starvation-dependent aversive navigation in Caenorhabditis elegans. Proc. Natl. Acad. Sci. USA *116*, 18673–18683.

2. Kim, K.W., and Jin, Y. (2015). Neuronal responses to stress and injury in C. elegans. FEBS Lett. *589*, 1644–1652.

3. Prahlad, V., Cornelius, T., and Morimoto, R.I. (2008). Regulation of the cellular heat shock response in Caenorhabditis elegans by thermosensory neurons. Science *320*, 811–814.

4. Kagias, K., Nehammer, C., and Pocock, R. (2012). Neuronal responses to physiological stress. Front. Genet. *3*, 222.

5. Cattaneo, A., and Riva, M.A. (2016). Stress-induced mechanisms in mental illness: a role for glucocorticoid signalling. J. Steroid Biochem. Mol. Biol. *160*, 169–174.

6. Fogaça, M.V., and Duman, R.S. (2019). Cortical GABAergic dysfunction in stress and depression: new insights for therapeutic interventions. Front. Cell. Neurosci. *13*, 87.

7. Guan, Z.Z. (2008). Cross-talk between oxidative stress and modifications of cholinergic and glutaminergic receptors in the pathogenesis of Alzheimer's disease. Acta Pharmacol. Sin. *29*, 773–780.

8. Juárez Olguín, H., Calderón Guzmán, D., Hernández García, E., and Barragán Mejía, G. (2016). The role of dopamine and its dysfunction as a consequence of oxidative stress. Oxid. Med. Cell. Longev. *2016*, 9730467.

9. Murnane, K.S. (2019). Serotonin 2A receptors are a stress response system: implications for post-traumatic stress disorder. Behav. Pharmacol. *30*, 151–162.

10. Chen, C., Wang, L., Rong, X., Wang, W., and Wang, X. (2015). Effects of fluoxetine on protein expression of potassium ion channels in the brain of chronic mild stress rats. Acta Pharm. Sin. B *5*, 55–61.

11. Zhou, J.J., Gao, Y., Kosten, T.A., Zhao, Z., and Li, D.P. (2017). Acute stress diminishes M-current contributing to elevated activity of hypothalamic-pituitary-adrenal axis. Neuropharmacology *114*, 67–76.

12. Park, J.Y., Dus, M., Kim, S., Abu, F., Kanai, M.I., Rudy, B., and Suh, G.S.B. (2016). Drosophila SLC5A11 mediates hunger by regulating K(+) channel activity. Curr. Biol. *26*, 1965–1974.

13. Nuñez-Villena, F., Becerra, A., Echeverría, C., Briceño, N., Porras, O., Armisén, R., Varela, D., Montorfano, I., Sarmiento, D.,

and Simon, F. (2011). Increased expression of the transient receptor potential melastatin 7 channel is critically involved in lipopolysaccharide-induced reactive oxygen species-mediated neuronal death. Antioxidants Redox Signal. *15*, 2425–2438.

14. Roedding, A.S., Tong, S.Y., Au-Yeung, W., Li, P.P., and Warsh, J.J. (2013). Chronic oxidative stress modulates TRPC3 and TRPM2 channel expression and function in rat primary cortical neurons: relevance to the pathophysiology of bipolar disorder. Brain Res. *1517*, 16–27.

15. Benemei, S., Fusi, C., Trevisan, G., and Geppetti, P. (2014). The TRPA1 channel in migraine mechanism and treatment. Br. J. Pharmacol. *171*, 2552–2567.

16. Wang, S., Yuan, F., and Li, D.P. (2017). M channels and stress response. Oncotarget *8*, 34026–34027.

17. Goodman, M.B., Hall, D.H., Avery, L., and Lockery, S.R. (1998). Active currents regulate sensitivity and dynamic range in C. elegans neurons. Neuron *20*, 763–772.

18. Liu, Q., Kidd, P.B., Dobosiewicz, M., and Bargmann, C.I. (2018). C. elegans AWA olfactory neurons fire calcium-mediated all-or-none action potentials. Cell *175*, 57–70.e17.

19. Bargmann, C.I. (1998). Neurobiology of the Caenorhabditis elegans genome. Science *282*, 2028–2033.

20. Lockery, S.R., and Goodman, M.B. (2009). The quest for action potentials in C. elegans neurons hits a plateau. Nat. Neurosci. *12*, 377–378.

21. Hanukoglu, I., and Hanukoglu, A. (2016). Epithelial sodium channel (ENaC) family: phylogeny, structure-function, tissue distribution, and associated inherited diseases. Gene *579*, 95–132.

22. Qadri, Y.J., Rooj, A.K., and Fuller, C.M. (2012). ENaCs and ASICs as therapeutic targets. Am. J. Physiol. Cell Physiol. *302*, C943–C965.

23. Dwyer, J.M., Rizzo, S.J.S., Neal, S.J., Lin, Q., Jow, F., Arias, R.L., Rosenzweig-Lipson, S., Dunlop, J., and Beyer, C.E. (2009). Acid sensing ion channel (ASIC) inhibitors exhibit anxiolytic-like activity in preclinical pharmacological models. Psychopharmacology (Berl) *203*, 41–52.

24. Zhou, W., Ye, S., Luo, R., Wu, L.M., and Wang, W. (2019). Inhibition of acid-sensing ion channels reduces the hypothalamus–pituitary–adrenal axis activity and ameliorates depression-like behavior in rats. RSC Adv. *9*, 8707–8713.

25. Ilatovskaya, D.V., Pavlov, T.S., Levchenko, V., and Staruschenko, A. (2013). ROS production as a common mechanism of ENaC regulation by EGF, insulin, and IGF-1. Am. J. Physiol. Cell Physiol. *304*, C102–C111.

26. Xu, H., and Chu, S. (2007). ENaC alpha-subunit variants are expressed in lung epithelial cells and are suppressed by oxidative stress. Am. J. Physiol. Lung Cell Mol. Physiol. *293*, L1454–L1462.

27. Andrey, F., Tsintsadze, T., Volkova, T., Lozovaya, N., and Krishtal, O. (2005). Acid sensing ionic channels: modulation by redox reagents. Biochim. Biophys. Acta *1745*, 1–6.

28. Cadiou, H., Studer, M., Jones, N.G., Smith, E.S.J., Ballard, A., McMahon, S.B., and McNaughton, P.A. (2007). Modulation of acid-sensing ion channel activity by nitric oxide. J. Neurosci. *27*, 13251–13260.

29. Arteaga, M.F., Coric, T., Straub, C., and Canessa, C.M. (2008). A brain-specific SGK1 splice isoform regulates expression of ASIC1 in neurons. Proc. Natl. Acad. Sci. USA *105*, 4459–4464.

30. Liu, W., Yuen, E.Y., and Yan, Z. (2010). The stress hormone corticosterone increases synaptic alpha-amino-3-hydroxy-5-methyl-4-isoxazolepropionic acid (AMPA) receptors via serum- and glucocorticoid-inducible kinase (SGK) regulation of the GDI-Rab4 complex. J. Biol. Chem. *285*, 6101–6108.

31. Pearce, D. (2003). SGK1 regulation of epithelial sodium transport. Cell. Physiol. Biochem. *13*, 13–20.

32. Xiong, Z., Liu, Y., Hu, L., Ma, B., Ai, Y., and Xiong, C. (2013). A rapid facilitation of acid-sensing ion channels current by corticosterone in cultured hippocampal neurons. Neurochem. Res. *38*, 1446–1453.

33. Ye, S., Yang, R., Xiong, Q., Yang, Y., Zhou, L., Gong, Y., Li, C., Ding, Z., Ye, G., and Xiong, Z. (2018). Acute stress enhances learning and memory by activating acid-sensing ion channels in rats. Biochem. Biophys. Res. Commun. *498*, 1078–1084.

34. Etchberger, J.F., Lorch, A., Sleumer, M.C., Zapf, R., Jones, S.J., Marra, M.A., Holt, R.A., Moerman, D.G., and Hobert, O. (2007). The molecular signature and cis-regulatory architecture of a C. elegans gustatory neuron. Genes Dev. *21*, 1653–1674.

35. McWilliam, H., Li, W., Uludag, M., Squizzato, S., Park, Y.M., Buso, N., Cowley, A.P., and Lopez, R. (2013). Analysis tool web services from the EMBL-EBI. Nucleic Acids Res. *41*, W597–W600.

36. An, J.H., and Blackwell, T.K. (2003). SKN-1 links C. elegans mesendodermal specification to a conserved oxidative stress response. Genes Dev. *17*, 1882–1893.

37. Murphy, C.T., McCarroll, S.A., Bargmann, C.I., Fraser, A., Kamath, R.S., Ahringer, J., Li, H., and Kenyon, C. (2003). Genes that act downstream of DAF-16 to influence the lifespan of Caenorhabditis elegans. Nature *424*, 277–283.

38. Trinklein, N.D., Murray, J.I., Hartman, S.J., Botstein, D., and Myers, R.M. (2004). The role of heat shock transcription factor 1 in the genome-wide regulation of the mammalian heat shock response. Mol. Biol. Cell *15*, 1254–1261.

39. Hibshman, J.D., Doan, A.E., Moore, B.T., Kaplan, R.E., Hung, A., Webster, A.K., Bhatt, D.P., Chitrakar, R., Hirschey, M.D., and Baugh, L.R. (2017). daf-16/FoxO promotes gluconeogenesis and trehalose synthesis during starvation to support survival. Elife *6*, e30057.

40. Weinkove, D., Halstead, J.R., Gems, D., and Divecha, N. (2006). Long-term starvation and ageing induce AGE-1/PI 3-kinase-dependent translocation of DAF-16/FOXO to the cytoplasm. BMC Biol. *4*, 1.

41. Kaplan, R.E.W., and Baugh, L.R. (2016). L1 arrest, daf-16/FoxO and nonautonomous control of post-embryonic development. Worm *5*, e1175196.

42. Hardie, D.G. (2018). Keeping the home fires burning: AMP-activated protein kinase. J. R. Soc. Interface *15*, 20170774.

43. An, J.H., Vranas, K., Lucke, M., Inoue, H., Hisamoto, N., Matsumoto, K., and Blackwell, T.K. (2005). Regulation of the Caenorhabditis elegans oxidative stress defense protein SKN-1 by glycogen synthase kinase-3. Proc. Natl. Acad. Sci. USA *102*, 16275–16280.

44. Sawin, E.R., Ranganathan, R., and Horvitz, H.R. (2000). C. elegans locomotory rate is modulated by the environment through a dopaminergic pathway and by experience through a serotonergic pathway. Neuron *26*, 619–631.

45. Chase, D.L., Pepper, J.S., and Koelle, M.R. (2004). Mechanism of extrasynaptic dopamine signaling in Caenorhabditis elegans. Nat. Neurosci. *7*, 1096–1103.

46. Mahoney, T.R., Luo, S., and Nonet, M.L. (2006). Analysis of synaptic transmission in Caenorhabditis elegans using an aldicarb-sensitivity assay. Nat. Protoc. *1*, 1772–1777.

47. Gründer, S., and Pusch, M. (2015). Biophysical properties of acid-sensing ion channels (ASICs). Neuropharmacology *94*, 9–18.

48. Bartoi, T., Augustinowski, K., Polleichtner, G., Gründer, S., and Ulbrich, M.H. (2014). Acid-sensing ion channel (ASIC) 1a/2a heteromers have a flexible 2:1/1:2 stoichiometry. Proc. Natl. Acad. Sci. USA *111*, 8281–8286.

49. Canessa, C.M., Schild, L., Buell, G., Thorens, B., Gautschi, I., Horisberger, J.D., and Rossier, B.C. (1994). Amiloride-sensitive epithelial Na+ channel is made of three homologous subunits. Nature *367*, 463–467.

50. Yang, L., and Palmer, L.G. (2014). Ion conduction and selectivity in acid-sensing ion channel 1. J. Gen. Physiol. *144*, 245–255.

51. Kaulich, E., McCubbin, P.T.N., Schafer, W.R., and Walker, D.S. (2023). Physiological insight into the conserved properties of Caenorhabditis elegans acid-sensing degenerin/epithelial sodium channels. J. Physiol. *601*, 1625–1653.

52. Eastwood, A.L., and Goodman, M.B. (2012). Insight into DEG/ENaC channel gating from

genetics and structure. Physiology *27*, 282–290.

53. Collier, D.M., and Snyder, P.M. (2009). Extracellular chloride regulates the epithelial sodium channel. J. Biol. Chem. *284*, 29320–29325.

54. St-Pierre, F., Marshall, J.D., Yang, Y., Gong, Y., Schnitzer, M.J., and Lin, M.Z. (2014). High-fidelity optical reporting of neuronal electrical activity with an ultrafast fluorescent voltage sensor. Nat. Neurosci. *17*, 884–889.

55. Krashia, P., Nobili, A., and D'Amelio, M. (2019). Unifying hypothesis of dopamine neuron loss in neurodegenerative diseases: focusing on alzheimer's disease. Front. Mol. Neurosci. *12*, 123.

56. Masato, A., Plotegher, N., Boassa, D., and Bubacco, L. (2019). Impaired dopamine metabolism in Parkinson's disease pathogenesis. Mol. Neurodegener. *14*, 35.

57. Simunovic, F., Yi, M., Wang, Y., Macey, L., Brown, L.T., Krichevsky, A.M., Andersen, S.L., Stephens, R.M., Benes, F.M., and Sonntag, K.C. (2009). Gene expression profiling of substantia nigra dopamine neurons: further insights into Parkinson's disease pathology. Brain *132*, 1795–1809.

58. Houghton, P.J., and Howes, M.J. (2005). Natural products and derivatives affecting neurotransmission relevant to Alzheimer's and Parkinson's disease. Neurosignals *14*, 6–22.

59. Austin, K.W., Ameringer, S.W., and Cloud, L.J. (2016). An integrated review of psychological stress in Parkinson's disease: biological mechanisms and symptom and health outcomes. Parkinsons Dis. *2016*, 9869712.

60. Rothman, S.M., and Mattson, M.P. (2010). Adverse stress, hippocampal networks, and Alzheimer's disease. NeuroMolecular Med. *12*, 56–70.

61. Cao, S., Gelwix, C.C., Caldwell, K.A., and Caldwell, G.A. (2005). Torsin-mediated protection from cellular stress in the dopaminergic neurons of Caenorhabditis elegans. J. Neurosci. *25*, 3801–3812.

62. Fatouros, C., Pir, G.J., Biernat, J., Koushika, S.P., Mandelkow, E., Mandelkow, E.M., Schmidt, E., and Baumeister, R. (2012). Inhibition of tau aggregation in a novel Caenorhabditis elegans model of tauopathy mitigates proteotoxicity. Hum. Mol. Genet. *21*, 3587–3603.

63. Bangsbo, J., Johansen, L., Graham, T., and Saltin, B. (1993). Lactate and H+ effluxes from human skeletal muscles during intense, dynamic exercise. J. Physiol. *462*, 115–133.

64. Guo, Y., Zhou, I.Y., Chan, S.T., Wang, Y., Mandeville, E.T., Igarashi, T., Lo, E.H., Ji, X., and Sun, P.Z. (2016). pH-sensitive MRI demarcates graded tissue acidification during acute stroke - pH specificity enhancement with magnetization transfer and relaxation-normalized amide proton transfer (APT) MRI. Neuroimage *141*, 242–249.

65. Ichihara, K., Haga, N., and Abiko, Y. (1984). Is ischemia-induced pH decrease of dog myocardium respiratory or metabolic acidosis? Am. J. Physiol. *246*, H652–H657.

66. Engin, K., Leeper, D.B., Cater, J.R., Thistlethwaite, A.J., Tupchong, L., and McFarlane, J.D. (1995). Extracellular pH distribution in human tumours. Int. J. Hyperther. *11*, 211–216.

67. Simmen, H.P., and Blaser, J. (1993). Analysis of pH and pO2 in abscesses, peritoneal fluid, and drainage fluid in the presence or absence of bacterial infection during and after abdominal surgery. Am. J. Surg. *166*, 24–27.

68. Johnson, D., Allman, E., and Nehrke, K. (2012). Regulation of acid-base transporters by reactive oxygen species following mitochondrial fragmentation. Am. J. Physiol. Cell Physiol. *302*, C1045–C1054.

69. Johnson, D., and Nehrke, K. (2010). Mitochondrial fragmentation leads to intracellular acidification in Caenorhabditis elegans and mammalian cells. Mol. Biol. Cell *21*, 2191–2201.

70. Benomar, S., Lansdon, P., Bender, A.M., Peterson, B.R., Chandler, J.R., and Ackley, B.D. (2020). The C. elegans CHP1 homolog, pbo-1, functions in innate immunity by regulating the pH of the intestinal lumen. PLoS Pathog. *16*, e1008134.

71. Rook, M.L., Musgaard, M., and MacLean, D.M. (2021). Coupling structure with function in acid-sensing ion channels: challenges in pursuit of proton sensors. J. Physiol. *599*, 417–430.

72. Wang, Y., Apicella, A., Jr., Lee, S.K., Ezcurra, M., Slone, R.D., Goldmit, M., Schafer, W.R., Shaham, S., Driscoll, M., and Bianchi, L. (2008). A glial DEG/ENaC channel functions with neuronal channel DEG-1 to mediate specific sensory functions in C. elegans. EMBO J. *27*, 2388–2399.

73. Zhang, P., Fyfe, G.K., Grichtchenko, I.I., and Canessa, C.M. (1999). Inhibition of alphabeta epithelial sodium channels by external protons indicates that the second hydrophobic domain contains structural elements for closing the pore. Biophys. J. *77*, 3043–3051.

74. Amin, M.S., Wang, H.W., Reza, E., Whitman, S.C., Tuana, B.S., and Leenen, F.H.H. (2005). Distribution of epithelial sodium channels and mineralocorticoid receptors in cardiovascular regulatory centers in rat brain. Am. J. Physiol. Regul. Integr. Comp. Physiol. *289*, R1787–R1797.

75. Geffeney, S.L., Cueva, J.G., Glauser, D.A., Doll, J.C., Lee, T.H.C., Montoya, M., Karania, S., Garakani, A.M., Pruitt, B.L., and Goodman, M.B. (2011). DEG/ENaC but not TRP channels are the major mechanoelectrical transduction channels in a C. elegans nociceptor. Neuron *71*, 845–857.

76. Liu, X., Liu, C., Ye, J., Zhang, S., Wang, K., and Su, R. (2020). Distribution of acid sensing ion channels in axonal growth cones and presynaptic membrane of cultured hippocampal neurons. Front. Cell. Neurosci. *14*, 205.

77. Voglis, G., and Tavernarakis, N. (2008). A synaptic DEG/ENaC ion channel mediates learning in C. elegans by facilitating dopamine signalling. EMBO J. *27*, 3288–3299.

78. Hooper, P.L., Durham, H.D., Török, Z., Hooper, P.L., Crul, T., and Vígh, L. (2016). The central role of heat shock factor 1 in synaptic fidelity and memory consolidation. Cell Stress Chaperones *21*, 745–753.

79. Kim, S.Y., and Webb, A.E. (2017). Neuronal functions of FOXO/DAF-16. Nutr. Healthy Aging *4*, 113–126.

80. Martínez, G., Khatiwada, S., Costa-Mattioli, M., and Hetz, C. (2018). ER proteostasis control of neuronal physiology and synaptic function. Trends Neurosci. *41*, 610–624.

81. Staab, T.A., Griffen, T.C., Corcoran, C., Evgrafov, O., Knowles, J.A., and Sieburth, D. (2013). The conserved SKN-1/Nrf2 stress response pathway regulates synaptic function in Caenorhabditis elegans. PLoS Genet. *9*, e1003354.

82. Wilson, M.A., Iser, W.B., Son, T.G., Logie, A., Cabral-Costa, J.V., Mattson, M.P., and Camandola, S. (2017). skn-1 is required for interneuron sensory integration and foraging behavior in Caenorhabditis elegans. PLoS One *12*, e0176798.

83. Taylor, H.B.C., and Jeans, A.F. (2021). Friend or foe? The varied faces of homeostatic synaptic plasticity in neurodegenerative disease. Front. Cell. Neurosci. *15*, 782768.

84. Ortega-Ramírez, A., Vega, R., and Soto, E. (2017). Acid-Sensing ion channels as potential therapeutic targets in neurodegeneration and neuroinflammation. Mediat. Inflamm. *2017*, 3728096.

85. Mari, Y., Katnik, C., and Cuevas, J. (2010). ASIC1a channels are activated by endogenous protons during ischemia and contribute to synergistic potentiation of intracellular Ca(2+) overload during ischemia and acidosis. Cell Calcium *48*, 70–82.

86. Aoyama, K., Burns, D.M., Suh, S.W., Garnier, P., Matsumori, Y., Shiina, H., and Swanson, R.A. (2005). Acidosis causes endoplasmic reticulum stress and caspase-12-mediated astrocyte death. J. Cerebr. Blood Flow Metabol. *25*, 358–370.

87. Swanson, R.A., Farrell, K., and Simon, R.P. (1995). Acidosis causes failure of astrocyte glutamate uptake during hypoxia. J. Cerebr. Blood Flow Metabol. *15*, 417–424.

88. Kirby, J., Ning, K., Ferraiuolo, L., Heath, P.R., Ismail, A., Kuo, S.W., Valori, C.F., Cox, L., Sharrack, B., Wharton, S.B., et al. (2011). Phosphatase and tensin homologue/protein kinase B pathway linked to motor

neuron survival in human superoxide dismutase 1-related amyotrophic lateral sclerosis. Brain *134*, 506–517.

89. Lu, B., Su, Y., Das, S., Liu, J., Xia, J., and Ren, D. (2007). The neuronal channel NALCN contributes resting sodium permeability and is required for normal respiratory rhythm. Cell *129*, 371–383.

90. Cochet-Bissuel, M., Lory, P., and Monteil, A. (2014). The sodium leak channel, NALCN, in health and disease. Front. Cell. Neurosci. *8*, 132.

91. Berends, A.C., Luiten, P.G.M., and Nyakas, C. (2005). A review of the neuroprotective properties of the 5-HT1A receptor agonist repinotan HCl (BAYx3702) in ischemic stroke. CNS Drug Rev. *11*, 379–402.

92. Eijkelkamp, N., Linley, J.E., Baker, M.D., Minett, M.S., Cregg, R., Werdehausen, R., Rugiero, F., and Wood, J.N. (2012). Neurological perspectives on voltage-gated sodium channels. Brain *135*, 2585–2612.

93. Rasheed, N., Ahmad, A., Pandey, C.P., Chaturvedi, R.K., Lohani, M., and Palit, G. (2010). Differential response of central dopaminergic system in acute and chronic unpredictable stress models in rats. Neurochem. Res. *35*, 22–32.

94. Schneider, C.A., Rasband, W.S., and Eliceiri, K.W. (2012). NIH Image to ImageJ: 25 years of image analysis. Nat. Methods *9*, 671–675.

95. Nonet, M.L., Holgado, A.M., Brewer, F., Serpe, C.J., Norbeck, B.A., Holleran, J., Wei, L., Hartwieg, E., Jorgensen, E.M., and Alfonso, A. (1999). UNC-11, a Caenorhabditis elegans AP180 homologue, regulates the size and protein composition of synaptic vesicles. Mol. Biol. Cell *10*, 2343–2360.

96. Sanjiib Guha, G.C., and Kapahi, P. (2018). Morphological analysis of dopaminergic neurons with age using Caenorhabditis elegans GFP reporter strains. bio-protocol.

97. Brenner, S. (1974). The genetics of Caenorhabditis elegans. Genetics *77*, 71–94.

98. Fay, D.S. (2013). Classical Genetic Methods (WormBook), pp. 1–58.

99. Mello, C.C., Kramer, J.M., Stinchcomb, D., and Ambros, V. (1991). Efficient gene transfer in C.elegans: extrachromosomal maintenance and integration of transforming sequences. EMBO J. *10*, 3959–3970.

100. Praitis, V., Casey, E., Collar, D., and Austin, J. (2001). Creation of low-copy integrated transgenic lines in Caenorhabditis elegans. Genetics *157*, 1217–1226.

101. Sieburth, D., Madison, J.M., and Kaplan, J.M. (2007). PKC-1 regulates secretion of neuropeptides. Nat. Neurosci. *10*, 49–57.

102. Dittman, J.S., and Kaplan, J.M. (2006). Factors regulating the abundance and localization of synaptobrevin in the plasma membrane. Proc. Natl. Acad. Sci. USA *103*, 11399–11404.

103. Kaulich, E., Carroll, T., Ackley, B.D., Tang, Y.Q., Hardege, I., Nehrke, K., Schafer, W.R., and Walker, D.S. (2022). Distinct roles for two Caenorhabditis elegans acid-sensing ion channels in an ultradian clock. Elife *11*, e75837.

104. Paukert, M., Babini, E., Pusch, M., and Gründer, S. (2004). Identification of the Ca2+ blocking site of acid-sensing ion channel (ASIC) 1: implications for channel gating. J. Gen. Physiol. *124*, 383–394.

105. Hardege, I., Xu, S., Gordon, R.D., Thompson, A.J., Figg, N., Stowasser, M., Murrell-Lagnado, R., and O'Shaughnessy, K.M. (2015). Novel insertion mutation in KCNJ5 channel produces constitutive aldosterone release from H295R cells. Mol. Endocrinol. *29*, 1522–1530.

106. Awayda, M.S., and Subramanyam, M. (1998). Regulation of the epithelial Na+ channel by membrane tension. J. Gen. Physiol. *112*, 97–111.

107. Hedgecock, E.M., Culotti, J.G., Thomson, J.N., and Perkins, L.A. (1985). Axonal guidance mutants of Caenorhabditis elegans identified by filling sensory neurons with fluorescein dyes. Dev. Biol. *111*, 158–170.

108. Morley, J.F., and Morimoto, R.I. (2004). Regulation of longevity in Caenorhabditis elegans by heat shock factor and molecular chaperones. Mol. Biol. Cell *15*, 657–664.

109. You, Y.J., Kim, J., Cobb, M., and Avery, L. (2006). Starvation activates MAP kinase through the muscarinic acetylcholine pathway in Caenorhabditis elegans pharynx. Cell Metabol. *3*, 237–245.

STAR★METHODS

KEY RESOURCES TABLE

REAGENT or RESOURCE	SOURCE	IDENTIFIER
Bacterial and virus strains		
Escherichia coli: OP50	Jonathan Ewbank lab; *Caenorhabditis* Genetics Center (CGC)	WB-STRAIN: WBStrain00041971; WormBase ID: WBStrain00041971
Escherichia coli: HB101 strain: *E. coli* [supE44 hsdS20(rB-mB-) recA13 ara-14 proA2 lacY1 galK2 rpsL20 xyl-5 mtl-1]	*Caenorhabditis* Genetics Center (CGC)	WB-STRAIN: WBStrain00041075; WormBase ID: WBStrain00041075
Escherichia coli: Ht115 (DE3): *E. coli* [F-, mcrA, mcrB, IN(rrnD-rrnE)1, rnc14::Tn10 (DE3 lysogen: lacUV5 promoter -T7 polymerase].	*Caenorhabditis* Genetics Center (CGC)	WB-STRAIN:HT115; WormBase ID: WBStrain00041079
Escherichia coli: Na22	*Caenorhabditis* Genetics Center (CGC)	WB-STRAIN: WBStrain00041948; WormBase ID: WBStrain00041948
Chemicals, peptides, and recombinant proteins		
Levamisole	Sigma-Aldrich	Product No.: PHR1798; CAS: 16595-80-5
Tetramisole hydrochloride	Sigma-Aldrich	Product No.: L9756; CAS: 16595-80-5
Paraquat (N, N′-dimethyl-4,4′-bipyridinium dichloride)	Sigma-Aldrich	Product No.: 36541; CAS: 75365-73-0
Tunicamycin from *Streptomyces sp.*	Sigma-Aldrich	Beilstein No.: 6888090;CAS: 11089-65-9
Dopamine hydrochloride	Sigma-Aldrich	Beilstein No.: 3656720; CAS: 62-31-7
UltraPure Agarose	Invitrogen	Cat.#: 16500500
Ethidium Bromide	Sigma-Aldrich	Cat.#: 1.11615.0010; CAS: 1239-45-8
Nanobeads NIST Traceable Particle Size Standard 100 nm	Polysciences	Cat.#: 64010-15
DiI (dioctadecyl tetramethylindodicarbocyanine-disulphonic acid)	Invitrogen	Cat.#: N22880
Aldicarb	Sigma-Aldrich	Product No. 33386; CAS: 116-06-3
TRIzol reagent	Invitrogen	Cat.#: 15596026
pcDNA3.1 /Puro - CAG - ASAP1 plasmid	Schnitzer et al., 2014[53]	Addgene plamid#52519; RRID:Addgene_52519
pPD95.77 (L2464)	Fire Lab *C. elegans* Vector Kit – 1995; http://n2t.net/addgene:1495	Addgene plasmid# 1495; RRID:Addgene_1495
pL4440	Fire Lab *C. elegans* Vector Kit – 1999; http://n2t.net/addgene:1654	Addgene plasmid# 1654; RRID:Addgene_1654
pPD96.52 (L2534)	Fire Lab *C. elegans* Vector Kit – 1999; http://n2t.net/addgene:1608	Addgene plasmid#1608; RRID:Addgene_1608
pPK719 (unc-119) rescue	Roger Pocock lab (BRIC, Copenhagen, Denmark); http://n2t.net/addgene:38149	Addgene, plasmid #38149; RRID:Addgene_38149
Critical commercial assays		
NucleoSpin Tissue, Mini kit for DNA from cells and tissue	Macherey-Nagel	Cat. # 740952.250
Topo TA Cloning Kit	Invitrogen	Cat.# K457501
iScript™ cDNA Synthesis Kit	Bio-Rad	Cat.#: 1708890
SuperScript™ III First-Strand Synthesis System	Invitrogen	Cat. # 18080051

(*Continued on next page*)

Continued

REAGENT or RESOURCE	SOURCE	IDENTIFIER
NEB Q5® Site-Directed Mutagenesis Kit	New England BioLabs	Cat. # E0554S
NEBuilder® HiFi DNA Assembly Master Mix	New England BioLabs	Cat. # E2621L
mMESSAGE mMACHINE™ T7 Transcription Kit	Ambion	Cat.# AM1344
Deposited data		
WormBase	International consortium for *C. elegans* and related nematodes	https://wormbase.org//#012-34-5
Blast: Basic Local Alignment Search Tool - NCBI	NIH: National Library of Medicine – National Center for Biotechnology Information	https://blast.ncbi.nlm.nih.gov/Blast.cgi
WormBook	THE ONLINE REVIEW OF *C. elegans* BIOLOGY	http://wormbook.org/
Experimental models: Organisms/strains		
C. elegans strains, see Table 1		
Xenopus laevis oocytes	EcoCyte Bioscience (Dortmund, Germany)	N/A
Oligonucleotides		
For primers, see Table 2		
Recombinant DNA		
del-2 (exons 5-12) in pL4440 (RNAi)	This paper	N/A
del-3 (exons 2-7) in pL4440 (RNAi)	This paper	N/A
del-4 (exons 1-10) in pL4440 (RNAi)	This paper	N/A
p_{del-2}DsRed transcriptional reporter in the pPD95.77 plasmid vector	This paper	N/A
p_{del-3}DsRed transcriptional reporter in the pPD95.77 plasmid vector	This paper	N/A
p_{del-4}mCherry transcriptional reporter in the pPD95.77 plasmid vector	This paper	N/A
p_{del-2}DEL-2::mCherry translational reporter in pPD95.77	This paper	N/A
p_{del-3}DEL-3::DsRed translational reporter in pPD95.77	This paper	N/A
p_{del-4}DEL-4::GFP translational reporter in pPD95.77	This paper	N/A
p_{del-4}DEL-4::DsRed translational reporter in pPD95.77	This paper	N/A
p_{del-4}SNB-1::DsRed synaptic vesicle marker in pPD95.77	This paper	N/A
p_{dat-1}ASAP-1 voltage sensor in pPD96.52	This paper	N/A
pEK230: *del-4* cDNA in the KSM vector	This paper	N/A
pEK238: *del-4(tm717)* cDNA in the KSM vector	This paper	N/A
Software and algorithms		
ImageJ 1.48V	Schneider et al.[93]	https://imagej.nih.gov/ij/index.html; RRID: SCR_003070
GraphPad Prism 8.0.2	GraphPad Software	https://www.graphpad.com/
Photoshop CS5	Adobe	https://www.adobe.com/gr_en/products/photoshop/landpb.html
Volocity High-Performance 3D imaging software	Volocity	https://www.volocity4d.com/

(*Continued on next page*)

Continued

REAGENT or RESOURCE	SOURCE	IDENTIFIER
SnapGene Viewer	SnapGene by Dotmatics	https://www.snapgene.com/snapgene-viewer
CenGen	CeNGEN - THE COMPLETE GENE EXPRESSION MAP OF THE C. ELEGANS NERVOUS SYSTEM	https://www.cengen.org/
Phobius tool	Stockholm Bioinformatics Centre; McWilliam et al.[35]	http://phobius.sbc.su.se/

RESOURCE AVAILABILITY

Lead contact

Further information and requests for resources and reagents should be directed to and will be fulfilled by the lead contact, Tavernarakis Nektarios (tavernarakis@imbb.forth.gr).

Materials availability

Plasmids and *C. elegans* lines generated in this study will be available upon request.

Data and code availability

- All data reported in this paper will be shared by the lead contact upon request.
- This paper does not report original code.
- Any additional information required to reanalyse the data reported in this paper is available from the lead contact upon request.

EXPERIMENTAL MODEL AND STUDY PARTICIPANT DETAILS

Caenorhabditis elegans

Nematodes were maintained following standard procedures, as previously described.[97] Stocks were maintained on 5cm NGM plates seeded with OP50 (KRT). Animal rearing temperature was kept at 20°C unless otherwise noted. The OP50 *E. coli* strain was preferably used as a food source except for RNAi experiments, where NGM plates were seeded with HT115 (DE3) bacteria (KRT), carrying the desired RNAi plasmid construct. HB101 *E. coli* bacteria (KRT) were used to form a thin bacterial lawn for the basal slowing response assay.

Isogenic hermaphrodite populations of the same developmental stage were used in all experiments. *C. elegans* has a lifespan of approximately 20 days at 20°C, during which it passes through four larval stages (l1-l4) before reaching adulthood. All experiments were performed during adulthood, with the only exception being the starvation survival assay that monitors animals from the l1 stage until adulthood. Imaging after heat stress and starvation was conducted on day two of adulthood. Animals grown on RNAi plates were imaged on day three or four of adulthood. Animals from the rest of the experiments were imaged on day one of adulthood. The exact day of adulthood that each experiment was performed is also reported in the figure legends.

Males emerge spontaneously in a population (frequency ~0.02 %). A larger male population was obtained following a mild heat sock (3-4 hrs at 35°C or 2s hr at 37°C) of late l4 stage animals.[98] Males were maintained through mating with hermaphrodites. In this study, males were used only for genetic crossing.

Variations *tm717* and *tm5642* were verified by polymerase chain reaction (PCR) using the primers 5′-AAAAGTGTGGACCCGGATAT-3′ and 5′-ACCAAGAGAGGAAGCAGTTCC-3′, 5′-ATGTGGCTCCGAG GACTTTTC-3′ and 5′- GCAATCAGACACCACACCCAGTA-3′ (Table 2). The strains used in this study are listed in Table 1. Strains *unc-119(ed3)*;Ex[$p_{del\text{-}2}$DEL-$2_{1\text{-}27}$::DsRed; *unc-119*(+)], *unc-119(ed3)*;Ex[$p_{del\text{-}3}$DEL-$3_{1\text{-}45}$::DsRed; *unc-119*(+)] and *unc-119(ed3)*;Ex[$p_{del\text{-}4}$DEL-$4_{1\text{-}36}$::mCherry; *unc-119*(+)] are referred in the text as $p_{del\text{-}2}$DsRed, $p_{del\text{-}3}$DsRed and $p_{del\text{-}4}$mCherry, respectively (Table 1).

Xenopus oocytes

Electrophysiology experiments were performed with *Xenopus laevis* oocytes. *Xenopus* oocytes were obtained from EcoCyte Bioscience (Dortmund, Germany) (KRT). They were maintained at 16°C in 1X ND96 solution (96 mM NaCl, 2 mM $MgCl_2$, 2 mM KCl, 1.8 mM $CaCl_2$, pH 7.4).

METHOD DETAILS

Generation of *C. elegans* transgenic lines

Genetic transformation with microinjection

For the generation of transgenic animals, plasmid DNAs were mixed, at a concentration of 50 ng/ml of the plasmid of interest with 50 ng/ml of the pRF4 plasmid bearing the dominant mutation *su1006* of the *rol-6* gene.[99] The dominant mutation *su1006* causes the roller phenotype. The DNA mixtures were microinjected into the gonads of N2 young adult hermaphrodite animals. F1 transgenic progeny were selected based on the roller phenotype to establish independent lines. Translational reporter fusion lines of *del-4* with the DsRed and ASAP1 were generated by injection. The roller phenotype of the line $p_{del\text{-}4}$DEL-4:: DsRed; *rol-6(su1006)* was used for crosses with the strains BZ555, BZ555;BR5270 and UA44.

Biolistic transformation of C. elegans

The second method used to generate transgenic animals was the gold nanoparticle bombardment (biolistic transformation). We used 10 μg of the construct bearing the desired gene and 10 μg of the pPK719 rescue plasmid DNA, carrying the coding sequence of the *unc-119* gene.[100] Transformed animals bearing the *unc-119* rescue construct exhibit wild-type locomotion. DNAs were bombarded on hermaphrodite *unc-119(ed3)* locomotion defective mutant animals of stage L4 or young adulthood, cultured on 9 cm Na22-seeded plates (KRT). The remaining constructs, apart from the two generated with microinjection, including another one translational reporter of *del-4* with DsRed, were introduced into *C. elegans* with biolistic transformation. The $p_{del\text{-}4}$DEL-4::GFP;$p_{del\text{-}4}$SNB-1::DsRed line was generated by co-bombardment of a DNA mixture containing 7 μg $p_{del\text{-}4}$DEL-4::GFP, 7 μg $p_{del\text{-}4}$SNB-1::DsRed and 7 μg *unc-119* rescue plasmid DNA.

Genetic crosses

Generation of males was achieved with a mild heat sock (3-4 hrs at 35°C or 2 hrs at 37°C) of late l4 stage animals.[98] For each mating ~6 hermaphrodites of one genotype were placed in a 3 cm OP50-seeded petri plate with ~18 males. Mating was considered successful when an increased number of male progenies was observed in the plate. Selection of transgenic lines was achieved by exploiting the roller phenotype, by using a UV stereoscope (epifluorescence microscope NIKON SMZ800N) to select fluorescent reporters or by isolating genomic DNA (NucleoSpin Tissue, Mini kit for DNA) (KRT) and performing PCR when selection of genes mutations was needed (see Table 2 for primer sequences).

The following reporters and double mutants were generated by standard genetic crosses (also Tables 1, 2 and S4): *unc-119(ed3)*;Ex[$p_{del\text{-}2}$DEL-$2_{1\text{-}27}$::DsRed; $p_{flp\text{-}8}$GFP;*unc-119*(+)], *unc-119(ed3)*;Ex[$p_{del\text{-}2}$DEL-$2_{1\text{-}27}$::DsRed; OSM-10::GFP;*unc-119*(+)], *unc-119(ed3)*;Ex[$p_{del\text{-}2}$DEL-$2_{1\text{-}27}$::DsRed; $p_{dat\text{-}1}$GFP;*unc-119*(+)], *unc-119(ed3)*;Ex[$p_{del\text{-}3}$DEL-$3_{1\text{-}45}$::DsRed; $p_{flp\text{-}8}$GFP;*unc-119*(+)], *unc-119(ed3)*;Ex[$p_{del\text{-}3}$DEL-$3_{1\text{-}45}$::DsRed; OSM-10::GFP;*unc-119*(+)], *unc-119(ed3)*;Ex[$p_{del\text{-}3}$DEL-$3_{1\text{-}45}$::DsRed; $p_{dat\text{-}1}$GFP;*unc-119*(+)], *unc-119(ed3)*;Ex[$p_{del\text{-}3}$DEL-$3_{1\text{-}45}$::DsRed;TPH-1::GFP;*unc-119*(+);*rol-6(su1006)*], *unc-119(ed3)*;Ex[$p_{del\text{-}4}$DEL-$4_{1\text{-}36}$::mCherry; $p_{flp\text{-}8}$GFP;*unc-119*(+)], *unc-119(ed3)*;Ex[$p_{del\text{-}4}$DEL-$4_{1\text{-}36}$::mCherry; OSM-10::GFP;*unc-119*(+)], *unc119(ed3)*; Ex[p_{del4}DEL$4_{1\text{-}36}$::mCherry; p_{dat1}GFP;*unc-119*(+)], *unc119(ed3)*;Ex[p_{del4}DEL$4_{1\text{-}36}$::mCherry; TPH1::GFP; *unc-119*(+);*rol-6(su1006)*], *unc-119(ed3)*;Ex[$p_{del\text{-}4}$DEL-$4_{1\text{-}36}$::mCherry; $p_{acr\text{-}2}$GFP;*unc-119*(+)], *del-4(tm717)*; zcls4[$p_{hsp\text{-}4}$GFP], *del-4(tm717);* uthls202[aak-2(intron1)::aak-2(aa1-aa321)::Tomato::unc-54 3′UTR ; *rol-6(su 1006)]*, *del-4(tm717)*;skn-1b/c::GFP, *del-4(tm717)*; $p_{asic\text{-}1}$SNB-1::SEpHluorin; *rol-6(su1006)*, *del-4(tm717)*; [*unc-119(ed3)*; oxSi834[P $_{unc\text{-}47}$GFP::SNB-::unc-54 UTR; *unc-119*(+)], *del-4(tm717)*; nuIs183 [p_{unc129}NLP-21::Venus; $p_{myo\text{-}2}$NLS::GFP], *del-4(tm717);* $p_{dat\text{-}1}$ASAP-1; *rol-6(su1006)*], *del-4(tm717)*; egIs1[$p_{dat\text{-}1}$GFP], $p_{del\text{-}4}$ DEL-4:: DsRed; egIs1 [$p_{dat\text{-}1}$GFP]; *rol-6(su1006)*, byIs161 [$p_{rab\text{-}3}$F3(delta)K280 + $p_{myo\text{-}2}$mCherry]; egIs1 [$p_{dat\text{-}1}$GFP], *del-4(tm717)*; byIs161 [$p_{rab\text{-}3}$F3(delta)K280 + $p_{myo\text{-}2}$mCherry]; egIs1 [$p_{dat\text{-}1}$GFP], $p_{del\text{-}4}$DEL-4::DsRed; *rol-6(su1006)*; byIs161 [$p_{rab\text{-}3}$F3(delta)K280 + $p_{myo\text{-}2}$mCherry]; egIs1 [$p_{dat\text{-}1}$GFP], *del-4(tm717)*; baIn11[$p_{dat\text{-}1}$::a-Synuclein; $p_{dat\text{-}1}$GFP], $p_{del\text{-}4}$DEL-4:: DsRed; *rol-6(su1006)*]; baIn11[$p_{dat\text{-}1}$a-Synuclein; $p_{dat\text{-}1}$GFP], *del-4(tm717);dop-1(vs100)*, *del-4(tm717);dop-2(vs105)*, *del-4(tm717);dop-3(vs106)*, *del-4(tm717);pkc-1(ok563)*, *del-4(tm717);pkc-2 (ok328)*, *del-4(tm717);tpa-1 (k501)*, *del-4(tm717);kin-2*

(ce179), del-4(tm717);unc-43(tm1605), del-4(tm717); $p_{hsp-16.2}$::GFP, *del-4(tm717);* dvIs19 [(pAF15) gst-4p::GFP::NLS)], *del-4(tm717);*p_{sod-3}::GFP, *del-4(tm717);* $P_{let-858}$GCaMP2.0; *rol-6(su1006).*

Molecular cloning

All genomic sequences were retrieved from WormBase (www.wormbase.org). To generate a construct for induction of *del-4* RNAi, the *del-4* gene was amplified with PCR from wt genomic DNA isolated from the N2 strain (Nucleospin Tissue kit – see KRT). Subsequently, the PCR product was inserted into the Topo vector (KRT), and subcloned in the pL4440 plasmid vector. Amplified region corresponds to exons 1-10 of the *del-4* gene. The resulting construct was transformed into the Ht115 (DE3) *E. coli* strain (KRT). Ht115 bacteria carrying the empty pL4440 vector were used as a control food in the experiments that use the RNAi technique for gene downregulation. The primers used for the amplification of *del-4* (exons 1-10) were 5′-GATGGGTGTATTTTGGACCG-3′ and 5′-TCAAGACACGATTCTCCTGA-3′ (Table 2).

Conventional cloning procedures were followed for the construction of the translational and transcriptional reporters expressed in *C. elegans*. The promoter region and the first exon of each gene were amplified from wt genomic DNA isolated from the N2 strain, for the generation of p_{del-2}DsRed, p_{del-3}DsRed, and p_{del-4}mCherry transcriptional reporters (KRT). They were inserted in the Topo vector and subcloned in the pPD95.77 plasmid vector (KRT) in frame and at the amino (N) terminus of a pre-existing DsRed or mCherry fluorescent protein. The promoter regions amplified were 1.3 Kb upstream to the start codon of *del-2*, 2 Kb of *del-3*, and 1.5 Kb of *del-4*. The primers used were 5′-TCTTATGATGCACGGCG-3′ and 5′-GGTACCCGTCCACTATTAGTAAT-3′ for del-2, 5′-GCATGCTTACATTTGAGGGTTTAG-3′ and 5′-ACCG GTGTTTTCGATTCAGTTTT-3′ for del-3, 5′-CTGCAGGTCGACACATCATAAATC-3′ and 5′-ACCGGTCC TCAACCATCGAGCATTT-3′ for *del-4* (Table 2). Excision of DNA sequences from the Topo vector was performed with HindIII/XhoI for *del-2* and *del-3*, and with EcoRI for *del-4*.

To generate the p_{del-2}DEL-2::mCherry (KRT) translational reporter construct, we amplified from wt genomic DNA the sequence from the fifth until the eleventh exon, without the stop codon. The primers used were 5′-CTGCAGGATTTCTCTGTCAAGTGG-3′ and 5′-ACCGGTCATATTGTCAGGCAAGTT-3′ (Table 2). The PCR product was inserted into the Topo vector, and an AgeI/PstI was subcloned into the pPD95.77 plasmid vector, in frame with the mCherry coding sequence. Exons two to four were then amplified using the 5′-CTGCAGAGTTGATGATGATTAAAGAA-3′ and 5′-CTGCAGTGAAAATGCTCAAACAAA-3′ primers (Table 2) and subcloned into the Topo vector. A PstI/BglI fragment was then ligated upstream to exon five in pPD95.77 carrying *del-2* (exons 5-11) in frame with mCherry. Finally, the promoter and the first exon of *del-2* were excised from the Topo vector (created previously for the generation of the *del-2* transcriptional reporter) with SphI/PvuII and ligated into pPD95.77 carrying exons 2-11. The translational reporter p_{del-3}-DEL-3::DsRed was generated by amplifying the wild-type genomic region from exon two to exon seven, just before the stop codon, using the primers 5′-ACCGGTTGTTCACGATGATCAACTATT-3′ and 5′-ACC GGTGGTGTGTCTCCTGAAGCTA-3′ (Table 2). The amplified region was inserted into the Topo vector and an AgeI fragment was inserted downstream of exon 1 into pPD95.77 carrying the *del-3* promoter region and the first exon fused with DsRed, created during the construction of the *del-3* transcriptional reporter. For the *del-4* translational reporter p_{del-4}DEL-4::GFP, the promoter and the whole coding region were isolated from genomic wild-type DNA, using the primers 5′-ACGCGTCGACACATCATAAATCTCC ACCCAC-3′ and 5′-CGGGGTACCCCATCATTAGAATGAGGCTTTGG-3′, and inserted into the Topo vector. The promoter and coding regions were isolated using SalI/KpnI and fused with GFP in the pPD95.77 plasmid vector. To create p_{del-4}DEL-4::DsRed, the promoter and coding region of *del-4* were isolated from the GFP-tagged translational reporter construct using SphI/AgeI and inserted into pPD95.77, in frame with the coding sequence of the DsRed gene.

To monitor synaptic vesicle localization, we generated the construct p_{del-4}SNB-1::DsRed (KRT). The SNB-1 coding region and *del-4* promoter were amplified, with 5′-CGG GGTACCGAATTCGGACGCTCAAGGA GATGCCGGC-3′ and 5′-CGGGGTACCGAATTCTTTTCCTCCAGCCCATAAAACG-3′, 5′-CTGCAGGTCGA CACATCATAAATC-3′ and 5′-GGATCCCATCTGCAATTTTATTTT-3′ (Table 2), and inserted into Topo vectors. A KpnI DNA fragment of *snb-1* was excised from Topo and inserted into the pPD95.77 plasmid vector in frame with the DsRed coding sequence. An SphI/KpnI fragment of the *del-4* promoter was then fused upstream to *snb-1* gene. To estimate the resting membrane potential, we generated the construct p_{dat-1} ASAP-1 (KRT). Plasmid pcDNA3.1 /Puro - CAG - ASAP1[54] (plasmid #52519) (KRT) was retrieved from Addgene. We amplified ASAP-1 from plasmid #52519 and the *dat-1* promoter from wt genomic DNA

isolated from the N2 strain, with the primers 5′-TAGCCGCCACCATGGAGAC-3′ and 5′-AGATCTTTCATTA GGTTACCACTTCAAG-3′, 5′-CTGCAGATCCATGAAATGGAACTTGA-3′ and 5′-GGATCCGGCTAAAAA TTGTTGAG-3′. The PCR products were then inserted in Topo vectors. The *myo-3* promoter of pPD96.52 was replaced with a PstI/BamHI fragment containing the *dat-1* promoter. Next, a BamHI/EcoRV fragment containing ASAP1 was inserted downstream of the *dat-1* promoter into pPD96.52.

Total RNA isolation and qRT-analysis

Total RNA extraction from synchronized day-1 or day-2 adult animals was performed using the TRIzol reagent (Invitrogen). For cDNA synthesis the iScript™ cDNA Synthesis Kit (Bio-Rad) was used. Quantitative Real-Time PCR (qRT-PCR) was performed in a Bio-Rad CFX96 Real-Time PCR system and was repeated at least three times. Expression of the housekeeping gene pmp-3 was used as an internal control for normalization. The primers used for measuring pmp-3 mRNA levels were 5′- ATGATAAATCAG CGTCCCGAC-3′ and 5′- TTGCAACGAGAGCAACTGAAC -3′.

Protein blast

Protein BLAST analysis was performed in silico using the protein BLAST tool of the NCBI website (https://blast.ncbi.nlm.nih.gov/Blast.cgi). For this analysis, we retrieved the protein sequences of DEL-2 (isoforms a and b), DEL-3, and DEL-4 from the WORMBASE (https://wormbase.org//#012-34-5).

RNAi treatment

Specific gene downregulation was achieved using the RNA interference technique (RNAi). Animals were fed bacteria expressing double-stranded (ds) RNA, which targets the gene of interest. For the basal slowing assay and for hsf-1 downregulation, animals were synchronized with bleaching solution and eggs were placed on RNAi plates. They were allowed for 2 days at 20°C to grow until the l4 stage. Four to five l4 animals were transferred on new RNAi plates and allowed for 3-4 days to lay progenies. One-day-old adult animals from the second generation grown on RNAi plates were used to measure the basal slowing response. For imaging during *del-4* downregulation, isogenic populations of animals were synchronized with bleaching. Eggs were placed on NGM plates seeded with dsRNA for *del-4* and allowed to hatch and grow until the fourth day of adulthood. Animals were transferred on new RNAi plates every second day. RNAi plates were seeded with 200 μl of O/D culture inoculated with 50 μl O/N culture/ml of the O/D and incubated for 3-4 hrs shaking at 37°C.

Microscopy

Confocal imaging

Confocal images were acquired using an LSM710 Zeiss confocal microscope (Axio-observer Z1). Image z-stacks were captured, and maximum intensity projections were obtained using ZEN 2.3 software (Carl Zeiss, Jena, Germany). Animals were immobilized on a 5% agarose (in M9 solution) pad with a drop of 10 μl Nanobeads (Nanobeads NIST Traceable Particle Size Standard 100 nm, Polysciences) (KRT). The animals used were hermaphrodites on day one of adulthood unless otherwise stated. A 40x lens was used when the images were used for estimating the neuronal pattern of DELs, whereas for the rest of the confocal images, used to estimate colocalization or neurodegeneration, a 63x lens was used.

We followed previously suggested procedures to evaluate dense core and synaptic vesicle release.[62,101] Quantitation of synaptic and dense core vesicle numbers was performed in the dorsal nerve cord, when oriented towards the objective, at the turn of the posterior gonadal arm of young adults (day 1 of adulthood). Maximum intensity projection images were obtained from the dorsal neural cord of $p_{unc-129}$NLP-21::YFP and p_{unc-47}GFP::SNB-1 expressing animals (Table 1). We cross-fertilized *del-4(tm717)* mutants with animals carrying a GFP marker of synaptic vesicles (SVs) expressed under the GABAergic motor neuron-specific, *unc-47* promoter (p_{unc-47}GFP::SNB-1). Genetic tagging of synaptic vesicle-associated proteins or neuropeptides with fluorescent proteins can be used to estimate vesicle and neuropeptide density at presynaptic sites.[102] We quantified SVs at the presynaptic elements of the dorsal nerve cord at the turn of the posterior gonadal arm. We measured the number of puncta per 10 μm and the mean puncta intensity of neurons.

Previous studies assessed the levels of DCVs released via a YFP reporter of NLP-21 neuropeptide expressed under the *unc-129* promoter (KRT).[101] Using this reporter, we determined the relative amount of

DCVs in the dorsal neural cord cholinergic motor neurons. We assessed the release of DCVs by calculating the mean intensity ratio of the axon to coelomocytes, as coelomocytes retrieve the released NLP-21::YFP.[101] We crossed the DCVs reporter strain with the *del-4(tm717)* mutant (Table 1) and performed high-magnification confocal microscopy analysis.

Maximum intensity projections were also retrieved for the posterior coelomocytes of the $p_{unc-129}$NLP-21::YFP strain. The images were analysed using the Volocity Software (Quorum Technologies). We measured the mean fluorescence intensity of cholinergic motor neuron axons from the posterior coelomocytes of NLP-21:: YFP-expressing animals. The number of fluorescent puncta/10 μm was counted and the ratio of axon to coelomocyte mean fluorescence intensity was calculated. Likewise, the mean fluorescence intensity of puncta and the number of puncta per 10 μm were computed in p_{unc-47}GFP::SNB-1 animals.

To monitor neurodegeneration, we cross-fertilized animals overexpressing DEL-4 (p_{del-4}DEL-4::GFP) and *del-4(tm717)* mutants with *C. elegans* Parkinson's and Alzheimer's disease models (Table 1). The UA44 strain was used as the model for Parkinson's disease. It expresses human α-synuclein in dopaminergic neurons, labelled with GFP to monitor degeneration (p_{dat-1}GFP;p_{dat-1}a-synuclein).[61] We assessed neurodegeneration in the Parkinson's disease model at day seven of adulthood. We used the BR5270 strain that pan-neuronally expresses the pro-aggregation F3ΔK280 tau fragment as a tauopathy model.[62] To detect dopaminergic neuronal loss, we crossed the BR5270 strain with animals carrying the p_{dat-1}GFP (BZ555) reporter (Table 1). We measured the degenerated neurons in the tauopathy model at day 5 of adulthood.

Neurodegeneration was assessed based on the morphology of the six dopaminergic neurons in the head (4 CEP and 2 ADE), on days 5 and 7 of adulthood. Estimation of dopaminergic neuron degeneration was performed as previously described.[96] Neurons were considered degenerated when they exhibited either one of the following morphological defects: neuritic blebbing, breaks in neuronal processes or dendrites, absence of neuronal processes, cell body shrinkage, reduced fluorescence or absence. If one or more of the above-mentioned phenotypes were observed, then the neuron was considered degenerated. Fifty to sixty animals were examined per biological replicate for each genotype. The number of degenerated neurons per animal is plotted in graphs for each genotype. Scoring was performed by two investigators (DP and MG) and one of them performed it blindly.

Epifluorescence microscopy

Epifluorescence microscopy was performed using a Zeiss Axio Imager Z2 or EVOS™ FV Auto2 Imaging System (Thermo Fisher Scientific). Mounting of animals on slides was achieved with a 13 μl drop of 30 mM Tetramisole (Tetramisole hydrochloride, Sigma-Aldrich) for imaging with a 5x lens or with 2% agarose pads and 15 μl of 30 mM Tetramisole for imaging with the 20x lens (KRT). Imaging after heat stress and starvation was conducted on day two of adulthood. Animals grown on RNAi plates were imaged on day three or four of adulthood. Animals from the rest of the experiments were imaged on day one of adulthood.

To assess DEL-4 expression levels, we used the DEL-4::GFP translational reporter and measured the intensity of the most brightly fluorescent neuronal cell body in the head of each animal. The HSF-1::GFP expression levels were collected from entire animals and GFP-positive nuclei in the hypodermis. We overlooked the nuclei located above the gut to avoid intestinal autofluorescence. Measurements of SKN-1b/c::GFP were collected from entire animals and ASI neurons. The DAF-16::GFP expression levels were measured from the whole animal and from intestinal cells. We measured the intensity levels of DAF-16 in the nuclei and adjacent cytoplasm of gut cells and calculated the nucleus-to-cytoplasm ratio. The intensity of neuronal cell somas in the head of p_{asic-1}SNB-1::SEpHluorin animals was counted to estimate the basal levels of synaptic release from dopaminergic neurons. Super ecliptic phluorin (SEpHluorin) (Table S1) is a pH-sensitive GFP. When genetically tagged with SNB-1, SEPhluorin is expressed inside synaptic vesicles, where the low pH quenches its fluorescence. Upon vesicle release, SEpHluorin encounters the less acidic environment of the synaptic cleft and recovers its fluorescence, allowing for estimation of synaptic vesicle release. Similarly, the fluorescence intensity from the cell bodies of cholinergic motor neurons was measured in p_{acr-2}SNB-1::SEpHluorin-expressing animals. We acquired visualizations of the ventral cord posterior and anterior to the vulva. To estimate the voltage levels using ASAP1, we counted the intensity from the cell bodies of dopaminergic neurons. Expression levels of phsp-16.2GFP, p_{sod-3}GFP, p_{skn-1}SKN-1::GFP, p_{gst-4}GFP, p_{hsp-4}GFP, $p_{let-858}$GaMP2.0, and p_{aak-2}AAK-2::Tomato were measured from the entire body and expressed as mean pixel intensity in arbitrary units (a.u.).

Imaging with the EVOS™ Imaging System was performed for p_{acr-2}SNB-1::SEpHluorin, the voltage indicator p_{dat-1}ASAP1, and p_{daf-16}DAF-16::GFP in gut nuclei, and the z-stack analysis of the imaging system was used. Analysis of epifluorescence images was performed using Image J 1.48V. For presentation purposes only, the 'straighten' function of ImageJ software was utilized for isolating and straightening animals' heads, bodies, or neuronal processes. The line width in pixels used was 300 for Figures 5D, 7A, S1A, and S6E (ASI nuclei), 400 for Figure 7C, 80 for Figures 7K and 7L, 220 for 8C, 350 for S6E (gut nuclei), and 600 for S6E (hypodermis nuclei).

Behavioural assays

Basal slowing assay

The procedure followed for the basal slowing response was previously described.[44] NGM plates were seeded with HB101 (KRT) in a ring shape, leaving the centre of the plate without food. NGM plates seeded with HB101 bacteria and non-seeded plates were incubated for 16 h (O/N) at 37°C and allowed to cool to room temperature before use. Synchronized well-fed animals on day 1 of adulthood were washed in a 20 μl drop of M9 solution (3 g KH_2PO_4, 6 g Na_2HPO_4, 5 g NaCl, 1 ml 1 M $MgSO_4$, H_2O up to 1 litre) twice. Subsequently, the animals were placed in the unseeded region at the centre of the plate with eyelash hair and allowed to recover for 5 min. The bend number of the anterior body region was counted for each active animal during 20sec. The forward and backward movements were counted. The procedure was performed in the absence or presence of bacteria. Measurements on the seeded plate were performed only for animals that moved on the bacteria. Ten to fifteen hermaphrodite animals were placed on each assay plate, and 8-15 measurements were taken. Each experiment was repeated at least 3 times. To quantify the locomotory response, we calculated for each experiment the ratio of Δ body bends/20sec. Δ body bends/20sec corresponds to the body bends/20sec of each animal on an unseeded plate minus the body bends/20sec on a plate with food.

Population drop-test assay

The population drop test was performed following the standard protocol described in the WormBook (http://wormbook.org/chapters/www_behavior/behavior.html) (KRT), with minor modifications. In brief, 30 animals of each genotype were placed on a 6 cm unseeded NGM agar plate and allowed to rest for 5 min. Drops of M13 buffer (30 mM Tris-HCl pH 7.0, 100 mM NaCl, 10 mM KCl) were delivered with a 0.5 ml syringe at the animal's tail. Glacial acetic acid was used to prepare M13 solutions with pH values of 6.6, 4.5, and 2.2. Backward movement within 4 seconds of drop delivery was considered a positive avoidance response. Each animal was tested with 2-3 drops with an inter-stimulus interval of at least 2 min. We examined well-fed hermaphrodites on day one of adulthood. The avoidance index was calculated as the number of positive responses divided by the total number of trials. An avoidance index of 1 represents complete avoidance to the M13 solution, and 0 represents a total lack of avoidance response.

DEL-4 expression and TEVC on Xenopus oocytes

cDNA generation

C. elegans cDNA was obtained from N2 wild-type and purified using the Invitrogen™ SuperScript™ III First-Strand Synthesis System (KRT). The cDNA inserts were subcloned into the KSM vector under the control of the T7 promoter containing the 3′ and 5′ untranslated regions (UTRs) of the Xenopus beta-globin gene and the poly(A) tail.

Primer generation

The forward primer 5′-AGATCTGGTTACCACTAAACCAGCC-3′ and reverse primer 5′-TGCAGGAATTC GATATCAAGCTTATCGATACC-3′ were used to amplify the KSM vector. Based on the sequence on wormbase.org, the forward primer 5′-CTTGATATCGAATTCCTGCAATGGGTGTATTTTGGACCGGC-3′ and the reverse primer 5′-GTTTAGTGGTAACCAGATCTTCAATCATTAGAATGAGGCTTTGGTGGAAC-3′ were used for amplification of the *del-4* cDNA (based on the sequence in wormbase.org). To generate *del-4(tm717)* deletions, we used the NEB Q5® Site-Directed Mutagenesis Kit (KRT). Plasmids generated were pEK230 (*del-4* cDNA in the KSM vector[51] and pEK238 (*del-4(tm717)* cDNA in the KSM vector). The NEBuilder HiFi DNA Assembly Reaction Protocol was used to assemble the KSM vector and cDNA inserts using NEBuilder® HiFi DNA Assembly Master Mix (KRT) and a vector:insert ratio of 1:2.

mRNA synthesis and microinjection

The linear plasmid was used as the template for *in vitro* RNA synthesis from the T7 promoter using the mMessage T7 kit (Ambion #AM1344) (KRT) to produce 5′-capped RNA (KRT). Oocytes were injected with 25 nl of RNA solution at a total concentration of approximately 500 ng/μl using the Roboinject (MultiChannel Systems). Oocytes were kept at 16°C in 1X ND96 prior to TEVC.

Two-electrode voltage clamp (TEVC)

TVEC was performed 1-2 days post-injection at room temperature using the Robocyte2 (MultiChannel Systems) as previously described.[51,103] *Xenopus* oocytes were clamped at −60 mV using ready-to-use Measuring Heads from MultiChannel Systems filled with 3M KCl. All channels were tested using the Robocyte2 (MultiChannel Systems). Since millimolar concentrations of Ca^{2+} and other divalent ions except Mg^{2+} can block ASIC currents,[104] Ca^{2+}-free buffers were used for substitution experiments of monovalent cations adapted from a previous protocol[105]: 96 mM XCl, 1 mM $MgCl_2$, 5 mM HEPES, pH adjusted to 7.4 with XOH, where X was Na^+, K^+ or Li^+, respectively. To test ion permeability for Ca^{2+}, a previous protocol was used,[72] replacing Na^+ with equimolar Ca^{2+}. If necessary, D-Glucose was used to adjust the osmolarity. Osmolarity was checked and confirmed to be within an error of 210 m.[106] To test pH sensitivity, 1X ND96 solution was used; for solutions with a pH of 5 or lower, MES was used instead of HEPES and adjusted with HCl. I-V relationships for ion selectivity and proton conductance were calculated by subtracting the background leak current in the presence of 500 μM amiloride from the current observed in the absence of amiloride to get the actual current. Actual current I-V curves for each oocyte were fitted to a linear regression line, and the x-intercept was compared between solutions to calculate an average reversal potential (E_{rev}). The reversal potential shift (ΔE_{rev}) was calculated for each oocyte, when shifting between pH solutions or from a NaCl to a KCl, LiCl or $CaCl_2$ solution. To test the responses to pH, channel-expressing *Xenopus* oocytes were perfused with 1X ND96 (using HEPES for buffering pH above 5.5, and MES for pH below 5). The pH was adjusted with HCl and ranged from pH 7.4 (neutral pH of the ND96 solution) to pH 3.8 or pH 4. Background currents measured at pH 7.4 were subtracted from those measured during activation of the channels. For analysis, currents were normalized to maximal currents (I/I_{max}) and best fitted using the Hill's equation (variable slope).

DiI staining

To identify the DEL-4 subcellular localization, we labelled amphid and phasmid neurons with the lipophilic carbocyanine tracer DiI (dioctadecyl tetramethylindodicarbocyanine-disulphonic acid, Invitrogen) (KRT), prepared as described earlier.[107] DiI stains the membranes of amphids, phasmids, and chemosensory neurons with nerve endings exposed to the environment. In brief, one-day-old adult hermaphrodite animals were washed twice with 200 μl M9 free of bacteria and incubated in 200 μl 10 μg/ml DiI diluted in M9. Animals were rotated in a 200 μl tube with DiI for 2-3 hours, washed twice with M9, and then allowed to recover and de-stain for an hour on an OP50-seeded NGM plate before imaging.

Stress assays

Heat stress (HS)

To assess DEL-4 expression levels under the implementation of heat stress, 1-day adult animals expressing DEL-4::GFP were treated for 2 hrs at 37°C. Animals were allowed to recover O/N at 20°C on NGM plates seeded with OP50 and then imaged on day 2 of adulthood. To assess the effect of heat stress on the voltage of dopaminergic neurons, which was measured with ASAP1, 2-day adult hermaphrodite animals were stressed for one hour at 37°C on OP50-seeded plates and then imaged immediately.

Long term starvation (LTSt)

For the starvation assay, one-day-old adult hermaphrodite animals were placed with a platinum pick on unseeded NGM plates. They were allowed to starve for 24 hrs and then imaged on day two of adulthood.

Oxidative stress (OS)

To induce oxidative stress paraquat (N, N′-dimethyl-4,4′-bipyridinium dichloride, Sigma-Aldrich) (KRT) was added on top of OP50-seeded NGM. Paraquat was added to a final concentration of 8 mM diluted in water. Water was placed on the control plates. Plates were allowed to absorb the drug and animals at the L4 stage were placed in plates. Animals were stressed O/N and then imaged on day one of adulthood.

ER stress (ERS)

To induce ER stress tunicamycin (Sigma-Aldrich) (KRT) was plated on OP50-seeded NGM. Tunicamycin was added to a final concentration of 2.5 μg/ml in M9. M9 was placed on control plates. Plates were allowed to absorb the drug or M9 and animals at the L4 stage were placed in the assay plates. Animals were stressed O/N and then imaged on day one of adulthood.

Acidic stress (AS)

To elicit low-pH stress, we used an M13 solution adjusted with CH3COOH at the appropriate pH. Before treatment, one washing step was performed in a 20 μl drop of M13 pH 6.6. For the measurement of DEL-4 expression levels upon acidic stress, one-day adults were incubated for 1 hr within a 20 μl M13 drop of pH 6.6 (control) or pH 3.5 (at low pH stress). To estimate the ASAP1 levels after acidic stress, 2-day adult animals were incubated for 15 min in a 20 μl M13 drop of pH 6.6 (control) or pH 4.5 (low pH stress). After treatment, the animals were incubated in a 20 μl drop of M13 solution pH 6.6 to recover GFP fluorescence that quenches due to the pH sensitivity of GFP.

Survival assays

Survival assay after heat shock

For thermotolerance evaluation, 1-day adult animals were placed on OP50-seeded NGM plates and exposed to 37°C for 2.5 hours. Animals were allowed to recover overnight at 20°C, and on the following day, death events were monitored per day. Animals were scored as dead when they failed to respond to prodding with the platinum wire. Animals were transferred to new plates once every two days to avoid mixing with the progeny.[108]

Starvation survival assay

To analyse survival during starvation, we followed the procedure described previously[109], with a few modifications. After synchronization with the bleaching solution, ~3.500 eggs were incubated in 1.5 ml BSA-coated tubes filled with sterile M9 solution on a rotating carousel (Stuart Scientific SB1 Blood Test Tube Rotator) at 20°C. Twenty-four hours after egg preparation and every second or third day, 20 μl was collected from each tube, plated on OP50-seeded NGM and allowed to grow at 20°C for three days. Three samples (20 μl) were collected from each strain, and the average was calculated. We then counted the animals that reached L4 stage or young adulthood. Day 1 was considered the day after egg preparation and was used as a control and denominator to calculate the percentage of animals that recovered.

Pharmacological assays

Acute aldicarb resistance assay

Aldicarb is a cholinesterase inhibitor that causes paralysis due to acetylcholine (ACh) accumulation at the synaptic cleft. We used aldicarb (100 mM stock in 70% ethanol; Sigma-Aldrich) (KRT), as proposed by Mahoney et al.[46] Animals were collected and washed twice in M9. We differentiated the procedure by placing one-day adult animals in a 15 μl drop of 10 mM aldicarb in M9 instead of using NGM plates with aldicarb. The animals were monitored to identify the moment at which they stopped moving. Seven animals were used per condition in each experiment, with a total of six biological replicates.

Levamisole resistance assay

Levamisole is a nicotinic receptor agonist that paralyzes animals through continuous muscle stimulation. For the levamisole assay, we used 400 μM concentration in M9. Animals were collected with M9 and washed twice. Subsequently, they were placed in a 20 μl drop of 400 μM levamisole (KRT). Locomotion was evaluated by the number of animals not moving in the levamisole drop reported every 5 min until all animals were paralyzed.

Dopamine resistance assay

To monitor dopamine-induced paralysis, 30-40 animals of the selected genotypes and at day one of adulthood were collected with M9 and washed twice. Subsequently, we placed the animals in a 20 μl drop of 40 mM dopamine (Dopamine hydrochloride, Sigma-Aldrich) (KRT), diluted with M9. The number of moving animals was recorded every 5 min of exposure and until all animals were paralyzed. We always used freshly prepared dopamine to avoid oxidization.

QUANTIFICATION AND STATISTICAL ANALYSIS

Sample sizes were not predetermined using statistical methods. Statistical analysis and graphical illustrations were performed using Prism software package (GraphPad Software Inc., San Diego, CA, USA). The results are presented as XY graphs, with error bars representing the standard error of the mean (SEM). Two-way analysis of variance (TWO-WAY ANOVA) was performed for most of the experiments to compare the mean values and evaluate statistical significance. TWO-WAY ANOVA is selected where the mean values of independent biological replicates with pre-calculated SEM are represented in the graph. In the other cases One-way ANOVA is used. The post-hoc analysis to correct for multiple comparisons was performed using the Tukey's multiple comparisons test or the ordinary Two-way ANOVA test for the TWO-WAY ANOVA analysis, while the one-way Tukey's test was used in the One-way ANOVA. For survival analysis the Log-rank (Mantel-Cox) test was used to evaluate statistical significance. All experiments were repeated at least thrice. The number of biological replicates, the sample sizes, the specific type of ANOVA and any further statistical information related to each graph can be found in the Figure legends. The P-values in the graphs are indicated with the following symbols: ns $p=0.1234$, *$p=0.0332$, **$p=0.0021$, ***$p=0.0002$, ****$p<0.0001$.